8990

Hydrodynamic and Salinity Modeling for Estuarine Habitat Restoration at Herring River, Wellfleet, Massachusetts

Submitted to:

National Park Service
US Department of Interior
Cape Cod National Seashore
99 Marconi Site Road
Wellfleet, Massachusetts 02667
Attn: Dr. John Portnoy

Submitted by:

Malcolm L. Spaulding
Annette Grilli
Ocean Engineering
University of Rhode Island
Narragansett, RI 02881
Tel: 401-874-6666
Fax: 401-874-6837
Email: spaulding@oce.uri.edu

October 2001

Table of Contents

Appendices

Appendix A Spreadsheets containing data collected during the intensive tidal cycle survey programs performed on July 25, 2000 and September 27, 2000.

Appendix B Spreadsheets containing time series data of surface elevation, salinity, and temperature collected during 1999- 2000 at one station in Herring River and a second station just offshore of the Herring River dike.

Appendix C Spreadsheet containing grain size analysis of sediment samples collected in Herring River and adjacent area seaward of the dike.

Appendix D Web based animations of the surface area covered versus time and the high, low, and tidally averaged, mean salinity for the present control structure configuration (C2), all control structures removed in the dike(Case C5), and Case C5 for the 100 year storm. A second group of simulations is provided for the three cases above, but with Mill Creek diked and High Toss Road removed.

Executive Summary

A dike was constructed across the entrance to Herring River and the associated marsh system, located in Wellfleet, Massachusetts on Cape Cod in 1908. The dike has three box culverts, which allow water and salt exchange between the river and adjacent Wellfleet Harbor. Two of the culverts have flapper tidal gates and the third an adjustable sluice gate. The restriction in flow imposed by the hydraulic control structures has resulted in the conversion of hundreds of hectares of the original inter-tidal, salt marshes into upland vegetation eliminating habitat for estuarine plants and animals, including fish and shellfish. In addition it has resulted in adverse impacts on water quality including acidification of river waters, leaching of metals from the sediments and episodic anoxia. It has also resulted in subsidence of the wetlands.

As part of renewed interest in salt marsh restoration in the National Park Service (NPS) the Cape Cod National Seashore (CACO) managers, the public, and local and state environmental authorities are interested in restoring estuarine habitat in Herring River. In order to proceed NPS needs a comprehensive, scientifically rigorous, and clearly articulated restoration plan that meets the approval of local, state, and federal regulators, as well as the affected private property owners. One component of such a plan is the application, calibration, and validation of hydrodynamic and salinity models. These models allow the impact of various restoration options, including various configurations of the sluice and tidal gates located in the dike and alterations to the opening in the dike, on the flows, sea surface elevations, and salinity distribution in the river to be assessed. Based on earlier simplified modeling studies and field data collection programs sponsored by NPS as a starting point, the goals of the present study are: (1) to apply state of the art models to predict the tidal flows and salinity in the Herring River system, (2) to collect field data for selected periods of time to validate and calibrate the models, and (3) to perform a series of simulations, using the validated model, to determine the impact of various restoration options on the flows through the dike and the tidal ranges and salinities in the river.

To support model calibration and validation two separate field programs were performed. The first consisted of continuous time series measurements of sea surface elevation up and downstream of the dike for the period from June to October 2000. The second consisted of two intensive tidal cycle experiments, performed on July 25, 2000 and September 27, 2000, which collected data to characterize the currents and flows through the dike, sea surface elevations up and downstream of the dike, and salinity and temperature fields in the Herring River system and adjacent Wellfleet Harbor, over a lunar, semi-diurnal (M_2) tidal cycle (period-12.42 hrs). In addition the flux of freshwater into the system was determined by gauging flows at key locations.

An analysis of the data showed that the dike reduced the mean tidal range from 2.53 m in the bay to 0.56 m in the river. This is a reduction of a factor of 4.52 in the tidal range across the dike. High tide in the river lagged that in the bay by about 3.2 hours. The low tide phase difference was very small as a result of the truncated shape of the low tide portion of the tidal elevation curve. The surface elevation time series was dominated by the lunar semi-diurnal tide (M_2, 12.42 hr period), with all other components being significantly smaller. The

spring/neap tides were 32 % higher and 8 % lower than the mean downstream of the dike and 13 % higher and 4 % lower upstream.

The intensive tidal cycle survey showed that the tidal flows through the dike were controlled by the tidal and sluice gates. The majority of the inflow (flood) to the system was through the sluice gate while the outflow (ebb) was about equally divided between the three culverts. The data show that the two culverts, with tidal gates, exhibit minor leakage on the flood tide due to structural problems with the gate pins or hinges. The peak flow rates through the gates, based on the two tidal cycle surveys, are on the order of 6 to 10 m^3/sec, increasing with increasing tidal range. Tidal flows are substantially larger than the mean freshwater flows entering the system during the surveys (0.1 to 0.2 m^3/sec). The data show that salinity intrusion in the system reaches its maximum at high tide and its minimum at low tide. The maximum intrusion distance is normally south of High Toss Road.

An inlet-basin hydrodynamic model was developed to predict the flows through the culverts and the water level in the river. The model solves the one-dimensional conservation of mass and momentum equations for the inlet (culverts and associated hydraulic control structures) and a conservation of mass equation, with variable water storage (basin area vs. elevation), for the basin. The model includes frictional losses in the inlet due to bottom and boundary friction as well as losses due to flow through the sluice gate. The model is an extension of earlier work by the US Army Corp of Engineers. The salinity model assumes a simple balance between the seaward, advective flux of salt due to the mean freshwater input to the system and the landward flux of salt due to tidal diffusion.

The hydrodynamic model was applied to predict the flow through the dike and the surface elevation in the basin for the two intensive tidal cycle surveys to calibrate and validate the model. The model was forced by the observed bay tides. The surface area versus elevation curve for the basin was based on the merging of existing bathymetric and topographic data sets for the river plus transect data collected during the present study. Model predictions of surface elevation in the river were in excellent agreement with observations for both the calibration and validation exercises, with root mean square (rms) errors of 6 cm when a single value of the bottom friction (Manning) coefficient was selected. A detailed sensitivity study showed that model performance could be substantially improved (rms error of 2-3 cm) if a two-part formulation was used, with higher frictional losses on the ebb than on the flood tide. Additional simulations showed that model performance is weakly dependent on Manning coefficient (n), as long as n is in the range of 0.06 and 0.09. Model predictions of maximums, minimums, and range are much more sensitive to Manning coefficient, generally increasing (larger maximums, smaller minimums, and larger ranges) as n decreases.

Simulations were performed for a variety of restoration options that include alteration of the hydraulic control structures in the culverts (e.g. various sluice and tidal gate configurations and openings) and opening all gates. An additional set of simulations was performed diking off Mill Creek and allowing water to flow freely through the High Toss Road causeway. Taken as a group, the first set of simulations show that increasing the effective size of the opening at the dike increases the high and low tide water levels and the tidal range in Herring River. In general replacing a tide gate by a sluice gate results in an increase in the low tide

level but little change in the high tide level. Simulations with 100 year storm conditions show that the water level damping caused by the dike is similar to that for more typical tidal forcing but that the water levels are substantially increased due to the increase in the forcing from Wellfleet Harbor. The impact of increasing the effective cross sectional area opening of the dike, as a result of the restoration options, is similar to that for the simple tidally forced cases. Alternation of the basin geometry by diking Mill Creek and additional openings in the High Toss Road causeway has little impact on water levels for the current control structure configuration. If all control structures are removed however seawater penetrates well north of High Toss Road inundating the wetland at high tide and leaving pools of water at low. This occurs for both tidal and 100yr. storm forcing. The additional water storage capacity, afforded by the wetland above High Toss Road, increases the mean and minimum water levels and reduces the maximum level. The tidal range is substantially (over 50%) reduced.

Simulations were performed systematically increasing the width of the opening in the dike to determine the impact of these large scale modifications on the tidal range and minimum and maximum water levels in Herring River. The widths ranged from the present condition (width = 6 m, three culverts completely open) to complete removal of the dike (width = 200 m). This suite of simulations showed that the tidal range and water levels in the river asymptotically approached those in the bay as the opening width increased. For widths greater than about 30 m, the dike structure had little impact on conditions in the river.

The salinity model was calibrated with data from the July 25, 2000 intensive tidal cycle survey data and showed a very good ability to predict the vertically averaged tidal mean salinity profile (rms error – 1.6 ppt). This performance was confirmed by validation of the model with data from the September 27, 2000 experiment, which gave an rms error of 2.5 ppt. The model predicted flushing time and salt penetration distance were in reasonable agreement with the July 25 observations (26 hrs., 1.48 km) and the September 27 observations (34.7 hrs, 1.5 km). The salinity model was applied to predict the impact of the restoration options on the salt intrusion distance and flushing time. In general as the effective size of the opening in the dike increases the salinity intrusion distance and flushing time both increase. This result is directly due to the increased tidal exchange allowed by the increased size of the opening. A sensitivity analysis showed that the model predictions were very sensitive to the assumed freshwater input rate. The flushing time was predicted to decrease as the freshwater flow rate increased. Simulations for the alternate basin geometry (diked Mill Creek, additional openings in High Toss Road) show salt water penetrating to High Toss Road for the existing controls. Intrusion distances increase substantially with removal of all controls and allow salt water to reach the wetland, well north of High Toss Road. Flushing times increase as the tidal exchange volume increases.

Comparison of the present model predictions for tidal conditions (range, minimum, and maximums) and salt penetration distance and flushing time, for the current configuration and proposed restoration options that involve minor modifications in the current configuration, are in good agreement with prior modeling studies performed by Garvine and reported in Roman (1987). However, as the opening in the dike increases the present simulations show a much larger impact in terms of tidal range, minimum and maximum water level, salt penetration distance, and flushing time than Garvine's work. As an example the present simulations show

substantial increases in the maximum and minimum water levels, tidal range, salt penetration distance and flushing time, while Garvine's simulations predict little variation. A systematic sensitivity study shows that the principal differences are due to the assumed surface area versus elevation curve used to describe the storage capacity of the river between the dike and High Toss Road. Garvine's relationship has a much smaller storage area/volume in the critical 0.0 to 0.7 m elevation range than the relationship used in the present study. The second most important parameter is the difference in the representation of frictional losses through the dike. The present model reproduces Garvine's predictions very well when similar inputs are employed and assumptions made.

The construction of the dike across the mouth of Herring River, and the associated control structures in the dike, have generated a strong asymmetric pattern in the flood/ebb flow velocities in the lower river. Offshore sediments (sand) are transported through the dike into the lower river by the strong flood tide currents. This material falls to the seabed and is deposited landward of the dike, forming a flood tide delta. Ebb currents in the vicinity of the delta are insufficient to re-suspend the sediment and hence the delta has grown to the point that its peak is vegetated with marsh grass. Removal of the control structures in the dike, and the resulting reduction in the asymmetry of the flow field, are projected to have minimal impact on the sediments in the flood tide delta since the currents required for re-suspension will not be achieved in typical tidal forcing. Re-suspension and transport are however likely in rare, strong storm events.

It is cautioned that while the hydrodynamic and salinity model are well calibrated and validated for the current conditions, calibration/validation for restoration options, particularly those that represent significant increases in the effective opening of the flow cross sectional area in the dike, have not been possible due to the lack of field data. The results however are sufficiently definitive for park managers to proceed with an incremental, adaptive-management program, which could be verified by field experiments as described below.

The present field program and modeling investigation have provided a reasonable understanding of the tidal and salt dynamics of the Herring River system for the current configuration and operation of the hydraulic control structures in the dike. To advance our understanding additional intensive tidal cycle survey data should be collected and used to refine the model calibration. Particular attention needs to be directed at making more careful measurements of the water levels inside the culverts, particularly the one containing the sluice gate, where the flows are observed to be super-critical on a substantial portion of the flood tide. The largest uncertainty in the model application to the restoration options is the specification of the surface area versus elevation relationship, particularly in the range from 0.0 to 0.7 m. It is recommended that additional surveying be performed in this area to verify and refine the assumed topography used in the present model. It has not been possible, within the context of the present study, to evaluate the model predictive performance for conditions substantially different from the present configuration. This problem could be addressed by significantly altering the hydraulic control structures in the dike (opening of the sluice gate, removal of one or more of the tidal gates) and making similar intensive tidal cycle measurements to those performed in the present study. This would only need to be done for a short period of time (several tidal cycles) to obtain the necessary data. Note that in most cases

these experiments would explore conditions typical of the impact of storms on the river. Once this data was obtained and evaluated restoration options that were explored in the experiments could be considered for implementation.

List of Tables

List of Figures

1. Background and study objectives

The estuarine habitat of the Herring River, located in Wellfleet, Massachusetts (Figure 1) Cape Cod National Seashore, has been severely degraded by drainage and the construction of a dike, with sluice and tidal gates, at the entrance to the river starting in 1908 (Portnoy and Reynolds, 1997). Because of the dike and the associated operation of the tidal and sluice gates, seawater from Wellfleet Harbor and Cape Cod Bay has been prevented from entering most of the system. This has resulted in conversion of hundreds of hectares of the original inter-tidal, salt marshes into upland vegetation eliminating habitat for estuarine plants and animals, including fish and shellfish (Portnoy et al, 1987; Roman, 1987). Surface waters in the area have been acidified by the drainage and the oxidation of sulfur in the diked salt marsh peat (Portnoy and Giblin, 1997). These acidified waters have resulted in the leaching of metals from native clays to the surface waters. In the summer, river waters are seriously depleted of oxygen due to temperature effects and the lack of flushing. The acidity, metals levels, and episodic anoxia cause fish kills and generally leave depauperate aquatic fauna. The restricted fish access to the area, and particularly to mosquito breeding sites, has increased the nuisance mosquito problem; this in spite of the diking and drainage systems implemented in the early 1900s to control these mosquitoes. In addition the wetlands have subsided nearly one meter due to the increased decomposition rate, sediment de-watering and associated pore-space collapse and the loss of sediment supply from the bay.

The National Park Service (NPS) has funded or cooperated in a large number of multi-disciplinary investigations studying the impacts of the tidal gates on the Herring River system and evaluating alternatives for the restoration of the river since 1980 (Roman, 1987; Roman et al, 1995). In addition to assessing the ecological effects of the dike and evaluating the impact of restoration of tidal flows in the area, the protection of groundwater quality and the impact on private properties adjacent to the flood plain were also investigated.

As part of renewed interest in salt marsh restoration in the National Park Service the Cape Cod National Seashore (CACO) managers, the public, and local and state environmental authorities are interested in restoring estuarine habitat in Herring River. Although approximately 80 % of the flood plain directly affected by the tidal gate is within CACO boundaries, and nearly all of this land is federally owned, two homes, a golf course, and the dike at the entrance to the system are outside NPS's control. In addition NPS lands are subject to other jurisdictions. In order to proceed NPS needs a comprehensive, scientifically rigorous, and clearly articulated restoration plan that meets the approval of local, state, and federal regulators, as well as the affected private property owners.

In earlier studies (Roman, 1987; Roman et al, 1995) hydrodynamic and salinity modeling were performed to assess the impact of the operation of the sluice and tidal gates located in the dike at Chequesset Neck on flows, sea surface elevations and salinity distribution in the river. Model simulations for a variety of options, including removal of tidal gates and adjustments of the sluice gate, showed that the system could be restored to former estuarine conditions. This would require removal of the tide gates, diking in Mill Creek to protect the golf course, rehabilitation/addition of selected culverts, and removal of spoil piles that resulted from prior dredging of the channels in the system to promote drainage.

The prior hydrodynamic and salinity modeling provided important insight into the fundamental physical behavior of the system but had several important limitations. The simulations were hampered by the lack of long term field data on sea surface elevation and salinity necessary to accurately calibrate and verify the model. Only three data sets were available, each lasting only one tidal cycle. Data to accurately characterize the current flood plain topography, particularly in the upper reaches of the river, were also limited. These data are critical to assessing the dynamics of the system and to evaluating the impact of restoration options. Finally the model conceptualized the system in the form of any entry channel and a single interior storage basin (i.e. Herring River). The model was unable to consider flows within the channel network in the marsh. Given these limitations model predictions remain uncertain and are not currently adequate to assess the physical impact of restoration options.

In addition NPS managers need to understand how restored tidal flows in the river would affect sedimentation and return the diked wetland surface back into equilibrium with current sea level. Managers also need to understand how the transport of fine-grained particulate organic and inorganic matter in the wetland will be affected if tidal flows in the area are increased. There is particular concern that this material will be transported seaward of the dike toward Wellfleet Harbor and adversely impact shellfish beds in this area. None of these issues were addressed in the earlier NPS studies (Roman, 1987).

Given this background the goals of the present study are:

1. To apply state of the art models to predict the tidal flows and salinity in the Herring River system.

2. To collect field data for selected periods of time to validate and calibrate the models,

3. To perform a series of simulations, using the validated model, to determine the impact of various restoration options on the flows, salinities, and sediment transport in the river.

Section 2 of this report presents an overview of the hydrodynamic and salinity models used to study the tidal dynamics of the system and assess the restoration alternatives. The data collected to support the modeling program including application, calibration and validation is provided in Section 3. Sections 4 and 5 address model calibration and validation, respectively. Application of the model, to assess the impact of restoration options on hydrodynamics and salinity in the river, is provided in Section 6. This section also discusses the impact of restoration on sediment transport dynamics using a conceptual model. Conclusions of the work are presented in Section 7 and references in Section 8.

The data collected during two intensive tidal cycle surveys in July and September 2000 are provided in Appendix A. Time series data of sea surface elevation, salinity, and temperature collected during 1999 and 2000 at one station in Herring River and a second just seaward of the dike are provided in Appendix B. Appendix C provides data on grain size analysis from surficial sediments in Herring River and the adjacent area just off shore of the dike. Appendix

D provides web-based material that helps better understand the water level and salinity dynamics of the study area. (The web-based software has been provided to the National Park Service as part of this study.) The web-based system includes topographic and bathymetric maps of the study. In addition animations of the surface area covered by water versus time, over a lunar semi-diurnal cycle (12.42 hours), are provided for the current gate configurations, under mean and 100 year flood forcing, and for the case when all control structures in the dike are removed, with mean tidal forcing. Two sets of animations are provided, the first assuming that tidal waters do not penetrate north of High Toss Road and the second for a restoration option that assumes that Mill Creek is diked and that additional openings are made in High Toss Road so that tidal waters are free to penetrate north of High Toss Road. Finally model predictions of the salinity distribution at high and low tide and for the tidally averaged case are provided for each of the six simulations.

2. Hydrodynamic and salinity models for tidal inlet systems

An overview of the inlet-basin hydrodynamic model used in the present study is presented here. In the context of this investigation the box culverts, through the dike, are the inlets and Herring River, upstream of the dike, acts as a basin, alternately storing and releasing water as the tidal floods and ebbs through the dike. The region downstream of the dike is the bay, which forces the system. The spatially integrated numerical model is based on the equations derived from the complete equations of motion by Harris and Bodine (1977). Extensions of the model, to account for the presence of sluice gates and the presence and operation of tidal gates, are provided. The presentation of the basic model follows that given by Seelig et al (1977).

Assumptions made in the process of model derivation were:

- Sea level is a specified function of time.

- The bay water level remains horizontal. This means that the bay water level rises and falls at the same rate throughout the entire bay at each point in time. This occurs when the length of the long wave (tidal wave) forcing the system is much longer in the bay than the longest axis of the bay.

- The bay is connected to the sea by one or more inlets.

- At least one inlet must continuously connect the bay to the sea. Some areas of inlets may go dry during the water level cycle, and one or more inlets may go dry as long as one inlet contains water.

- Bay water surface area is a function of bay water level (or a function of time).

- Inlet cross-sectional area is a function of local depth (or a function of time).

- The local, water level slope in the inlet is assumed to be linearly related to the local friction loss along the inlet, between the sea and bay levels.

- There is a water level drop along the inlet that is proportional to the un-recovered velocity head lost through turbulent eddy diffusion in the bay (flood flow) or sea (ebb flow).

- Storage of water in the inlet is negligible. This means that the flow into the inlet is equal to the flow exiting the inlet at any time. In addition, the volume of water stored in the inlet between high and low water should be small compared to the tidal prism. This is generally the case if the surface area of the bay is much larger than the surface area of the inlet.

- Wind stress on the inlet and bay surfaces is negligible. This means that

the model is most useful for cases when the wind is light, has a short duration, or has a short fetch over the bay.

- Water has constant properties throughout the inlet and bay. No attempt has been made to model saltwater intrusion or other density gradient effects.

- Radiation stress (the interaction with wind waves) is neglected.

- Coriolis effects are neglected.

The derivation of the model begins with the one-dimensional equation of motion as derived by Harris and Bodine (1977),

$$\frac{\partial \bar{u}}{\partial t} + \frac{1}{2}\frac{\partial}{\partial x}\bar{u}^2 + g\frac{\partial h}{\partial x} + \frac{1}{A_c}\int_{y1}^{y2}(\tau_{zx})_z\,dy = R \qquad (1)$$

where

$\bar{u}$ = cross-sectional mean water velocity in the inlet (positive on flood flow)

t = time

x = distance along the main axis of the inlet

y = cross stream distance, from one side of the inlet, y1, to the other, y2.

h = water level above some datum

g = acceleration due to gravity

A_c = inlet cross-sectional flow area at x

$(\tau_{zx})_z$ = component of the stress tensor at the bottom of the inlet in the direction of the main axis of the inlet

R = remainder terms, which are neglected in this model (R=0). This means that the water level is taken as constant at each inlet cross section. See Harris and Bodine (1977) for a discussion of these neglected terms.

The first term on the left hand side of Equation 1 is the temporal acceleration, the second term is the convective or advective acceleration, the third term is the slope of the water surface along the inlet, and the fourth term is the bottom stress.

To obtain a simplified equation, the expressions in Equation 1 are integrated over the length of the inlet between the sea and the bay, where x_s and x_b are the respective limits,

$$\int_{x_s}^{x_b} \frac{\partial \bar{u}}{\partial t} dx + \int_{x_s}^{x_b} \frac{1}{2} \frac{\partial \bar{u}^2}{\partial x} dx + \int_{x_s}^{x_b} g \frac{\partial h}{\partial x} dx$$

$$+ \int_{x_s}^{x_b} \frac{1}{A_c} \int_{y_1}^{y_2} (\tau_{zx})_z \, dy dx = 0 . \qquad (2)$$

Carrying out selected integrations and rearranging, Equation 2 becomes,

$$\frac{\partial}{\partial t} \int_{x_s}^{x_b} \bar{u} dx + \frac{1}{2} \left[(\bar{u}_b)^2 - (\bar{u}_s)^2 \right]$$

$$+ g \left[h_b - h_s \right] + \int_{x_s}^{x_b} \frac{1}{A_c} \int_{y_1}^{y_2} (\tau_{zx})_z \, dy dx = 0 . \qquad (3)$$

In Equation 3, terms involving $\partial x_b/\partial t$ and $\partial x_s/\partial t$ have been set to zero since x_b and x_s are assumed to be independent of time.

From continuity the cross-section mean inlet water velocity is equal to the inlet discharge, Q, divided by the inlet cross-sectional area, A_c,

$$\bar{u} = Q / A_c \qquad (4)$$

Substituting Equation 4 and using the product rule for integration, the first term on the left of Equation 3 can be integrated to yield,

$$\int_{x_s}^{x_b} \frac{\partial \left(\frac{Q}{A_c} \right)}{\partial t} dx = \frac{\partial Q}{\partial t} \int_{x_s}^{x_b} \frac{dx}{A_c} + Q \frac{\partial}{\partial t} \left(\int_{x_s}^{x_b} \frac{dx}{A_c} \right), \qquad (5)$$

where the second part of the equation,

$$\frac{\partial}{\partial t}\left(\int_{x_s}^{x_b}\frac{dx}{A_c}\right),$$

is taken as zero because channel storage terms are neglected.

After substitution of Equation 4, the second and third terms on the left hand side of Equation 3 are,

$$\frac{1}{2}\left(\frac{1}{A_b^2}-\frac{1}{A_s^2}\right)Q^2+g(h_b-h_s) \qquad (6)$$

where A_b and A_s are the cross-sectional areas of the inlet at the bay and sea ends of the inlet, and h_b and h_s are the water levels in the bay and sea referenced to a common datum. The convective acceleration, the left term of Equation 6, may also be expressed in terms of empirical loss coefficients.

The bottom stress is evaluated by using Manning's equation,

$$(\tau_{zx})_z=\frac{gn^2}{kD^{1/3}}|u|\,u \qquad (7)$$

where u is the water velocity in the inlet, D is the water depth at that point, and k is a conversion factor to adapt Manning's equation to the system of units used. The value of k is [1.0 meter (3.2808 feet) per second cubed] $^{2/3}$. The absolute value function of u accounts for the alternating direction of bottom stress with flood and ebb tide. The bottom stress is approximated by determining the water velocity, u, at a number of grid points throughout the inlet.

The value of u is obtained from a plan view flow net system of channels and cross sections which are representative of flow throughout the tidal cycle. The main axis of each channel is drawn approximately parallel to the direction of flow and the cross sections are drawn approximately perpendicular to the flow. The subscript, i, then denotes the cross-section number and the subscript, j, indicates the channel number. Section i=1 is the seaward cross section and section i=IS is the inlet cross section at the entrance to the bay. Channel j=1 and channel j=IC are the two channels adjacent to land. A typical cell, denoted as cell (i,j), consists of that part of channel j situated between cross-sections i and i+1. The water velocity in cell (i,j), u_{ij}, is assumed to be at the centroid of cell (i,j) and to act parallel to the axis of channel j.

A weighting function, W_{ij}, is then used to determine what fraction of the total inlet flow, Q, passes through a grid cell (i,j) at an instant in time.

$$Q_{ij} = W_{ij} Q \tag{8}$$

where Q_{ij} is the discharge in cell (i,j). Various weighting functions are discussed later in this section.

The mean water velocity in cell (i,j), u_{ij}, is taken equal to the discharge in the cell divided by the mean cross-sectional area of the cell perpendicular to the flow, A_{ij} ; i.e.,

$$u_{ij} = W_{ij}\, Q / A_{ij}. \tag{9}$$

Substituting Equations 7 and 9 into the fourth term of Equation 3 and integrating over x and y give the total bottom friction, F,

$$F = \sum_{i=1}^{IS-1} \frac{1}{\sum_{j=1}^{IC} (A_{ij})} \sum_{j=1}^{IC} \frac{g (n_{ij})^2 \left| W_{ij} Q \right| W_{ij} Q\, B_{ij}\, L_{ij}}{k (D_{ij})^{1/3}\, A_{ij}^{\,2}} \tag{10}$$

where n_{ij} is the Manning's coefficient of friction for each grid cell, D_{ij} is the mean instantaneous water depth in a cell, and B_{ij} and L_{ij} are the mean cell width and length, respectively. All of the cell parameters are taken to apply to the centroid of the cell.

Let I_g be a geometry integral defined for convenience as,

$$I_g = \frac{1}{\int_{x_s}^{x_b} \frac{dx}{A_c}} = \frac{1}{\sum_{i=1}^{IS-1} \left(\frac{\sum_{j=1}^{IC} L_{ij} / IC}{\sum_{j=1}^{IC} A_{ij}} \right)} \tag{11}$$

which has units of length.

Substituting Equations 5, 6, and 10 into Equation 3, multiplying by I_g, and setting dQ/dt equal to the other terms gives,

$$\frac{dQ}{dt} = \frac{-I_g}{2} \left(\frac{1}{A_b^{\,2}} - \frac{1}{A_s^{\,2}} \right) Q^2 - g\, I_g\, (h_b - h_s) - I_g F \tag{12}$$

where F is defined by Equation 10.

If M inlets connect the bay to the sea, there will be one equation (Equation 12) for each inlet. Let Q_m be the discharge of the m th inlet, then the total discharge for all inlets, Q_T, is the sum of inlet discharges,

$$Q_T = \sum_{m=1}^{M} Q_m \,. \tag{13}$$

The rate of change of water level in the bay, dh_b/dt, is related to inlet discharge, Q_T, plus discharge into the bay from other sources, Q_{inflow}, by the continuity equation,

$$\frac{dh_b}{dt} = \frac{Q_T}{A_{bay}} + \frac{Q_{inflow}}{A_{bay}} \tag{14}$$

where A_{bay} is the instantaneous surface area of the bay.

There are several methods available for solving the simultaneous differential equations (Eq. 12 for M inlets, and Eq. 14 for a total of M+1 equations). The method selected for this model is a fourth-order Runge-Kutta-Gill technique. Advantages of this method are that it is self-starting, extremely stable, may use a longtime step, has wide application, and converges quickly. The main disadvantage of this technique is that it may cost approximately twice as much as other methods because of the technique that the Runge-Kutta-Gill method uses to calculate each time step, to check error bounds, and to establish the next time step.

The weighting function, W_{ij} (the fraction of the total flow that passes through a grid cell at a time step), provides a systematic method of distributing flow throughout an inlet for use in evaluating the bottom stress. There are three weighting functions that can be used.

First, a weighting function to distribute flow between channels at each cross section so that total friction in the section is minimized. This function may allow some water to move perpendicular to the main axis of the flow net at each cross section, but the flow should be small for a well-drawn net.

Second, a weighting function is developed by assuming that all flow is parallel to the streamlines of the flow net and distributes the discharge in each channel of the inlet to minimize overall friction. This method is consistent with the equations of motion used in the model derivation and assumes that the grid system permits an accurate representation of the inlet streamline patterns.

In practice both of the minimum friction weighting functions produce similar results for many inlets. Comparisons with prototype measurements show that either minimum friction weighting function adequately predicts the flow distribution across inlet cross sections tested.

Jet formation in flow exiting the inlet throat, not accounted for in these weighting functions, may also cause differences between observed and predicted flow patterns. However, an empirical coefficient may be used to account for these losses.

The third weighting function is the same as that used in lumped parameter models. It assumes that discharge is the same in all grid cells throughout the inlet at any instant in time. This means that the flow in each grid (channel) is equal to the total flow for the inlet divided by the number of channels, IC.

In the above model bottom frictional losses are parameterized in terms of the Manning coefficient. For dike systems, with a sluice gate, additional losses due to the flow around the gate must be included in the model. The gate introduces a constriction such that, (when the gate is totally immersed), the water height at the gate, on the riverside, is lower than the height at the end of the channel. Figure 2 provides a definition of geometric parameters that are needed to understand the presentation of the formulation of the loss term given below.

The bottom of the culvert is at a height h_{g0} from mean sea level (NGVD) . The water levels in the harbor (ocean side) and in the river are given by y_h and y_r, , respectively. Both elevations are referenced to mean water level. The gate opening is given by g_0. The depth, d, is defined as the depth of water on the ocean side of the gate. The depth, d_c, is the average depth of water in the channel, on the river side of the gate. The gate elevation, referenced to the mean water level, is y_g and the water level in the channel on the river side of the gate, also referenced to the mean water level, is given by y_{hs}.

The fluid velocity is given by U, with the subscripts h, g, and r referring, respectively to the harbor side of the gate, under the gate, and the river side of the dike.

The head loss can be estimated from Bernoulli's equation in terms of the differences of velocities on both sides of the gate. In addition Belanger's formula (Lejeune, 1982), relates the loss to the fluid velocities upstream of the dike and under the gate.

Bernoulli's equation, between A to C, is expressed as:

$$y_h + U_h^2 / 2g = y_r + U_r^2 / 2g + \Delta h \qquad (15)$$

with Δh representing the head loss term. Belanger's formula states that:

$$\Delta h = (U_g - U_r)^2 / 2g . \qquad (16)$$

Combining Belanger's formula with Bernoulli 's equation, as well as the continuity equation,

$$Q = s_g U_g = s_r U_r, \qquad (17)$$

(where s_g and s_r indicates cross-sectional areas, under the gate and in the channel, respectively) reduces the head loss to a function of the cross sectional areas in the channel and of the square of the discharge Q.

In case of a gate totally immersed (on both sides), we find

$$\Delta h = (\alpha_1 / 2g)\ Q^2 / s_g^2 \qquad (18)$$

and

$$y_h - y_r = (\alpha / 2g)\ Q^2 / s_g^2 \qquad (19)$$

where α_1 and α are function of the cross sectional areas, under the gate, and at the end of the channel, given by,

$$\alpha = (1 - 2 (s_g / s_r) (1-(s_g/s_r))) \quad ; \quad \alpha_1 = (1 - s_g / s_r)^2 \qquad (20)$$

According to the relative position of the gate to the water levels in the harbor and in the river(gate submerged or partially emerged) this general formula can be slightly modified. Only in the case of the gate being totally immersed is the head loss calculated as above. The hypothetical alternative situations are summarized below.

- When the gate is partially submerged on river side, when the water level on the river side is between the bottom and the top of the gate opening and when the level on the harbor side is still above the top of the gate opening, the equations above have to be modified in order to take into account the free surface occurring under the gate. In this case the inflow is calculated as the sum of two superimposed flow, one at the bottom of the channel not affected by the free surface,Q_1, and another at the top having the free surface,Q_2. The resulting inflow, Q_0, is expressed by the following formula (Lejeune, 1982):

$$Q_0 = \mu\, w\, [\, (y_r - y_{g0}) \sqrt{[2g\, (y_h - y_r)]} + (y_g - y_r) \sqrt{[2g\, (y_h - 1/2(y_r + y_g)]]}. \qquad (21)$$

where w is the channel width and μ an empirical coefficient of contraction (0.7).
In such a situation, the water velocity is usually very large under the gate, and much lower in the ocean and in the channel. In some cases, a hydraulic jump may even form downstream of the gate (this was observed during the field experiments). Hence, following Belanger's equation and assuming $U_g >> U_r$ (or U_h), the head loss under the gate is given by the total kinetic energy of the flow corresponding to Q_0,

$$\Delta h = Q_0 / (s_g^2\ 2g) \qquad (22)$$

- When the gate is now partially submerged on the harbor side, which means that the river level is above the top of the gate opening and the level in the harbor is under the gate opening, the same equations as above are applied but with a change of sign.

- Finally, when the gate is totally emerged, there is not any head loss due to the gate.

- The tide gates do not introduce any particular constraint in the flow except that there is no inflow at all at flood tide, when the level in the harbor is above the level in the river. The flow is assumed to be re-established normally at ebb tide when the level in the river is higher than the level in the harbor.

Salinity intrusion model

A review of the data on the Herring River system shows that there is progressive increase in salinity from very low levels in the upper reaches of the river at High Toss Road to higher values typical of Wellfleet Harbor at the dike. The data show that the system is characterized by large tidal flow rates at the dike (peak values of 6 to 10 m^3/sec) with small, net seaward flux of freshwater (0.1 to 0.3 m^3/sec). The water depths in the river are typically quite limited (0.5 to 1.5 m) and the system appears, from both prior and present measurements, to be well mixed or at most weakly stratified for the majority of the tidal cycle.

A review of the data and prior work by Garvine (Roman, 1987) suggest that the salt is transported upstream (up river) by tidal diffusion and down stream by net freshwater advection. Within this steady state framework the semi-diurnal tides advect the salinity field upstream on the flood tide and down stream on the ebb, without a basic change in the longitudinal salinity profile. This basic pattern has been confirmed by the intensive tidal cycle surveys performed during this study and presented in Section 4.

The goal of the present model is to allow prediction of the change in salt penetration into the river and the change in flushing time of the system caused by alterations in the configuration of the culvert system located at the dike. Attention is restricted to the steady state distribution of salt in the river.

Given this background a simple, one dimensional salt balance model is employed. The model balances advection of salt seaward by net freshwater flow with landward transport by tidal diffusion (Officer, 1976). The salt conservation equation can be expressed as,

$$\frac{d}{dx}(AuS) = \frac{d}{dx}(KA\frac{dS}{dx}) \qquad (23)$$

where S(x), A(x), and U(x) are the tidal mean, cross sectional averaged salinity, cross sectional area, and net velocity as a function of upstream distance (x) measured from the dike. K is the longitudinal eddy diffusivity or dispersion coefficient that parameterizes the tidal diffusive flux of salt.

Assuming that the net flux of water is seaward and constant and integrating Equation 23 over x gives,

$$\frac{dS}{dx} = -\frac{Q_f S}{KA} \tag{24}$$

where Q_f is the freshwater flow rate. If Q_f, K, and A are assumed constant then this equation can be integrated directly to show that the salinity decreases exponentially with distance upstream from a value of S(0) at the mouth. The coefficient of the exponent is given by Q_f/KA. Increases in Q_f or decreases in the product of K and A result in increases in salt intrusion distance.

For the present application the cross sectional area is a strong function of both the distance upstream (Figure 5a) and the tidal mean water level. Because of this dependence it is impossible to analytically integrate Equation 24. The equation can however be integrated numerically.

Given this constraint bathymetric and topographic data on the Herring River system(Section 3) were curve fit using a multi-component regression equation to determine A(x) as a function of the tidal mean water level. The value of K is typically determined by selecting a value that minimizes the rms error between observations and model predictions for the salinity field for a known freshwater flow rate and tidal mean water level.

Given a value for Q_f and the A(x) Equation 24 can be integrated to determine S(x). S(x) can then be integrated over the length of the river to determine the tidal mean volume of freshwater, V_f, in the estuary as follows,

$$V_f = \int_0^{x_L} \{1 - \frac{S(x)}{S(0)}\} A(x) dx \tag{25}$$

where x_L is the upstream limit of salinity penetration.

The flushing time of the system can then be defined as,

$$t_f = \frac{V_f}{Q_f} \tag{26}$$

Results of the simulation are typically reported in terms of a measure of the salt penetration distance and the flushing time. One commonly used metric for salt penetration is the distance for the salinity to achieve 10% of its value at the river mouth.

3. Data collection programs in support of model application

The data collection program was divided into separate activities and included collecting data on the topography of the river, time series data on the sea surface elevation, temperature, and salinity at one station in the Herring River and one seaward of the dike, two intensive tidal cycle surveys of the system during the summer and fall of 2000 and a surficial sediment sampling program to characterize the sediment grain size distributions in the river and adjacent bay area. Each program is defined in detail below.

Time series data collection

Time series data for surface elevation, water temperature, salinity, and dissolved oxygen were collected using two YSI/Endeco 6000 water quality, sensing systems. One system was installed seawater of the dike to collect data representative of conditions in the ocean and the second about mid-way between the dike and High Toss Road on the main stem of the Herring River to collect data to characterize the river. Figure 1 shows the location of both instruments (water level stations). The seaward instrument was mounted inside a stilling basin driven into the seabed to provide secure anchoring for the instrument, to minimize observation of the instrument by local water users, and to prevent vandalism or theft. The instrument in Herring River was deployed on a mounting bracket secured to the sea-bed in the central channel of the river. Water depths were very shallow for both instruments during low tide, particularly spring lows. Data were recorded and stored in memory every 15 minutes over the typical 30 day deployment periods. In practice, for each deployment cycle, the instruments were retrieved, data downloaded and the instrument redeployed within the next day or two. The data sets therefore have a characteristic one to two day gap during consecutive deployments. The instruments were initially deployed in May 2000 and removed in November 2000. The location sensing systems of the instrument were established, relative to a National Geodetic Vertical Datum (NGVD) reference, by NPS using standard surveying techniques. NPS personnel subsequently corrected surface elevation records to an NGVD reference.

Overview of the Intensive Tidal Cycle Experiments for the Herring River System

The overall goal of the two intensive tidal cycle experiments, performed on July 25, 2000 and September 27, 2000, was to collect data to characterize the currents/flows, sea surface elevations, salinity, and temperature field in the Herring River system and adjacent Wellfleet Harbor over a lunar, semi-diurnal (M_2) tidal cycle (period-12.42 hrs). Given the narrow width of the system and the stratification that might be induced by the mixing of fresh and salt water the focus was on characterizing these fields along the central axis of the river and with depth. The data will be used to provide insight into the flow and salt transport dynamics and to calibrate and validate the hydrodynamic and salinity models of the system described earlier in the report.

A brief summary of the experimental protocol is given below. The protocol was the same for both surveys, except as noted. The presentation is divided by type or location of the measurement.

Dike Flux Measurements

There are three box culverts located under the causeway that forms a dike at the entrance to the Herring River. Figure 3 shows photographs of the dike on the landward and seaward sides. The culverts are clearly noted in the landward side (Figure3a) photograph. The eastern culvert (left side of photograph) has a sluice gate, while the center and western culverts have flapper tidal gates. The sluice and tidal gates are mounted on the seaward side of the dike. The vertical position of the sluice gate can be adjusted by a hand operated, coarse threaded screw drive (Figure 3b). According to earlier work by Roman (1987) the widths of the culverts are 1.83 m (eastern side, with sluice gate), 2.19 m (center, with tidal gate), and 2.1 m (western side, with tidal gate). All culverts have a height from floor to ceiling of 1.75 m and a length of 20.4 m. The top surface of the floor of the culverts were estimated to be 0.53 m above mean low water (MLW). These basic measurements were confirmed during the intensive tidal cycle survey. Data from the present study further shows that the mean sea level (MSL) water depth in the culverts is 0.84 m.

A single axis, electromagnetic current meter (Marsh McBirney) was deployed during the intensive tidal cycle survey, through the grating in the apron on the landward side of the dike, in the eastern culvert (with sluice gate). A steel mounting bracket, held to the concrete apron by a come-along, with an adjustable vertical rod (1.9 cm diameter, stainless steel) on which the current meter was mounted (Figure 4), was used to hold the current meter. Currents were then measured at mid-depth in the center of the culvert. The vertical structure of the currents at this location was measured at 0.25 m increments by adjusting the vertical position of the rod. Currents at other lateral positions (0.5 m increments) and vertical (0.25 m increments) locations were made using the same type of meter mounted on a moveable rod. This rod was located and held by hand during the survey. Based on the results of the first survey, which showed a well-developed turbulent flow field, the bracket mounted meter was positioned at mid-depth, in the center of the culvert during the second deployment. The vertical location of the meter was continuously adjusted to mid-depth throughout the tidal cycle. No measurements of the lateral and vertical structure were otherwise made during the second survey. The data were recorded by hand at 30 minute intervals throughout the tidal cycle (12.5 hours).

In addition a second single axis Marsh McBirney electromagnetic current meter was employed to make measurements at mid-depth in the center of each of the two culverts with tidal gates (center and west). The current meter was mounted on a stainless steel rod, which was hand held in the center of the channel. Measurements were again made at 15 minutes intervals over the tidal cycle.

Measurements of the water level (referenced to NGVD) were made on the eastern side of the culvert with the sluice gate (Figure 14b). Measurements were made at 15 minute intervals throughout the tidal cycle. The depth from NGVD to the top surface was measured at 0.84 m. With data from the current measurements noted above and the depth of water in the culvert, estimates can be made of the volumetric flow through the culvert.

During the experiment flows on the flood tide were almost exclusively through the sluice gate. A small flow was observed to enter via the center and western tidal gates during flood tide due to leakage caused by a missing gate hinge pin and a broken hinge. Flows during the ebb were approximately equal through all three culverts.

High Toss Road Flux Measurements

The goal of this portion of the experiment was to measure the flux of water over the tidal cycle through the 1.5 m diameter culvert on the main stem of the Herring River at High Toss Road (Figure 1). Measurements were made of the culvert flow cross sectional area versus time. This was done by measuring the water depth using an aluminum measuring rod, located at the center of the culvert. Measurements of the current speed were made using a hand held Swoffer propeller current meter located at two thirds of the water depth. The current meter was swivel mounted on a line with a lead counter-weight. This assured that the meter was correctly located vertically and that the meter axis could automatically orient to the direction of the flow. The direction of the flow (flood (landward) or ebb (seaward)) was made by visually noting the orientation of the tail fin of the current meter. Measurements of current speed and direction were made at 15 minute intervals and recorded by hand over one tidal cycle.

Vertical section hydrographic measurements

Measurements were made, from canoes, to characterize the vertical structure of the salinity and temperature (density) fields at the 12 hydrographic stations noted in Figure 1. There were two stations located seaward of the dike (prefix OS) and ten landward (prefix S). The stations landward of the dike were in similar locations to those given in Roman (1987). The stations were located along the central axis of the river channel and about evenly spaced between the dike and High Toss Road. Measurements were made using YSI/Endeco, HydroProducts, and Beckman systems. Calibrations of the instruments were verified prior to the field program. At each station the water depth was measured first followed by salinity and temperature measurements at 0.5 m intervals from the surface to the bottom. The water depths varied considerably, from measurement to measurement, due to small changes in horizontal location and the substantial variability in river bottom topography. If the local water depths were less than the 1 m hydrographic measurements were made at the surface (10 cm below the surface) and the bottom (10 cm above the bottom). For depths less than 0.5 m only mid-water depth measurements were made. Water depths were characteristically very shallow near low tide and access to sampling locations was often difficult, even by canoe. The time of each measurement was recorded. Measurements were made in a round robin fashion, starting at one end of the station line, proceeding to the next and subsequent stations, and then returning to the starting point. Two canoes, with separate crews (two individuals) were used to sample Herring River Stations S1- 4, and S5 -10, respectively (Figure 1). A separate crew, using two canoes, sampled the stations seaward of the dike (OS 1 and 2). This three-crew system was used to ensure that samples at all stations would be synoptic within about 30 to 40 minutes. Given transit times sampling at each station was performed at approximately hourly intervals.

Freshwater flow measurements

The goal of this part of the experiment was to gather data to make a first order estimate of the freshwater input to Herring River (seaward of High Toss Road) for the time of intensive tidal cycle survey.

Freshwater input into Herring River is known to be quite low (less than 0.3 m^3/sec) and generally comes from ground water discharge and to a more limited extent runoff, via a series of small streams and creeks from the watershed. In prior work Roman (1987) monitored the flows for the lower reach of Herring River at a culvert above High Toss Road (Culvert #1, see Roman, 1987), a culvert on Bound Brook, and Pole Dike Creek (at the intersection with Rte 6)(Figure 1). He used the summation of these flows to represent the total freshwater input into the lower reaches of the river. Even though Bound Brook enters the river upstream of Culvert #1 he selected it as a surrogate for Duck Harbor Creek, which enters the river south of Culvert # 1, for which no data were collected. An analysis of Roman's observations shows that Bound Brook contributes less than 10 % of the total freshwater input. Freshwater flows were therefore measured at Culvert #1 and on Pole Creek at the intersection with Rte 6. The summation of the flows from these two sources can be used to approximate the total input of freshwater. In the absence of significant rainfall the flows through both culverts were observed not to vary substantially over the days prior to and during the experiment. Measurements of these flows were therefore made on the day prior to each intensive tidal cycle survey.

Water depths in each culvert were measured at the culvert centerline using an aluminum measuring rod, with a foot pad. Current speeds were measured at 2/3 rd of the water depth using a Swoffer propeller current meter, swivel mounted on a counter weighted line. Current directions were determined based on the orientation of the current meters. The instrument was deployed for five minutes at each sight and showed little variation in flow speed and direction.

Sediment sampling

Surficial sediment samples were diver collected on July 26, 2000 to characterize the composition and grain size distribution up and downstream of the dike. The sampling locations are shown in Figure 1. The sample locations in the Herring River are located at the same sites as the hydrographic survey stations. For the lower portion of the Herring River the sites are located to sample geomorphic features of particular interest (i.e. flood and ebb tide deltas). All samples were stored in plastic sample tubes and brought to the University of Rhode Island, Geosciences Department for analysis. Sediment size distributions were determined for all samples and are included in Appendix C.

Topographic data

Based on earlier modeling work by Garvine (Roman, 1987) it was clear that the data available during his study were inadequate to accurately characterize the detailed topography of the 600 hectare flood plain of the Herring River. These data are critical to predicting the flooding and

drying of the flood plain for various restoration options. Additional topographic data for the system was collected by NPS personnel (J. Portnoy and M. Adams) in 1999 using a Trimble 4700-4800 total station, integrated real time, kinematic system. The data included eight transects across the flood plain of the Herring River and measurements at sites along the main axis of the river channel. NPS personnel converted these data to National Geodetic Vertical Datum (NGVD) reference and provided it to us in the form of *Excel* spreadsheets. They also provided US Geological Survey (USGS) topographic data for the 0, 3, and 6 meter contour lines, again in *Excel* form. SURFER and various kriging algorithms were then employed to develop a two dimensional, gridded topographic map of the area. Maps were produced on grids of 10, 15, 25, and 50 m resolution for the study area. Given the quality of the input data, a grid size of 15 m was deemed appropriate for the current application.

A review of the base map from the merged USGS and NPS transect data, after kriging by SURFER, showed that there was substantial uncertainty in the topography in the region very near and slightly above (0 to 1 m) NGVD. The topography in this region, as approximated by SURFER interpolation, was quite variable and at odds with the gently sloping flood plain observed in the field. NPS personnel fine tuned the Herring River elevation data by adding channels and ditches and interpolated elevation values based on their field survey data. They generated 0.1 meter contours from the field data and then modified them to reflect channel locations.

They also added some average flood plain values for areas where no field data were available. The altered, merged data set represents the bathymetry and topography based on best currently available data and the NPS personnel's intimate knowledge of the area. Figure 5a shows the final contour map of the bathymetry of the Herring River system. Figure 5b shows the combined topographic and bathymetric data in the form of a three dimensional perspective view.

4. Analysis of data from collection programs

This section presents an analysis of the data collected during the field programs noted in Section 2. To facilitate the presentation each major analysis effort is presented in a separate section. The complete data sets are given in Appendices A and B.

Topography and bathymetry

The best available representation of the topography and bathymetry of the Herring River system is shown by the SURFER generated contour map in Figure 5a. The data set shows that the Herring River system is characterized by a shallow depth river channel running through its central axes with a broad, flat flood plain.

The bathymetric and topographic data given in Figure 5 for the area between the dike and High Toss Road was used to generate a basin surface area versus elevation curve (Figure 6a and b). These curves were prepared since they are required as input to the hydrodynamic model described in Section 2. The curves are also very useful for understanding the storage capacity of the river as a function of water level.

Figure 6a shows that the surface area increases approximately linearly with elevation, but with two distinct regions. The slope of the curve is much lower for elevations above NGVD than for those below. This reflects the broad flood plain above NGVD and the more channelized bathymetry below this level. For comparison Garvine's (Roman, 1987) approximation of this curve is also shown. The curves are broadly comparable. Both show that the water storage capacity of the river increases with an increase in water elevation and does so substantially for water levels above NGVD. The present analysis however results in a much larger surface area for a given elevation in the elevation range from NGVD to 0.7 m than Garvine's, but a smaller area for elevations above 0.7 m.

One restoration option, under active consideration, would place a dike across the opening to Mill Creek in the lower Herring River to prevent flooding of the adjacent golf course and remove or place additional openings in High Toss Road to allow tidal waters to more readily penetrate the portion of Herring River north of the road. In anticipation of addressing this case Figure 6b shows the surface area versus elevation curve with the area above High Toss Road included and the area of Mill Creek excluded. Portnoy and Adam's and Garvine's curves are repeated from Figure 6a and included on Figure 6b. When the area above High Toss Road is included the amount of water storage capacity above NGVD increases dramatically compared to the case when the area is restricted to that below High Toss Road.

As an independent check of this relationship data from the two intensive tidal cycle surveys can be used to generate a portion of this curve. Using estimates of the flux through the three culverts and the water surface elevation from the time series surface elevation measurement in the middle of the river,the surface area versus elevation curve can be estimated by using water mass conservation. Specifically the amount of water entering/exiting through the dike during a given period of time is stored/removed from Herring River. Using this approach the surface area versus elevations was generated using the data from the two intensive tidal cycle surveys.

The results are shown on Figure 6a. A linear, least squares regression line was determined for each experiment. The figure shows that the data collected during the two intensive tidal cycle surveys give basin area versus elevations relationships that are generally consistent with the Portnoy and Adams topographic map. The R^2 are significant at about 0.6. Representation of the area versus elevation curve, using the tidal survey data, shows a decided hysteresis however. This is a direct result of the lack of balance between the ebb and flood flow volumes over the tidal cycle for the two intensive tidal cycle surveys (See analysis later in this section).

Surface elevation time series

Figure 7a and b show the surface elevation time series data collected at the upstream (a) and downstream (b) stations from May 2000 to November 2000. The data were generally collected on a monthly basis and the instruments removed at the end of the month to down load the data. Longer gaps represent times when the instruments were not deployed or under-going repair. The two records clearly show that the surface elevation time series is dominated by the lunar semi-diurnal tides, with two cycles per day. The neap-spring cycle, with a period of 14.8 days, is evident although not easy to see in the figure given its temporal scale.

The range of tides varies dramatically from a mean of 2.53 m for the downstream station to a mean of 0.56 m for the upstream station. The upstream to downstream tidal range ratio is 4.52 showing that the size of the culverts and the associated hydraulic control structures dramatically reduces the water level range in the river relative to that in the bay. The time of high water in the river is observed to lag that in the bay by 3.2 hours. The low water phase lag however is very small and close to zero. This unexpected result can be explained by a close inspection of one tidal cycle of data; June 25, 2000 for example (Figure 8). One notes that the bay tides are asymmetric with high water showing a characteristic sinusoidal shape while the low water portion of the cycle is abruptly truncated or chopped off. The period of low water extends for several hours until the flood tide results in a very rapid increase in the water level. Because of this characteristic shape the time of low water is almost simultaneous at the upstream and downstream stations. The feature is consistently observed in the bay time series and was previously observed by Garvine (see Roman, 1987) in his experimental program.

The spring tidal range is 132 % downstream and 113 % upstream of the mean range at the corresponding locations. The neap range is 92 % and 95% of the downstream and upstream mean ranges, respectively. The combination of the dike and the shape of the Herring River basin are seen to be very effective in limiting the maximum tidal range upstream of the dike.

Given the dominant tidal nature of the surface elevation record (Figure 7) a tidal harmonic analysis was performed using the principal 13 diurnal, semi-diurnal and associated over tides. To perform the analyses all data were sampled at 15 minute intervals. Data gaps of a few hours or less were filled by linear interpolation. Table 1 shows the resulting amplitudes and phases (based on Greenwich reference) for the thirteen constituents at upstream and downstream (dike) stations.

At the dike station the semi-diurnal components, M_2 (1.218 m), N_2 (0.253 m), and S_2(0.166 m), dominate the tidal signal. M_4 (0.130), the first overtide of the lunar semi-diurnal tide, is the next most important contributor in terms of tidal energy. These are followed by the diurnal components K_1 and O_1, all with magnitudes less than 0.124 m.

At the upstream station the semi-diurnal component, M_2 (0.253 m), clearly dominates the signal. N_2 and L_2 are the next most important contributors. M_4 is quite small (0.006 m) as are the K_1 and O_1 diurnal component at about 0.025 m. This analysis shows that the tides at both stations are mixed but primarily semi-diurnal, with the lunar semi-diurnal component dominant.

Based on the M_2 tidal component the dike is responsible for a factor of 4.8 reduction in the tidal range. This is in reasonable agreement with a value of 4.52 based on a statistical analysis of the data, described earlier.

A study of the phase differences shows that there is a consistent phase lag between the downstream and upstream stations. For the dominant M_2 component the upstream station lags that at the downstream site by about 67 degrees or 2.3 hours. This compares to a high tide phase lag of 3.2 hours and a low tide phase lag of 0.0 hour based on a statistical analysis of the data. The difference between the two can be attributed to the fact that the downstream tidal record has been distorted by local effects. The harmonic analysis is unable to provide a good approximation of the surface elevation record for this case since the local distortions can not be represented by a harmonic series.

Using the amplitudes and phases above a time series was generated for the upstream and downstream stations. These synthesized records were compared to the original record. This analysis shows that the synthesized surface elevation record is able to reproduce the upstream time series with an rms error of 9.6 cm and the downstream series with an rms error of 26.7 cm. The significant size of the downstream rms error is due to the inability of the harmonic re-composition to reproduce local effects (truncated low tide) observed in the record, as noted above (Figure 7 and 8).

Intensive tidal cycle survey of flux through the dike

In this section the surface elevation response and flux through the culverts, in response to bay tidal forcing, are characterized based on intensive tidal cycle surveys.

Figure 8 shows the surface elevation time series for the day on the July 25, 2000 experiment for stations up and downstream of the dike. These data are extracted from the time series surface elevation data sets described above. The data show a reduction in the tidal range from 2.5 m in the bay to 0.5 m in the river, a high tide phase lag of about 3 hours, and a low tide lag of 0.5 hours. The tides for this period are typical of the mean for the area. The observed reduction in tidal range is consistent with the analysis of the time series data presented above.

The fluxes through each of the culverts were calculated by multiplying the mean current speed in each culvert by the local water depth from the bottom of the culvert to the free surface and by the culvert width. For the eastern culvert the velocities measured vertically and horizontally across the section were averaged to estimate the mean velocity. The velocity measured at 2/3 ^{rds} depth, mid-span were used for the center and western culverts. The flux was calculated every 15 minutes throughout the experiment. Figure 9 shows a plot of the flux versus time for each of three culverts. G1 with sluice gate, east side, G2- tidal gate, center, G3- tidal gate, west side. The prefix "O" indicates observed. At the beginning of the experiment peak flood is observed to have a flux of 6 m^3/sec through the sluice gate. There is no substantial flow through either of the other two gates (G2 and G3). The flood flow rate decreases until about 9:30 when slack water occurs. With water levels decreasing (Figure 8) below mean sea level (MSL), flows are ebbing from the river, approximately uniformly through all three culverts. Peak ebb flows of 4 to 5 m^3/sec are observed at about 11:00 to 11:30. Flows continue to ebb until 15:00 but at ever decreasing rates. The ebb portion of the cycle is characterized by a sharp increase in ebb flow for the first 1.5 hours of the ebb and then a long (10:30 to 15:00, 4.5 hour) period with the ebb growing progressively weaker. This flow signature is directly attributable to the asymmetry in the sea surface elevation (low tide), as shown in Figure 8. With rising tides, flood flows are observed in the culvert with the sluice gate (G1) and increase with time until they reach a peak of 6.5 m^3/sec by 18:00. The tidal gates prevent any significant flows in G2 and G3 during the flood portion of the tidal cycle.

Figure 10 shows the observed sea surface elevation record based on measurements made at the dike, at the culvert on High Toss Road, and from the YSI/Endeco sensor located about half way between the dike and High Toss Road. The data show that, within the margin of uncertainty in the measurements, the sea surface elevations are in phase and the amplitudes the same at all stations. This analysis shows that Herring River responds as a simple water storage container and operates in a pumping mode in response to tidal forcing.

The analysis of the second experiment, September 27, 2000 followed the same protocol as for the first. The results are shown in terms of the up and downstream sea surface elevations (Figure 11), flows through each of the three culverts (Figure 12), and sea surface elevation at the dike, mid Herring River, and at High Toss Road, all versus time (Figure 13). These plots are similar to their first experiment counterparts (Figures 8, 9, and 10, respectively). The basic characteristic of the tidal response of the system is very similar, with those observed during the first intensive tidal cycle survey. The most striking difference is that the second experiment occurred during spring tides. The tidal range increased to 3 m and peak flow rates increased to 11 m^3/sec.

Water mass balance

In order to better understand the flow dynamics of the river it is instructive to study the long-term flow balance in the system. Specifically the interest is in determining the net flux of water through the system, caused by the inflow of freshwater via streams and runoff and how that flow compares to the tidal flows generated by tidal forcing at the mouth. To that end the flows through Pole Dike Creek, Bound Brook Island culvert, High Toss Road Culvert, and

through the three culverts at the dike were determined for the two intensive tidal cycle surveys. These are reported in Table 2. Flows in Pole Dike Creek and Brook Island culvert were unidirectional on the day of the measurement and hence the mean value is reported. At the High Toss Road culvert the flows are strongly influenced by the tides in the river. In this case the maximum and mean flows (m^3/sec) are presented for the flood and ebb portion of the tidal cycle and the maximum and mean for the entire cycle are also reported. For the dike, the maximum and mean flows for flood and ebb are presented.

A review of the data for the first experiment shows that the mean flows entering Herring River (south of High Toss Road) are generally quite small at 0.107 m^3/sec, especially in comparison to the magnitudes of the tidal flows at the dike (4- 7 m^3/sec). Similar results are observed during the second experiment. The two experiments show that the flows induced in the river by stream flow and runoff are very small and not important to our understanding of the tidal dynamics of the area.

In performing the experiment it was postulated that summing the flow measurements at Pole Dike Creek and Brook Island culvert would provide a reasonable first order estimate of the mean flow at High Toss Road. This assumption appears warranted based on the first experiment (0.120 m^3/sec vs. 0.107 m^3/sec) but is not reasonable for the second (0.094 m^3/sec vs. 0.239 m^3/sec.). The difference in the second experiment could potentially be attributed to higher ground water inflow to the river between the creeks and the High Toss Road culvert. The source of the difference is however unknown.

Assuming that there is no long term water storage in Herring River the difference in the amount of water that flows through the dike during the flood tide and the amount of water that exits through the dike during ebb must be the net flow through the system. The net flux should be equal to the freshwater input to the river. This calculation was performed for both experiments and showed that there was a 20 % excess in ebb water for the July 25, 2000 experiment and 14 % excess ebb for the September 27, 2000 experiment. The source of this difference is unknown. It was likely due either to a lack of detailed measurements of the current structure in the culverts or an inappropriately chosen location of the local surface elevation measurements. The measurement location was just landward of the culvert mouth and didn't account for draw-down effects in the entry of the culvert mouth during ebb tide. This is clearly demonstrated in Figure 14.

Salinity intrusion

The characteristics of salinity intrusion in the Herring River system can be appreciated through two different approaches. The first looks at the salinity time series at one location (Endeco/YSI water quality sensor) and the second at the movement of salt over selected tidal cycles from the two intensive tidal cycle surveys.

Time series

Figure 15 shows a plot of salinity at the upstream continuous measurement site (Figure 1) collected by the Endeco/YSI water quality sensor for the July 25, 2000 intensive tidal cycle

survey. The salinity is observed to be almost zero during the ebb portion of the tidal cycle. As the tide floods the salinity dramatically increases, as saltier water from downstream is advected upstream past the sensor. The salinity peaks at high slack water and the declines rapidly as the tide ebbs. The peak salinity value varies substantially from one cycle to the next (15 ppt at 9:00 to 20 ppt at 23:00) as a result of differences in the amplitude of tidal forcing. Studying the longer term record (not shown here) the salinity maximums increase and decrease approximately sinusoidally, with a period of about 15 days, and shows substantial diurnal inequalities. The basic salinity pattern can be explained by the tidal advection of the salt field past the observation point. As the salt wedge moves up the river during the flood tide the salinity is observed to increase rapidly, the rate dependent on the longitudinal gradient of the salinity field and the strength of the advective flow field. At high tide the currents are slack and the salinity reaches its peak. As the tide ebbs the salt wedge is transported down stream and the salinity decreases. The process is repeated on the next tidal cycle.

It was not possible to perform this analysis on the data from the bay station since the salinity measurements appear to have been contaminated by the flow of ground water into the stilling basin used to mount the instrument to the sea bed.

Hydrographic sections

Figure 16 shows the observed vertically averaged salinity at each hydrographic station (see Figure 1 for station locations) versus time for the July 25, 2000 experiment. The bay stations are noted with an OS and the river stations with an R. Station R1 is near the dike and R 10 near High Toss Road. It is instructive to study the general salinity pattern in both space and time. At the beginning of the experiment the salinities in the bay and at stations in the lower river (R1 and 2) are at their peak values. The salinities at stations further up river are increasing during this period of time, not reaching their highest values until about 9:30. The peaks at the upstream stations (R3 to R10) correspond to the time of slack before ebb. Salinity begins to decline at all stations after 9:30 and reaches its lowest values at 13:00 for the bay stations and at about 15:00 for the stations in the river. The later time corresponds to slack before flood. The lowest salinity values in the river hence lag those at the bay stations by several hours. For stations R6 through R10 the lowest levels are achieved by 11:00 and remain low throughout the remainder of the experiment. Salinities at stations R4 and all stations seaward increase after 15:00 through the end of the experiment. The final values are similar to those at the start of the experiment.

Viewed in terms of its spatial structure the salinity decreases with distance upstream, at any time, over the tidal cycle. The values at stations R1 and R2 approach those in the bay(OS1 and OS2) at high tide and at stations R6- R10 decrease to almost zero at low tide.

The observed salinity pattern is characteristic of a salt wedge being advected up and down the river in response to the flooding and ebbing tide. The salinity is, to a first order, in phase with the tidal elevations in the river. The phase lag between the peak salinity in the bay and that at the mouth of the river is caused by the phase lag in high tide between the river and the bay stations. Figure 17 shows the vertically averaged high and low tide salinity versus distance

down the river and clearly illustrates this characteristic of the system. The salinity structure is approximately independent of time but is advected up/down stream by the tides.

Figures 18 and 19 show identical plots but for the second experiment (September 27, 2000). The results are qualitatively similar to those shown for the first experiment, with the exception that the time of the experiment, relative to the tidal cycle, is different.

It is noted in both intensive tidal cycle surveys (Figures 16 and 17, survey - July 25, 2000 and Figure 18 and 19, survey - September 27, 2000) that the maximum salinities at the bay stations are lower than those at the most downstream river stations. This observation is contrary to the first order assumption that salinity should increase monotonically with distance down river and into the bay, in the absence of significant freshwater sources. The explanation for the local structure is unknown.

Sediment distribution

The spreadsheets presented in Appendix C provide data on the particle size distributions for each sample collected. To simplify the presentation we will aggregate the material into silt-clay, sand, and gravel size components. For the majority of the stations in Herring River (S1, 4, 6, 8, 9, and 10) (see Figure 1 for station l locations) and those just downstream of the dike (S11 and 12 correspond to OS1 and OS2 on Figure 1.) the bottom sediments are comprised primarily of sand (90 to 99 %) with the remainder being gravel (1 to 10 %). There is very little fine-grained material (silt-clay). For stations S2, 3, 5, and to a more limited extent S7, the bottom sediments are composed primarily of sand (52 to 85 %) with the remainder being silt-clay (48 to 15%). There is essentially no gravel found in these samples. The sites, with the high silt-clay content, are all located along the central channel axis and typically in deeper water, than the sand dominated samples.

A review of this data and the general coastal geomorphology suggests the following conceptual model for sediment transport. Sand, suspended by tidal and storm action downstream of the dike, is transported landward by flood tidal currents. Once the suspended sediments enter the sluice gate equipped box culvert they are rapidly transported by the very strong flood tidal currents through the dike and carried into the lower portion of the Herring River. The flood flow exiting the sluice gate forms a well-defined plume as it enters the much wider, lower reaches of Herring River. As the plume widens the velocity along the plume centerline decreases proportionally. The fine-grained, suspended sediment begins to settle from the water column as the plume velocity and turbulence levels decrease. This sediment transport pattern has resulted in the formation of a large flood tide delta (ramp like in shape, with the lower edge of the ramp located closer to the dike), at the very end of the flood tide plume. The peak elevation of the delta is now populated with marsh grass and is exposed during spring tidal forcing. This deposit is readily seen in the field but barely evident in the topographic and bathymetric maps shown in Figure 5 because of the resolution of the graph. Figure 3c provides a photograph clearly showing the flood tidal plume and the sea grass growing on the upper portion of the flood tide delta.

During the ebb tide the velocities in the vicinity of the flood tide delta are very small (few cm/sec) and hence the sediment deposited there on the flood tide is not normally re-suspended on the ebb. Sediments, that are deposited on the flood tide delta, maybe subject to re-suspension and subsequent transport in Herring River during extreme high tides and storms. The re-suspension and subsequent transport is quite rare (a few times a year) given the isolation of the lower river from the adjacent bay and the limited fetch for generating wind waves in the river. Once mobilized this sediment is likely transported, either as bed load or suspended sediment, upstream along the central axis of the river. This explains the substantial sand concentrations observed in the lower river and the high sand concentrations observed in the upper river.

Deeper areas in the lower river are observed to have a much higher fraction of silt and clay than at other sites in the river. It is probable that this very fine material has its origins in the upper reaches of Herring River. This material is advected seaward during strong freshwater flow events and is deposited in the deeper areas in the lower reaches of the river. Currents in these areas are not strong enough, even during strong tidal forcing or storm events, to re-suspend and move these materials and hence they tend to accumulate.

5. Hydrodynamic and salinity model application and calibration

The inlet basin hydrodynamic model presented in Section 2 was applied to the Herring River study area. This model is appropriate for the present application since all the key assumptions listed in Section 2 are met in the present application.

The basin surface area versus water level, shown in Figure 6, was used to represent the water storage capacity as a function of elevation in Herring River. Three parallel inlets wereused in the model to represent the three box culverts. The physical dimensions of the box culverts, previously noted, were used to describe each. Two of the culverts were specified as being fitted with tidal gates, allowing flow only during ebb tide. The third culvert included a sluice gate, set at 61 cm.

Calibration of the model was performed using the data collected on December 4, 1984 and reported in Roman (1987). During this period the sluice gate was open to 130 cm and the other two culverts were equipped with tidal gates. This period was selected for calibration since it would have the minimum influence of the sluice gate on the model predictions and allow for calibration of bottom frictional losses. Simulations were performed varying the Manning coefficient, n, which parameterizes frictional losses in the culvert (see Equation 7). The results of the simulation are presented in Table 3 in terms of the root mean square (rms) error between model predictions and observations over the tidal cycle, and the maximum and minimum predicted water levels and tidal range in Herring River for various values of the Manning coefficient. The maximum and minimum water levels and tidal range, based on the observations, are also provided for reference. Also provided are the results of Garvine's simulations for the same case. Cases S1 through S6 represent simulations with Manning coefficients increasing from 0.06 to 0.11, in increments of 0.01. The best fit to the data is for an n =0.09 which gives an rms error of 0.07 m. Using this value however slightly under predicts the maximum, minimum, and tidal range in comparison to observations. It is noted that the rms error is relatively insensitive (0.07 to 0.09 m) to variations in n while the maximum, minimum, and range are much more sensitive to its variation.

Finally simulations were performed using different Manning coefficients on flood and ebb tides to determine if model predictions could be improved (Case S0). Based on the observation that the model under predicted the maximum height, over predicted the extent of the minimum tides, and under predicted the tidal range, simulations were performed with larger Manning coefficients on the ebb than on the flood tide. The optimum performance (Case S0) was for n of 0.06 on flood and 0.09 on ebb. For this case the rms error is 0.05 m. The maximum, minimum, and tidal range are in excellent agreement with observations. The choice of differential values of n is partially justified by the observation that there is a significant set down in the water level in the entry region of the culvert on the landward side of the dike during ebb tide but no similar set down on the seaward side of the dike on the flood tide. This indicates that there are additional losses on ebb tide, relative to flood, due to flow entry effects.

The same suite of simulations was performed for the July 25, 2000 experiment. During this period the sluice gate was set at 61 cm and the other two culverts were equipped with tidal gates. These results are also presented in Table 3. Once again the best model performance (rms error – 0.06 m), if one value of n is selected, is for the case $n = 0.09$. Model performance is further improved, particularly for the maximum, minimum, and range predictions, if the two-part formulation described above ($n = 0.06$ on flood and 0.09 on ebb) is used. Similar results are also found when the model is applied to the September 27, 2000 experiment.

To provide additional insight the results of simulations for the July 25, 2001 intensive tidal cycle survey, using the two-part formulation, are shown in Figures 8 and 9. Figure 8 shows the final model predictions for the water level in Herring River. The model does an excellent job in reproducing the observed time series in Herring River. The model correctly predicts the phase lag between the bay and river stations and the substantial reduction in tidal amplitude. For the one day long simulation period the rms error in prediction of the river tidal elevation curve is 0.020 m.

A careful study of the simulations shows that bottom friction losses control the flow through the tidal gates, while those through the sluice gate are dominated by gate losses, rather the bottom friction. Gate losses are approximately seven times larger than bottom friction losses on the flood tide and twice those of bottom friction losses on the ebb tide. The differential behavior between flood and ebb losses is caused by the presence of supercritical flow in the vicinity of the sluice gate on flood tide and its absence on ebb.

Figure 9 shows the model predicted flux through the three box culverts for the July 25, 2000 experiment. Also shown are the observed values measured during the experiment. The model does a very good job of predicting the flood flows through the culvert with the sluice gate, correctly representing the magnitude and phasing over the cycle. The model also correctly represents the basic character of the ebb tide showing about equal flow through all three culverts during ebb, with a rapid increase to peak values early in the ebb cycle followed by a gradual decrease with time throughout the remainder of the ebb cycle. The model, however, under predicts the observed flow strength throughout the ebb. Based on the data analysis presented in Section 4 the observations are shown to over estimate the total volume of the ebb flow by about 14 %. The model in contrast predicts total ebb and flood tidal volumes in exact balance for the same period. Given this situation it is not surprising that the model under predicts the observed ebb tide flow rates.

The simplified salinity model, described in Section 2, was calibrated with the July 25, 2000 data. The A(x) relationship was determined using the SURFER based and merged topographic and bathymetric data sets. The merged data set had a resolution of 15 m. The along stream distance was discretized into 21 increments from the dike to High Toss Road. The mean water level was determined for the river for the experiment period. The bay salinity measurements at station OS 1 and 2 were used to set the salinity value at the dike. The value of the eddy diffusion coefficient was systematically adjusted until the rms error between simulation results and observations was minimized. Figure 20 shows the tidal mean observed and model predicted salinities as a function of distance measured from the dike for various values of the longitudinal dispersion coefficient. For a value of 6 m^2/sec the rms error was 2.5

ppt, for 5 and 4 m^2/sec the value was 1.8 ppt, and for 3 m^2/sec the value was 3.2 ppt. Rms errors were minimum (rms error - 1.6 ppt) for K equal to 4.5 m^2/sec. For the lower values of K the model under predicts the salt penetration while it over predicts the penetration for the highest values. Figure 21 shows the model predicted and observed salinity for the optimum value of K. In the lower reach (0 to 1 km) and the upper reach (1.5 to 2.1 km) of the river the model predicts the salinity quite well. In the mid reach area (1.1 to 1.3 km) the model over predicts the salinity. Given the simplicity of the model agreement between predictions and observations seems quite reasonable.

The salinity model predicts a flushing time and salt penetration distance of 31.3 hours and 1.6 km, respectively. Equivalent observed values are 26 hours and 1.5 km. The agreement is reasonable given the simplicity of the salinity model.

6. Hydrodynamic and salinity model validation

The calibrated model described in Section 5 was next applied to predict the surface elevation and flow rates through the dike for the September 27, 2000 experiment. As for the first experiment the model was forced by the downstream sea surface elevation time series. The sensitivity of model predictions to variations in Manning coefficient for this case are reported in Table 3. Once again predictive performance is optimal for $n = 0.09$ if a single value is selected and $n = 0.06/0.09$ if a two part formulation is used.

Figure 11 shows the driving surface elevation and the model predicted and observed sea surface elevation time series in Herring River. The predictions are once again in very good agreement with the observations, with an rms of 0.03 m.

Model predicted and observed flow rates through the three culverts for this experiment are shown in Figure 12. As in the first experiment the model reproduces the basic character of the flows throughout the cycle, correctly representing the staging of the flows and the approximate asymmetric shapes of the flood and ebb portions of the cycle. In this case the model under estimates the peak values of the observed flood and ebb flows. The observations are known to overestimate the ebb volume by about 20 % for this experiment (see Section 4). The source of the under prediction of the flood tide flows is unknown. This may be due to the procedure used to estimate the observed flows; specifically the water level used in the calculations was measured near the mouth of the culverts (Figure 14 b) and not in the culvert proper. The water level measurement hence didn't represent the fact that the flow becomes supercritical during the peak tidal flows. Supercritical flow occurs when the current speed exceeds the local shallow water wave speed. The water level in the culverts was below that observed at the measuring station in the river during the period of supercritical flows.

A final test of the model simulations was performed for the entire time period, June to October 2000, for which sea surface elevation time series were collected up and downstream of the dike. The results are provided in Table 3. Model predictions were compared to observations and yielded an rms error of 0.08 m (case S0). This uncertainty in model predictions is very reasonable and establishes the model's ability to predict the response of Herring River to tidal forcing.

In performing the simulations above it was observed that the present model predictions, using the optimum Manning coefficient, differed from those provided by Garvine and presented in Roman (1987). Gravine's and the present model differ in three important aspects.

1. The two model's assume a different empirical based expression for the surface area versus elevation curves. Garvine uses a three section, piecewise linear representation based on limited field transect data and available bathymetric and topographic maps (A0). The present analysis has generated a continuous curve based on a careful analysis of recent GPS transect data plus updated topographic and bathymetric maps (A1). Both relationships are provided in Figure 6. For water levels below NGVD both curves are similar. For water levels above NGVD to an elevation of 0.7 m the present

representation predicts a larger surface area than Garvine's work. For elevations above 0.7 m the relationship is reversed.

2. In Garvine's formulation the frictional loss is a function of the wetted perimeter of the culverts and the culvert length. The frictional effects associated with the sluice gate are parameterized by a correction of the bottom frictional loss by the relative gate opening. In the present model the frictional loss is similarly dependent on the length of the culvert and water depth, but with a slightly different formulation that used by Garvine. The losses associated with the sluice gate, in the present work, are handled by a separate loss parameterization, as given in Section 2.
3. Garvine's model assumes that the flow through the culverts is always in direct, steady state balance with the pressure gradient along the channel. The present model accounts for the unsteady nature of the flow in the inlet.

To assess the impact of the differences between the two models, simulations were performed for a variety of hypotheses about the three assumptions noted above.

The following keys have been used in the text to facilitate the presentation:

Basin area vs elevation curve
A0 – Garvine
A1 – Present analysis (Portnoy and Adams)

Friction:
M0 – Present analysis (Manning function of length & sluice gate losses)
M1- Garvine (wetted perimeter, Manning formulation)

DQ/Dt:

0.0 - Garvine
Model calculation – Present analysis

Hypothesis A is the base case and the results are summarized in Table 3. Hypothesis B employs the Portnoy and Adams basin area versus elevation relationship(A1) and Garvine's frictional representation (M1). Hypothesis C employs Garvine's basin area (A0) and friction (M1) and assumes that the unsteady term in the momentum equation (DQ/Dt) is zero. Garvine's area relationship (A0) and friction (M1) are employed in Hypothesis D, with DQ/Dt calculated by the present model. Finally Hypothesis E includes Garvine's area (A0), the present frictional representation (M0), and DQ/Dt calculated by the present model. Results for Hypothesis A, B, C, D, and E are presented in Tables 3, 4, 5, 6, and 7, respectively.

Simulations were typically performed for Garvine's December 4, 1984 experiment and the July 25, 2000 and September 27, 2000 intensive tidal cycle surveys. In each case the sensitivity to Manning coefficient (single value) was investigated. Only selected values were addressed. Also provided for reference are the observations for the experiment noted. The results are once again given in the form of rms errors between model predictions and

observations, and predicted and observed maximum, minimum, and range of the tide in Herring River. The results of the analysis are systematically summarized below with a goal to understanding the impact of each factor.

Effects of friction:

Comparing results of simulations using Hypothesis A (present model, M0) and B (Garvine, M1) shows the impact of frictional dissipation in the culverts. For the suite of simulations performed the frictional losses for a given Manning coefficient are larger for Garvine's formulation than for present procedure. The optimum value for the Manning coefficient (if a single value is selected) is 0.09 for the present analysis and 0.07 if Garvine's formulation is used.

Effects of DQ/Dt:

The impact of including the acceleration term can be evaluated by comparing the results of Hypothesis C with D (Table 5 and 6). These simulations show that inclusion of the acceleration term in the governing equations for the inlet (Hypothesis D) has little impact on the model predictions, slightly increasing the maximum, minimum, and range for comparable Manning coefficients. The model performs best with a Manning coefficient of 0.07. The analysis also shows that model performance is not significantly impacted if n varies from 0.06 to 0.09.

Effects of basin area:

The impact of basin area can be investigated by comparing the results of Hypothesis A (Portnoy and Adams, A1) (Table 3) and E (Garvine, A0) (Table 6). For comparable Manning coefficients use of Garvine's basin area versus elevation curve predicts higher maximums, lower minimums, and larger tidal ranges than when the Portnoy and Adams relationship is used. The best model performance is obtained for n of 0.11 if Garvine's representation of the area is employed and 0.09 if the present area-elevation representation is used. This behavior is due to the nonlinear impact of the basin area versus elevation curve on model predictions. For water elevations above about 0.7 m the Portnoy and Adam's curve (present analysis) gives a smaller basin area for a given elevation than Garvine's relationship (Figure 6). The opposite is true for elevations between 0.0 (NGVD) and 0.7 m.

Studying the simulations as a group it is noted that the model performance, as measured by rms error, is weakly dependent on Manning coefficient, as long as n is in the range of 0.06 and 0.09. Model predictions of maximums, minimums, and range are much more sensitive to Manning coefficient, generally increasing (larger maximums, smaller minimums, and larger ranges) as n decreases. The present model sensitivity studies show that the present predictions are consistent with Garvine's analysis, both giving a Manning coefficient of 0.09 if a minimum rms error is sought.

As a note of caution the present simulations have only evaluated the model performance for small variants of the current operation (namely two culverts equipped with tidal gates and one

with a sluice opening 61 and 130 cm). These gate configurations typically restrict the tidal range to approximately 0.65 m and hence don't give a sense as to the impact of more substantial alterations of the gate operations.

The salinity model, described earlier in the report, was applied to the second field experiment to validate the model, using the same longitudinal dispersion coefficient as in the calibration exercise. Model predictions of the tidally mean salinity as a function of distance along the river are shown in Figure 21. Also shown for comparison are the observations for the day of the experiment. Comparison of model predictions to observations gives an rms error of 2.5 ppt. The model correctly predicts the basic shape of the profile, but under predicts the value at intermediate locations in the river. Model performance is judged to be acceptable given the simplicity of its formulation and a reasonable tool to understand the impact of remedial measures on salt penetration into the river.

The model predicts a salinity penetration distance and flushing time of 1.4 km and 24.6 hours, respectively. This compares to observed values of 1.5 km and 34.7 hours. Model performance is very good for the salt penetration distance but over predicts the flushing time.

7. Application of hydrodynamic model to proposed restoration options

In managing the Herring River system the National Park Service is considering options that would increase the amount of salt water entering the river by either modifying the operation of the existing culverts or removal of a portion or all of the dike structure. A total of ten options or cases were evaluated. These are summarized in Table 8 and include progressively opening the sluice gate on the eastern culvert (Cases 1-3), removing one of the existing tidal gates (Case 4), removing all sluice and tidal gates (Case 5), employing three sluice gates with progressively decreasing openings (Cases 6-9), and removal of all restrictions in the culverts (Case 10). Case 10 assumes that all control structures are removed from the existing culverts and that water is allowed to follow unimpeded through the existing openings. Note there is no height restriction imposed on the water level for this case. Cases 1 through 9 are the same as employed by Garvine (Roman, 1987) in his restoration option analysis.

To simplify the analysis of the resulting predictions the model was forced with a sinusoidal, lunar semi-diurnal tide (12.42 hour) with amplitude of 1.19 m. Garvine estimated MLW as 0.53 m below the bottom of the box culverts. Measurements during the present study show that NGVD is 0.84 m above the bottom of the culvert. Mean Low Water (MLW) in Herring River was therefore set at 1.37 m (NGVD). This forcing was selected since it is the same as that used by Garvine. Note this choice of forcing doesn't reflect the extended period of low water that characterizes the actual system.

Predictions of high and low water and the tidal range in Herring River, using the present model and the two part formulation for the Manning coefficient (n = 0.06/0.09) (A0), are reported in Table 9. Also reported for comparison are similar estimates made using the present model with a single Manning coefficient (n=0.09) (A4), the present model but using Garvine's assumptions (C4), and the results of Garvine's simulations (Garvine).

It is instructive to study the results in several major groupings. Cases 1 through 3 address the impact of increasing the opening of the sluice gate, while leaving the other two gates unchanged and operated as tidal gates. The current opening is 61 cm or Case 2. Progressively increasing the sluice opening results in modest (10s of cm) but corresponding increases in both the high and low tide levels. The tidal range increases, but only by about 10 cm. The increase in high and low tidal levels is a direct result of the shape of the basin surface area versus elevation curve (Figure 6a).

Cases 3 through 5 explore the impact of progressively increasing the opening in the dike by systematically removing tidal gates, with the sluice gate at its maximum extent (130 cm). Case 3 has one sluice and two tidal gates, Case 4 two sluice and one tidal gates and Case 5 no gates. Once again high and low water and the tidal range all increase as the tidal gates are removed. Comparing the one sluice/two tidal gates case (Case 3) to the no gates case (Case 5) the high tide amplitude increases from 1.99 m to 2.63 m (MLW), or by about 60 cm, while the low tide counterpart increases from 1.42 m to 1.61 m (MLW) or by about 20 cm. The tidal range increases from 0.57 to 1.03 m, or by approximately 40 cm.

Cases 6 through 9 investigate the impact of progressively decreasing the sluice opening (102, 76, 51, and 25 cm), assumed to be installed in all three box culverts. The high tide level and tidal range progressively decrease as the effective size of the opening decreases over the range of cases tested. The decrease is 52 cm for high tide (2.57 m to 2.05 m) and 64 cm (1.02 m to 0.38 m) for the tidal range. The low tide level remains approximately constant, within 12 cm (1.55 m to 1.67 m).

The tidal range increases from 0.47 m for the present case to 1.03 m for the no gates case. Similarly the maximum increases from 1.76 m to 2.63 m (MLW) and the minimum from 1.29 to 1.61 cm (MLW).

Taken as a group the simulations show that increasing the effective size of the opening at the dike increases the high and low tide water levels and increases the tidal range in Herring River.

For comparison Table 9 also shows Garvine's (Roman, 1987) predictions for each of the first nine cases. His values for high and low tide levels and tidal range are reported. The differences between his simulations and the present results are generally quite small (8 cm or less) for cases where the gates are typically partially closed. (Cases 1,2,3,8 and 9). As the effective opening in the dike increases (Cases 4,5,6, and 7) the present simulation predicts higher high tides and lower low tides. The predicted tidal ranges for these cases are hence higher than those predicted by Garvine. For the most open three sluice gates cases (Cases 6 and 7) the tidal range is substantially larger and the high and low tides correspondingly higher and lower than from his simulation. The present simulation shows that the tidal range increases from 38 cm for the most restrictive case (Case 9) to 1.09 cm for the most open case (Case 10). Garvine's analysis, on the other hand, shows that the tidal range is almost invariant with dike opening (0.51 m versus 0.53 m).

Comparing the results from C4 to those of Garvine show that the present model is in excellent agreement with Garvine's, when similar assumptions are made. Comparing the results from A0 to A4 show that using the single Manning coefficient (A4) reduces the predicted maximum, minimum, and tidal range compared to the two-part formulation (A0). The difference increases as the dike becomes more open.

The cases selected above show the impact of modifying the openings and operation of the hydraulic control structures in the existing box culverts. Case 10 provides the maximum opening cross section and imposes no other control on the flow. It is of interest to understand what the implications of further opening of the dike would be. These options might be exercised in the event that dike-causeway system was reconstructed to allow additional exchange of water between the river and adjacent coastal waters. These simulations will also be useful to understand the extent to which the present dike structure impacts water levels, compared to the case of the absence of the dike. To this end simulations were performed with the model progressively increasing the width of the openings in the dike from Case 10 (6.1 m existing three culvert system) to the full width at the river mouth of approximately 200 m.

Table 10 shows the model predicted maximum, minimum, and range of water elevations in the river for various widths of the opening. The model is forced by a realistic representation of the semi-diurnal tide with a maximum elevation of 1.65 m and a minimum elevation of -0.73 m. A review of the simulations shows that the magnitude of the maximum and minimum elevations and the tidal range all increase as the width increases. The increases are quite rapid for small changes from the current size but decrease asymptotically as the opening size increases. The rate of increase is fastest for the maximum elevation and slower for the minimum elevation and tidal range. This is a result of the much larger incremental change in water storage capacity at high water versus that at low water. For widths greater than about 30 m the dike has little impact on the elevations in the river. Removing the dike increases the tidal range to 2.38 m compared to 1.1 m for the case with the present structure and all culverts fully open.

Figure 22 shows the same results, but in the form of time series of tidal elevations in the river for the various opening widths. The asymptotic response of the surface elevation to changes in the opening is clearly demonstrated. In addition the figure also shows that the phase lag between the surface elevation in the bay and in the river decreases as the opening size increases.

The set of simulations given above show the impact of various modifications to the culvert system on typical tidal conditions. It is of interest to understand the impact of these modifications in the event of storm conditions, which typically result in higher water levels.

Following Garvine, simulations were performed for a 100-year storm event, based on the February 6-7, 1978 nor'easter. The tidal forcing was selected from Boston, MA for this period. The highest water level was 4.51 m referenced to MLW. The forcing had an amplitude of 2.7 m and a period of 12.42 hours. Results of simulations for Cases 2, 5, and 10 are provided in Table 11. Case 2 represents the current configuration, Case 5 has three sluice gates open to 130 cm and Case 10 has all restrictions to the flow removed. As expected the maximum, minimum, and tidal range increase as the configuration of the culverts increases the flow cross sectional area. The tidal range increases from 0.93 m to 1.71 m (Case 2 to 10).

Comparisons are also shown in Table 11 to simulations performed by Garvine (Roman, 1987) for Cases 2 and 5. Garvine predicts a higher maximum for Case 2 (2.08 m) than the present simulation (1.80 m) and a substantially lower value (2.76 m vs. 3.21 m) for Case 5.

Finally simulations were performed for neap and spring tides for Cases 2, 5, and 10. The forcing was based on observations from the June to October 2000 time series data set. Model predictions (Table 11) are consistent with earlier simulations and show that the maximum, minimum, and range all increase as the culvert configuration becomes less restrictive (progressing from Case 2 to 10). The results for Case 2 are consistent with Garvine's simulations.

The salinity model, as described in Section 6, was employed to predict the salinity distribution and the associated flushing time for each restoration option. The tidal mean water level for each case was first determined from the hydrodynamic model simulations. A freshwater

inflow rate of 0.1 m^3/sec was assumed. The results are summarized in Table 12 in terms of the salt penetration distance and the flushing time. The salt penetration distance is defined as the location of the point where the salinity decreases to 10 % of its value at the mouth of the river. Also shown for comparison are the observed and model predicted results for the two field experiments. The same results are presented in Figures 23 and 24, which provide the salt penetration distance and flushing time versus mean water elevation, respectively. The case numbers are shown on the figures. The values of the mean water elevation are a result of simulations for these restoration option cases using the hydrodynamic model.

The model predictions are observed to be in good general agreement with the observations correctly predicting both the salt penetration distance as well as the associated flushing time. In general the mean water level, salt penetration distance and flushing time all increase as the configuration of the dike system allows more salt water to enter the system (in order: Cases C1, C2, C3, C9, C8, C7, C6, C4, C5, C10) (Figure 23 and 24). The minimum penetration distance is about 1.5 km and the maximum is 4.8 km. This compares to a distance of about 2 km between the mouth of the river and High Toss Road. For the more restricted cases (Cases C1, C2) the salt penetration distance is below High Toss Road while for the cases with larger tidal exchange (Cases C4 to C8 and C10) the penetration distance is well beyond High Toss Road. The flushing time increases from 29.5 hrs (1.23 days) for the most restrictive case (C1) to 14. 875 days (357 hours) for the case with the largest tidal exchange (Case 10). These results are all directly attributed to the increase in the tidal exchange as the hydraulic control structures are systematically removed or opened to their widest extent.

A series of simulations was performed to assess the sensitivity of the predictions to changing the segmentation length used to represent the cross sectional area versus distance relationship. These simulations showed the variations in the predictions were typically on the order of 10 %.

Simulations reported on the left hand side of Table 12 assume a freshwater input of 0.1 m^3/sec. As noted in the model development section mean freshwater flow rates are a key parameter controlling the salt penetration and flushing time of the river. To assess the impact of freshwater input on model predictions were made using a freshwater flow rate of 0.28 m^3/sec. This is the maximum value observed by Garvine. The results are also shown in Table 12. Figures 23 and 24 show the results for the 0.28 m^3/sec freshwater flow case as well. In general as the freshwater input increases the salt penetration distance and the flushing time decrease. The model is seen to be very sensitive to the specified flow rates.

Figures 23 and 24 both show a dramatic change in the salt penetration distance and the flushing time at a distance of approximately 2.3 km. This behavior is directly attributed to the rapid increase in the surface area north of High Toss Road.

In earlier modeling studies, for the same suite of restoration cases, Garvine found that the salinity penetration distance varied from about 1.4 to 1.9 km. Similarly the predicted flushing time varied little, ranging from 1.27 to 1.77 days. Garvine assumed that the freshwater input was 0.28 m^3/sec. Comparison of Garvine's predictions with the present model results show they are approximately equivalent for the base and minimal modification cases (Cases 1, 2,

and 3) but differ substantially when the tidal exchange becomes more substantial. As an example for Case 5, the salt penetration distance for the present simulation is predicted to be 4.8 km. This compares to Garvine's estimate of 1.87 km. The present simulation gives a flushing time of 2.8 days compared to Garvine's estimate of 1.77 days. The difference between the two can be principally explained by the difference in the surface area versus elevation curves (Figure 6) between the two simulations. The present model allows a significantly larger tidal exchange for elevations in the range of 0.0 to 0.7 m NGVD than does Garvine's representation. This larger exchange volume allows increased salt penetration and longer flushing times, since the volume that needs to be flushed is increased. These sensitivity studies clearly show the importance of correctly characterizing the basin surface area versus elevation relationship.

The above restoration options have assumed that flows are effectively blocked by High Toss Road and hence have included only the basin area seaward of the road. These simulations give a reasonable sense of the impact of the more restrictive restoration options (C1 to C4, C6 to C9) but don't adequately address the most open options investigated (C5 and C10) which allow the culverts at the dike to remain fully open. For the later two cases tidal waters will clearly penetrate north of High Toss Road. It is also likely that any future restoration program would include the construction of a dike across Mill Creek to protect the adjacent golf course. This dike would become particularly important for Cases C5 and C10.

To more carefully assess options that allow water to penetrate north of High Toss Road and with a dike across the mouth of Mill Creek, model simulations were performed for Case C2 (existing configuration), Case C5 (all controls removed), Case C10 (all control structures and vertical restrictions removed), and Case C5 for the 100 yr. storm event. For these simulations the basin surface area versus elevation curve provided in Figure 6b (no High Toss Road and Mill Creek) was used to represent the storage capacity of the river. Forcing was the same as for the other restoration cases. In describing the results of the simulations B0 refers to the existing basin configuration and B1, the configuration where High Toss Road is effectively removed (either removal or placement of additional culverts) and Mill Creek is diked.

The results of the simulations, in terms of the model predicted average, maximum and minimum tidal levels and tidal range in the river, are presented in Table 13. The results are also presented in Figure 25a, b, and c (a for Case C2, b for Case C5, and c for Case C10). In each plot the simulations for B0 and B1 are provided for typical tidal and 100 yr storm forcing. The results will first be discussed by case. For Case C2 the results are insensitive to basin geometry. This result can be attributed to the fact that little water penetrates north of High Toss Road and that the water storage capacity in Mill Creek is small compared to the main stem of the Herring River. For the 100 yr forcing case the mean water level, minimum and maximum tidal levels all increase and the tidal range decreases, compared to the tidally forced cases. The tidal range is substantially reduced for the B1 basin geometry, compared to the case using the B0 basin geometry. This is a direct result of the increased storage capacity above High Toss Road included in the B1 configuration.

For Case C5 changing the basin representation from B0 to B1 has little effect on the mean water level, substantially decreases the tidal range and the maximum water level and

increases the minimum water level. Similar trends with basin geometry are observed for the 100 yr storm forcing case, but with the mean basin water level increased by about 30%.

For Case C10 the same general trends, as observed in Case C5, but with significantly higher values for the maximums, means, and tidal ranges and lower values for the minimums, are seen.

For Cases C5 and C10 increasing the basin size from B0 to B1 results in a substantial decrease in tidal range and maximum water level, a slight increase in the mean water level, and a larger increase in the minimum water level. This holds true for both tidal and 100 yr storm forcing. Case C2 is insensitive to basin geometry for tidal forcing, but shows similar trends to those noted above for 100 yr forcing. The sensitivity of the model predictions for Cases C5 and C10 can be directly attributed to the increased storage capacity, at a given elevation, provided once water is allowed to penetrate north of High Toss Road. The loss of water storage capacity from diking of Mill Creek is overwhelmed by the increased capacity provided by the extensive marsh area north of High Toss Road. With the increased storage capacity afforded by B1 the minimum water level increases, the maximum water level decreases, the mean water level decreases slightly, and the tidal range decreases for both tidal and 100 yr storm forcing. A study of the surface area covered for Cases C5 and C10 show that a substantial portion of the area north of High Toss Road is inundated at high water. At low tide the water is observed to pool in low lying areas. This is clearly shown in the animations presented in Appendix D.

Simulations were performed to assess the impact of selecting the B1 basin geometry on the salt penetration distance and the flushing time for Herring River. These results are summarized in Table 14 for Cases C2, C5, and C10, with mean and 100 yr. tidal forcing. The values of the mean elevation in the system were determined from the hydrodynamic simulations. For both the mean tidal and 100 yr storm forcing the mean elevation, salinity penetration distance, and flushing time all increase as increasing amounts of water are allowed to enter the river (progressing from Case C2 to C10). The trend is similar to that observed in Table 12, with the B0 basin geometry. For the cases with the largest openings in the dike (C5, C10), with mean tidal forcing and for all cases with 100 yr storm forcing the salt penetration distance is well north of High Toss Road (about 2 km from dike).

If the flow controls in the dike at the mouth of Herring River are removed, one issue of particular concern is the impact this will have on sediment transport in the river and in the long term on the geomorphology of the study area. While no formal analysis has been completed as part of this study use of the conceptual model provided earlier can provide insight into the probable consequences of the remedial options investigated.

With the progressive opening, or removal, of the flow control structures in the dike, the flood flow velocities will decrease through the dike because there be an increasing flow cross sectional area compared to the existing system. For the no control structures case the flow cross sectional area increases by over a factor of three, compared to existing conditions. The inequality in flow speed, between the ebb and flood, will be progressively reduced as the opening area increases. The tidal range upstream of the dike and the resulting tidal velocities

in Herring River proper will increase as the cross sectional opening increases. The velocities upstream of the dike are nevertheless expected to remain quite small (peak velocities less than 10 cm/sec), and generally below the threshold for sediment re-suspension (20 cm/sec), even for the no control structure case. This is a result of the limited length of the basin relative to the tidal wave length.

The flood tide delta will adjust to the changes in the flow field but is likely to remain much as it is at present, with only very slow erosion and dispersal of sand into the river as the result of storm forcing. The fine grained, silt and clay material in the lower reaches of the river is expected to remain essentially in place during typical tidal forcing because the velocities required for re-suspension (i.e. greater than 20 cm/sec) are not likely to be reached, even for the no flow control structures case. If this material is re-suspended, say during a storm event, it is likely to be transported both up and downstream of the dike. This sediment will be widely dispersed if transported downstream of the dike because of its low settling velocity and the stronger tidal currents seaward of the dike. Clay and silt sediments that are transported up river during storms are likely to be transported down river during subsequent major freshwater discharge events and re-settle in the deeper waters of the lower river.

To help better appreciate and visualize the circulation and salinity dynamics of the Herring River, under both present and selected restoration options, and to allow the public ready access to this information as part of their review of NPS proposed restoration, a web site was developed as part of this project. It is nominally listed as Appendix D to this report. The site includes the following information: (1) reproductions of the study area topography and bathymetry, as provided in Figure 5 of this report. This is provided as background reference to help the viewer interpret the visual material provided. (2) animations (e.g. hourly intervals) of the surface area covered by water over one lunar, semi-diurnal tidal cycle for Herring River (south of the dike to High Toss Road or the entire marsh system). Animations are provided for three cases: C2 (current configuration of control structures in the dike), mean tidal forcing; C5 (all control structures in the dikes removed), mean tidal forcing; and C5 with 100 yr. storm forcing. These animations are provided for two different assumptions on the river's storage capacity. For the first case (basin geometry, B0) the storage basin consists of the area north of the dike and seaward of High Toss Road (no water is allowed to penetrate north of High Toss Road). For the second case (basin geometry, B1) Mill Creek is diked to prevent any water from entering this area. Water however is allowed to penetrate into the marsh system north of High Toss Road (the later can be achieved, either by removal of High Toss Road or additional breaching of the High Toss Road causeway with culverts.). In addition contour maps of the model predicted mean, tidally averaged and high and low tide salinity fields are provided. The model predicted values of salinity at the observation stations are also provided. The animations and salinity fields are provided for a total of six cases (two basin geometries x three cases of control structure configuration/forcing). The viewer is cautioned that the C5 and C5/100 yr storm forced cases for the B0 geometry overestimate the water levels in the lower river (below High Toss Road) and under-estimate the salinity intrusion. This is a result of the fact that the simulations assume that no water can penetrate north of High Toss Road, whereas the existing culvert on the western end of the road allows water to penetrate into the marsh system to the north. For these two cases simulations with the B1

basin geometry give more realistic pictures of the circulation and salinity dynamics for removal of flow control structures.

8. Summary and conclusions

The present study has resulted in the development, application, calibration, and validation of hydrodynamic and salinity models to allow prediction of the water level variations in the river, flow through the dike, and salt penetration distance and flushing time for the Herring River system. Model predictions are in very good agreement with data collected during intensive tidal cycle surveys and time series measurements of sea surface elevations in the river. Model predictions are consistent with earlier simulations performed by Garvine for the current configuration and operation of the hydraulic control structures in the dike.

Application of the present models to various restoration options shows that the tidal range, maximum and minimum water levels, salt penetration distance, and flushing time all increase as the effective flow cross sectional area of the opening in the dike increases. This is directly attributable to the increased tidal exchange volume with increased opening size. Even with all control structures removed the existing system of culverts results in a reduction in the exchange of water between bay and the river compared to the case before the dike was constructed. Restoration of pre-existing conditions in Herring River, defined as similar tidal ranges up and downstream of the dike, will require increasing the width of the opening to at least 30 m (total width of 200 m for unaltered system). The current width of the openings for all culverts is about 6 m. Diking Mill Creek and construction of additional culverts across High Toss Road has little impact on water levels and salt penetration and flushing time under the current control configuration. Removal of all gates from the dike for this case allows seawater to penetrate well north of High Toss Road. It increases the mean tidal level and significantly reduces the tidal range compared to the present system.

The present simulations are in very good agreement with earlier work by Garvine for configurations similar to those that presently exist. The present model predicts larger impacts on tidal and salinity conditions, than Garvine, as the restoration options allow substantially increased tidal exchange. The differences between the two have been investigated by a detailed series of sensitivity studies varying input data and model formulation. The largest differences between the two model predictions are explained by differences in the relationship used to define the surface area versus elevation relationship. The next most important parameter is the representation of the frictional losses in the flow through the dike.

While model performance is reasonable for conditions typical of the current operation, the uncertainty increases as the flow cross sectional area in the dike increases. There are currently no data sets to validate model performance for these conditions. The results however are sufficiently definitive for park managers to proceed with an incremental, adaptive-management program, which could be verified by additional field experiments and modeling investigations. These additional studies need to investigate configurations that allow a substantially increased cross sectional opening in the dike. These experiments need only be performed over a short period of time (e.g. several tidal cycles) to collect the necessary data. In addition to the intensive tidal cycle measurement made in the present study a stake field study, marking the extent of the surface area covered at high and low water levels in the river

by stakes, would be useful for clearly delineating the basin surface area at these two elevation marks.

In performing the intensive tidal cycle surveys and the subsequent analysis of the field data it was impossible to balance the water fluxes through the culverts over the tidal cycle. This problem appears to be directly attributed to not making the water level measurement at the same location as the current velocity measurement. Measuring the water level in the river adjacent to the culvert, rather than in the culvert, did not account for the strong local effects of flow on the surface elevation, specifically the supercritical flows that are observed during much of the flood tide or the substantial set down effects in the entry region of the culvert on the ebb flow. This issue needs to be addressed in future field programs.

Sensitivity studies with the salinity model clearly show that predictions of the flushing time and salt penetration distance are very sensitive to the assumed freshwater flow rates. While the present study provided data on these flows during the intensive tidal cycle surveys it provided little information on the variations of the freshwater input rates. This type of data will be necessary if more accurate estimates of the variation in salt intrusion and flushing are required.

Given the impact of the basin surface area versus elevation relationship on model predictions and the uncertainty in the present relationship it is recommended that additional surveying work be performed using the Trimble based GPS system (or similar system) used in the present study. The key region of interest is in the water level range from 0.0 to 0.7 m. Simulations can then be made using the revised relationship and its impact on restoration options assessed.

A conceptual sediment transport model has been developed to explain the formation of a substantial flood tide delta just landward of the dike. The delta is a direct result of the asymmetry of the flood/ebb flow through the dike. If the control structures in the dike are removed the current speeds in the vicinity of the flood tidal delta will continue to remain low, below the threshold for sediment re-suspension. The delta is therefore unlikely to experience significant erosion. This conceptual model can be partially verified by collection of current data on the margins of the flood tide delta during the intensive tidal cycle surveys proposed above.

Acknowledgements

The authors would like to acknowledge the commitment and support of Dr. John Portnoy, Evan Gwilliam, Mark Adams, and Janet Cote, National Park Service, US Department of Interior, Cape Cod National Seashore, Wellfleet, Massachusetts and Charles Roman, US Geological Survey, Biological Resources Division, University of RI, Narragansett, RI. Special thanks are due to the following individuals who participated in the two, day long field programs: Nicole Castanet, Marie Claire Cornillon, Joseph and Eileen Keating, Marie Martin, Ronald Regnier, Hillary Welch, and Jan Hatchette-Hierholzer. The sediment grain size analysis was performed by Matt Zitello under the direction of Dr. Jon Boothroyd, Geology Department at the University of Rhode Island. Larry Simoneau and Fred Pease, University of Rhode Island, Ocean Engineering constructed and installed the mount for the current meter at the dike. Special thanks are extended to Thomas Opishinski, Interactive Oceanographics, who developed the web site for the project, as presented in Appendix D.

9. References

Lejeune, A., 1982. Note du cours d'element d'hydro et aero dynamique. Faculte des sciences appliquees. Universite de Liege, Liege, Belgium.

Nichol, M, and J. D. Boon, 1994. Sediment transport processes in coastal lagoons, Chapter 7, in *Coastal Lagoon Processes*, B. Kjerfve (editor), Elsevier Oceanography Series, New York, New York, p. 103-127.

Nielsen, P., 1992. Coastal bottom boundary layers and sediment transport, Advanced Series on Ocean Engineering, Volume 4, World Scientific, Singapore.

Officer, C. B., 1976. *Physical Oceanography of Estuaries and Associated Coastal Waters,* John Wiley and Sons, NY, NY.

Portnoy, J. E. and M. Reynolds, 1997. Wellfleet's Herring River: The case for habitat restoration, Environment Cape Cod, Vol. 1, No. 1, pp 35-43.

Portnoy, J. W. and A. E. Giblin, 1997. Effects of historic tidal restrictions on salt marsh sediment chemistry, Biogeochemistry, 36, pp. 275-303.

Portnoy, J. W., 1991. Summer oxygen depletion in a diked New England estuary, Estuaries, Vol. 14, No. 2, June 1991, p. 122-129,

Roman, C., 1987. An evaluation of alternatives for the estuarine restoration Management: The Herring River ecosystem (Cape Cod National Seashore), National Park Service Cooperative Research Unit, Rutgers- The State University of New Jersey, New Brunswick, NJ 08903, p. 304.

Roman, C. T., R. W. Garvine, and J. W. Portnoy, 1995. Hydrologic modeling as a predictive basis for ecological restoration of salt marshes, Environmental Management, Vol. 19, No. 4, pp. 559-566.

Seelig, W. M., D. L. Harris, and B.E. Herchenroder, 1977. A spatially integrated numerical model of inlet hydraulics, GITI Report 14, US Army Corps of Engineers, Coastal Engineering Research Center, Fort Belvoir, VA and US Army Engineers Waterways Experiment Station, Vicksburg, MS

Spaulding, M. L., 1994. Modeling of circulation and dispersion in coastal lagoons, Chapter 5 in *Coastal Lagoon Processes*, B. Kjerfve (editor), Elsevier Oceanography Series, New York, New York, p. 103-127.

Table 1 Amplitude and phase (Greenwich) of the thirteen primary tidal constituents for the upstream and downstream stations on Herring River.

Tidal constituents	Amplitude – Dike (m)	Phase – Dike (Degrees)	Amplitude – Upstream (m)	Phase – Upstream (Degrees)
Z_0	0.440	0.	0.088	0.
M_2	1.218	358.39	0.253	65.35
N_2	0.253	325.30	0.049	39.47
M_4	0.130	326.54	0.006	214.29
L_2	0.087	35.24	0.029	87.98
K_1	0.124	156.28	0.025	203.82
O_1	0.102	149.18	0.023	189.82
S_2	0.166	41.38	0.013	86.97
T_2	0.052	59.76	0.007	217.05
M_6	0.028	210.49	0.010	290.72
S_1	0.021	82.61	0.006	45.12
Q_1	0.019	143.64	0.006	188.41
P_1	0.026	146.84	0.008	225.01

Table 2 Mean and maximum flow rates for the dike and High Toss Road, Pole Dike Creek and Bound Brook Island culverts for the July 24, 2000 and September 26, 2000 intensive tidal cycle surveys.

Herring River – Flows Basic Statistics – (m^3/sec)

	Experiment #1: July 24-25, 2000			**Experiment #2: Sep 26-27, 2000**		
		Flood	**Ebb**		**Flood**	**Ebb**
Dike, Three gates						
Mean		4.6	7.46		6.39	9
Max.		7.36	12.45		11.55	13.82
High Toss Road Culvert						
Mean	0.107	0.012362	0.172216	0.239	0.160325	0.276769
Max.	0.233	0.028684	0.232827	0.440	0.439919	0.436018
Pole Dike Creek Culvert						
July 24,2000 1:42 PM	0.030					
Sep 26, 2000 12:00 PM				0.007		
Brook Island Culvert						
July 24, 2000	0.090					
Sep 26, 2000 11:49AM				0.087		

Table 3 Model calibration hypothesis A (Simulations Sa):

1) Area = A1 = Portnoy and Adams basin

2) Friction = M0 = f(Manning + wetted length in inlet) (Seelig et al, 1977)

Garvine's experiment December 4, 1984: Sluice gate opened 130 cm, 2 tide gates

	Case #	Manning	RMS (m)	Max(m)	Min(m)	Range(m)
Observations:				0.6	-0.06	0.66
Garvine's simulations			0.06	0.61	-0.07	0.68
Inlet Simulations:	S1	0.06	0.09	0.589	-0.29	0.879
	S2	0.07	0.08	0.56	-0.207	0.767
	S3	0.08	0.07	0.53	-0.153	0.683
	S4	0.09	0.07	0.5	-0.109	0.609
	S5	0.1	0.07	0.47	-0.07	0.54
	S6	0.11	0.08	0.46	-0.05	0.51
	S0	0.06/0.09	0.05	0.59	-0.06	0.65

Experiment #1 :July 25, 2000 : Case 2: Sluice gate opened 65 cm + 2 tide gates

	Case #	Manning	RMS (m)	Max(m)	Min(m)	Range(m)
Observations:				0.42	-0.18	0.6
Inlet Simulations:	S1	0.06	0.09	0.36	-0.36	0.72
	S2	0.07	0.08	0.35	-0.3	0.65
	S3	0.08	0.07	0.35	-0.26	0.61
	S4	0.09	0.06	0.34	-0.22	0.56
	S5	0.1	0.06	0.33	-0.2	0.53
	S6	0.11	0.07	0.33	-0.19	0.52
	S0	0.06/0.09	0.02	0.42	-0.239	0.659

Experiment #2:September 27, 2000, Case 2: Sluice gate opened 65 cm + 2 tide gates

	Case #	Manning	RMS(m)	Max(m)	Min(m)	Range(m)
Observations:				0.45	-0.18	0.63
Inlet Simulations:	S3	0.08	0.05	0.42	-0.23	0.65
	S4	0.09	0.04	0.41	-0.17	0.58
	S6	0.11	0.05	0.41	-0.09	0.5
	S0	0.06/0.09	0.03	0.42	-0.16	0.58

Total series: June 2, 2000 -October 2000 Case 2: Sluice gate opened 65 cm + 2 tide gates

	Max(m)	Min(m)	Range(m)
Observations:	0.52	-0.32	0.84

Conclusion: 1) n1=0.06 +n2 =0.09

or

2) n =0.09

Table 4 Model calibration hypothesis B (Simulations Sb):
1) Area = A1 = Portnoy and Adams basin
2) Friction = M1 = f(Manning + wetted perimeter in inlet) (Garvine, p.169, Roman, 1987)

Garvine's experiment December 4, 1984: Sluice gate opened 130 cm, 2 tide gates

	Case #	Manning	RMS (m)	Max(m)	Min(m)	Range(m)
Observations:				0.6	-0.06	0.66
Garvine's simulations			0.06	0.61	-0.07	0.68
Inlet Simulations:	Sb1	0.06	0.09	0.46	-0.15	0.61
	Sb2	0.07	0.01	0.43	-0.09	0.52
	Sb6	0.04	0.14	0.55	-0.34	0.89

Experiment #1: July 25, 2000 : Case 2: Sluice gate opened 65 cm + 2 tide gates

	Case #	Manning	RMS (m)	Max(m)	Min(m)	Range(m)
Observations:				0.42	-0.18	0.6
Inlet Simulations:	Sb1	0.06	0.09	0.3	-0.25	0.55
	Sb2	0.07	0.09	0.29	-0.23	0.52
	Sb6	0.04	0.12	0.34	-0.41	0.75

Experiment #2: September 27, 2000 : Case 2: Sluice gate opened 65 cm + 2 tide gates

	Case #	Manning	RMS (m)	Max(m)	Min(m)	Range(m)
Observations:				0.45	-0.18	0.63
Inlet Simulations:	Sb1	0.06	0.07	0.41	-0.25	0.66
	Sb2	0.07	0.06	0.43	-0.09	0.52

Total series: June 2000 -October 2000 Case 2: Sluice gate opened 65 cm + 2 tide gates

	Max(m)	Min(m)	Range(m)
Observations:	0.52	-0.32	0.84

Conclusion : n=0.07

Table 5 Model calibration hypothesis C (Simulations Sc):

1) Area = A0 = Garvine's area

2) Friction = M1 = f(Manning + wet perimeter in inlet) (Garvine, p.169, Roman, 1987)

3) dQ/dt=0 (Garvine, Roman, 1987, p.169)

Garvine's experiment December 4, 1984: Sluice gate opened 130 cm, 2 tide gates

	Case #	Manning	RMS (m)	Max(m)	Min(m)	Range(m)
Observations:				0.6	-0.06	0.66
Garvine's simulations		0.09	0.06	0.61	-0.07	0.68
Inlet Simulations:	Sc1	0.06	0.09	0.52	-0.2	0.72
	Sc2	0.07	0.08	0.509	-0.156	0.665
	Sc3	0.08	0.07	0.49	-0.11	0.6
	Sc4	0.09	0.07	0.48	-0.08	0.56

Garvine's experiment May 17, 1985: Sluice gate opened 61 cm, 2 tide gates

	Case #	Manning	RMS (m)	Max(m)	Min(m)	Range(m)
Observations:				0.46	-0.11	0.57
Garvine's simulations		0.09	0.09	0.43	-0.13	0.56
Inlet Simulations:	Sc1	0.06	0.07	0.53	-0.03	0.56
	Sc2	0.07	0.07	0.51	-0.04	0.55
	Sc3	0.08	0.07	0.49	0.01	0.48
	Sc4	0.09	0.07	0.48	0.02	0.46

Conclusion : n=0.09

Table 6 Model calibration hypothesis D (simulations Sd):

1) Area = A0 = Garvine's area

2) Friction = M1 = f(Manning + wetted perimeter in inlet) (Garvine, p.169, Roman, 1987)

Garvine's experiment December 4, 1984: Sluice gate opened 130 cm, 2 tide gates

	Case #	Manning	RMS(m)	Max(m)	Min(m)	Range(m)
Observations:				0.6	-0.06	0.66
Garvine's simulations		0.09	0.06	0.61	-0.07	0.68
Inlet Simulations:	Sd1	0.06	0.09	0.58	-0.197	0.777
	Sd2	0.07	0.07	0.55	-0.15	0.7
	Sd3	0.08	0.07	0.51	-0.11	0.62
	Sd4	0.09	0.075	0.47	-0.09	0.56

Garvine's experiment May 17, 1985: Sluice gate opened 61 cm, 2 tide gates

	Case #	Manning	RMS(m)	Max(m)	Min(m)	Range(m)
Observations:				0.46	-0.11	0.57
Garvine's simulations		0.09	0.09	0.43	-0.13	0.56
Inlet Simulations:	Sd2	0.07	0.08	0.56	0	0.56
	Sd3	0.08	0.09	0.52	0.01	0.51

Experiment #1 :July 25, 2000 : Case 2: Sluice gate opened 65 cm, 2 tide gates

	Case #	Manning	RMS(m)	Max(m)	Min(m)	Range(m)
Observations:				0.42	-0.18	0.6
Inlet Simulations:	Sd1	0.06	0.08	0.37	-0.27	0.64
	Sd2	0.07	0.07	0.355	-0.231	0.586
	Sd3	0.08	0.08	0.337	-0.198	0.535
	Sd4	0.09	0.09	0.32	-0.17	0.49

Experiment #2:September 27, 2000 : Case 2: Sluice gate opened 65 cm + 2 tide gates

	Case #	Manning	RMS(m)	Max(m)	Min(m)	Range(m)
Observations:				0.45	-0.18	0.63
Inlet Simulations:	Sd1	0.06	0.07	0.46	-0.26	0.72
	Sd2	0.07	0.08	0.45	-0.21	0.66
	Sd3	0.08	0.09	0.44	-0.168	0.608
	Sd4	0.09	0.1	0.43	-0.12	0.55

Total series: June 2000 -October 2000 Case 2: Sluice gate opened 65 cm + 2 tide gates

	Max(m)	Min(m)	Range(m)
Observations:	0.52	-0.32	0.84

Conclusion: n= 0.07

Table 7 Model calibration hypothesis E(simulations Se):
1) Area = A0 =Garvine's basin
2) Friction = M0 = f(Manning+ wetted length)

Garvine's experiment December 4, 1984: Sluice gate opened 130 cm, 2 tide gates

	Case #	Manning	RMS(m)	Max(m)	Min(m)	Range(m)
Observations:				0.6	-0.06	0.66
Garvine's simulations			0.06	0.61	-0.07	0.68
Inlet Simulations:	Se4	0.09	0.07	0.62	-0.16	0.78
	Se5	0.1	0.05	0.6	-0.13	0.73
	Se6	0.11	0.05	0.58	-0.1	0.68

Experiment #1 :July 25, 2000 : Case 2: Sluice gate opened 65 cm + 2 tide gates

	Case #	Manning	RMS(m)	Max(m)	Min(m)	Range(m)
Observations:				0.42	-0.18	0.6
Inlet Simulations:	Se4	0.09	0.05	0.43	-0.24	0.67
	Se5	0.1	0.04	0.42	-0.21	0.63
	Se6	0.11	0.04	0.41	-0.18	0.59

Experiment #2:September 27, 2000: Case 2: Sluice gate opened 65 cm + 2 tide gates

	Case #	Manning	RMS(m)	Max(m)	Min(m)	Range(m)
Observations:				0.45	-0.18	0.63
Inlet Simulations:	Se5	0.1	0.05	0.47	-0.18	0.65
	Se6	0.11	0.03	0.46	-0.15	0.61

Total series: June 2000 -October 2000 Case 2: Sluice gate opened 65 cm + 2 tide gates

	Case #	Manning	RMS(m)	Max(m)	Min(m)	Range(m)
Observations:				0.52	-0.32	0.84

Conclusion : n= 0.11

Table 8 Sluice and tidal gate configurations used in restoration option evaluations. G is the vertical opening of the sluice gate.

Case	Configuration
1.	1 sluice gate (G*=51 cm), 2 tide gates
2.	1 sluice gate (G=61 cm), 2 tide gates
3.	1 sluice gate (G=130 cm), 2 tide gates
4.	1 sluice gate (G=130 cm), 1 tide gate, 1 open gate
5.	no sluice (G=130 cm) or tidal gate 3 sluice gates
6.	3 sluice gates(G=102 cm)
7.	3 sluice gates (G=76 cm)
8.	3 sluice gates (G=51 cm)
9.	3 sluice gates (G=25 cm)
10.	Removal of all restriction in culverts**

* G is the vertical opening of the gate. The maximum gate opening is 130 cm.
**This case assumes not only that all flow restrictions are removed from the current culverts but that all vertical restrictions to the flow are removed as well.

Table 9 Results of simulations for restoration options

Sinusoidal Forcing : z bay = 0.46 +1.19 * sin (2*pi *t/T) (Garvine's forcing)
Case number corresponds to the gate configuration as described in Garvine (p177, Roman, 1987) and presented in Table 8

All values given in meters	**MLW**				**NGVD**			
	A0	**A4**	**C4**	**Garvine**	**A0**	**A4**	**C4**	**Garvine**
Case 1: 1SG =51 cm + 2TG								
Max	1.76	1.71	1.73	1.81	0.39	0.34	0.36	0.44
Min	1.29	1.25	1.29	1.32	-0.08	-0.12	-0.08	-0.05
Range	0.47	0.46	0.44	0.49	0.47	0.46	0.44	0.49
Case 2: 1SG=61 cm + 2TG								
Max	1.81	1.75	1.75	1.85	0.44	0.38	0.38	0.48
Min	1.31	1.26	1.30	1.34	-0.06	-0.11	-0.07	-0.03
Range	0.50	0.49	0.46	0.51	0.50	0.49	0.46	0.51
Case 3: 1SG = 130 cm + 2 TG								
Max	1.99	1.83	1.79	1.93	0.62	0.46	0.42	0.56
Min	1.42	1.34	1.34	1.38	0.05	-0.03	-0.03	0.01
Range	0.57	0.49	0.46	0.55	0.57	0.49	0.46	0.55
Case 4: 1 SG =130 cm + 1 TG + 1TG OPENED								
Max	2.61	2.42	2.21	2.20	1.24	1.05	0.84	0.83
Min	1.66	1.60	1.62	1.62	0.29	0.23	0.25	0.25
Range	0.95	0.82	0.60	0.58	0.95	0.82	0.60	0.58
Case 5: 3 SG =130 cm								
Max	2.63	2.52	2.31	2.33	1.26	1.15	0.94	0.96
Min	1.61	1.58	1.62	1.80	0.24	0.21	0.25	0.43
Range	1.03	0.94	0.69	0.53	1.03	0.94	0.69	0.53
Case 6: 3SG = 102 cm								
Max	2.57	2.45	2.29	2.32	1.20	1.08	0.92	0.95
Min	1.55	1.51	1.57	1.77	0.18	0.14	0.20	0.4
Range	1.02	0.94	0.72	0.55	1.02	0.94	0.72	0.55
Case 7: 3SG = 76 cm								
Max	2.44	2.38	2.28	2.29	1.07	1.01	0.91	0.92
Min	1.66	1.61	1.68	1.74	0.29	0.24	0.31	0.37
Range	0.78	0.77	0.60	0.55	0.78	0.77	0.60	0.55
Case 8: 3SG =51 cm								
Max	2.30	2.26	2.23	2.23	0.93	0.89	0.86	0.86
Min	1.68	1.66	1.72	1.69	0.31	0.29	0.35	0.32
Range	0.62	0.60	0.51	0.54	0.62	0.60	0.51	0.54
Case 9: 3SG = 25 cm								
Max	2.05	2.04	2.10	2.11	0.68	0.67	0.73	0.74
Min	1.67	1.66	1.71	1.60	0.30	0.29	0.34	0.23
Range	0.38	0.38	0.39	0.51	0.38	0.38	0.39	0.51
Case 10: no gates								
Max	2.88	2.73	2.52		1.51	1.36	1.15	

Min	1.79	1.75	1.78	0.42	0.38	0.41
Range	1.09	0.98	0.75	1.09	0.98	0.75

Case Summary:

A0- present model with two part formulation for the Manning coefficient (n= 0.06/0.09)

A4- present model with single Manning Coefficient (n= 0.09)

C4- present model using Garvine's assumptions for basin area and bottom friction

Garvine- results of Garvine's simulations taken directly from Roman (1987)

MLW- reference to Mean Low Water (MLW)

NGVD- reference to National Geodetic Vertical Datum (NGVD)

Table 10 Impact of changes in the width of the opening at the Herring River dike on the maximum and minimum water elevations and tidal range in the river.

Forcing: maximum 1.65 m, minimum - -0.73 m, semi diurnal period

	Elevations (m)		
	Maximum	Minimum	Range(m)
Width of the inlet (m)			
6.1*	1.53	+0.43	1.1
10	1.63	-0.044	1.59
20	1.65	-0.49	2.14
30	1.65	-0.63	2.28
40	1.65	-0.67	2.32
60	1.65	-0.7	2.35
100	1.65	-0.72	2.37
120	1.65	-0.72	2.37
200	1.65	-0.73	2.38

* Present width of existing box culverts

Table 11 Results of simulation for selected 100 year storm, and neap and spring tidal cases

100 years storm : z bay (NGVD) = 0.44 +2.7 * sin (2*pi *t/T)

All values given in meters	MLW				NGVD			
	A0	A4	C4	Garvine	A0	A4	C4	Garvine
100 years storm: Case 2								
Max	1.95	1.89	1.93	2.08	0.58	0.52	0.56	0.71
Min	1.39	1.34	1.35		0.02	-0.03	-0.02	
Range	0.57	0.55	0.57		0.57	0.55	0.57	
100 years storm: Case 5								
Max	3.21	3.08	2.68	2.76	1.84	1.71	1.31	1.39
Min	1.73	1.70	2.06		0.36	0.33	0.69	
Range	1.48	1.38	0.62		1.48	1.38	0.62	
100 years storm: Case 10								
Max	4.08	3.97	2.99		2.71	2.6	1.62	
Min	2.37	2.32	2.81		1.00	0.95	1.44	
Range	1.71	1.64	0.19		1.71	1.64	0.19	
Neap tide : Case 2								
Max	1.77	1.70	1.67	1.77	0.40	0.33	0.30	0.4
Min	1.18	1.12	1.18	1.15	-0.19	-0.25	-0.19	-0.22
Range	0.59	0.58	0.49	0.62	0.59	0.58	0.49	0.62
RMS error	0.04	0.05	0.07		0.04	0.05	0.07	
Neap tide: Case 5								
Max	2.66	2.53	2.31		1.29	1.16	0.94	
Min	1.22	1.22	1.25		-0.15	-0.15	-0.12	
Range	1.44	1.31	1.06		1.44	1.31	1.06	
Neap tide: Case 10								
Max	3.01	2.80	2.42		1.64	1.43	1.05	
Min	1.22	1.22	1.25		-0.15	-0.15	-0.12	
Range	1.79	1.58	1.17		1.79	1.58	1.17	
Spring tide : Case 2								
Max	1.87	1.80	1.82	1.81	0.50	0.43	0.45	0.44
Min	1.20	1.16	1.21	1.20	-0.17	-0.21	-0.16	-0.17
Range	0.67	0.64	0.61	0.61	0.67	0.64	0.61	0.61
RMS error	0.06	0.03	0.04		0.06	0.03	0.04	
Spring tide: Case 5								
Max	3.02	2.87	2.51		1.65	1.50	1.14	
Min	1.42	1.39	1.38		0.05	0.02	0.01	
Range	1.60	1.48	1.13		1.60	1.48	1.13	
Spring tide: Case 10								
Max	3.72	3.44	2.72		2.35	2.07	1.35	
Min	1.60	1.52	1.48		0.23	0.15	0.11	
Range	2.12	1.92	1.24		2.12	1.92	1.24	

Table 12 Impact of restoration options on salt penetration distance and flushing time of Herring River for varying freshwater inputs.

Impact of restoration K= 4.5 m^2/sec, So = 28 ppt			Fresh water input: 0.10 m^3/s		Fresh water input: 0.28 m^3/s	
Flushing time (hrs)		**Mean water elevation (m)**	**Salt pene-tration distance (km)**	**Flushing time (hrs)**	**Salt pene-tration distance (km)**	**Flushing time (hrs)**
Measurements:	Exp. #1	0.2	1.5	26.0		
	Exp #2	0.16	1.5	34.7		
Model:	Exp. #1	0.2	1.6	31.3		
	Exp. #2	0.16	1.4	24.6		
C1		0.18	1.5	29.5	0.97	14
C2		0.22	1.6	36.2	1.17	17.8
C3		0.35	2.1	50.4	1.61	34.7
C4		0.78	4.8	229	2.74	68.8
C5		0.78	4.8	229	2.74	68.8
C6		0.75	4.6	223	2.54	66.7
C7		0.72	4.3	217	2.29	57
C8		0.65	3.8	180	2.17	54.7
C9		0.51	2.2	59.4	1.95	48.5
C10		0.97	>5	357	3.75	173

Table 13 Impact of restoration options on the average, minimum, and maximum tidal elevation and tidal range in Herring River for Cases C2, C5, and C10, with mean and 100 yr forcing for two basin geometries (B0 and B1).

Impact of restoration
Gate configuration: Present conditions (C2) / all gates opened @ 130 cm (C5) / no gates (C10)
Basin configuration: Existing configuration (B0), High Toss Road opened and Mill Creek closed (B1)

Case Name		B0	B1	100 yr / B0	100 yr / B1
C2	Average	0.2	0.22	0.30	0.35
	Max	0.48	0.58	0.58	0.48
	Min	-0.08	-0.12	0.01	0.19
	Range	0.56	0.70	0.57	0.29
C5	Average	0.72	0.74	1.07	1.09
	Max	1.27	0.97	1.84	1.36
	Min	0.24	0.51	0.36	0.82
	Range	1.03	0.46	1.48	0.54
C10	Average	0.95	1.05	1.79	1.86
	Max	1.51	1.27	2.73	2.23
	Min	0.42	0.85	1.00	1.57
	Range	1.09	0.42	1.73	0.66

Table 14 Impact of restoration options on salt penetration distance and flushing time of Herring River for Cases C2, C5, and C10, with mean tidal and 100 yr storm forcing, for basin geometry B1.

Extended Basin (B1) : Mill Creek diked and High Toss Road opened
Initial salinity at dike (S0), mean tidal forcing (and Exp. #1) = 28 ppt
Initial salinity at dike (S0), 100 year storm forcing = 32 ppt
Diffusivity, K = 4.5 m^2/s
Fresh water input: 0.10 m^3/s

Gate Configuration	Forcing	Mean Water Elevation (m)	Salt Penetration Distance (km)	Flushing Time (hrs)
C2	Mean tidal sinusoidal	0.22	1.6	32.6
C5	Mean tidal sinusoidal	0.74	4.27	200.7
C10	Mean tidal sinusoidal	1.05	>5	377
C2	100 year, sinusoidal	0.35	2.2	49.8
C5	100 year, sinusoidal	1.07	>5	384
C10	100 year, sinusoidal	1.09	>5	392

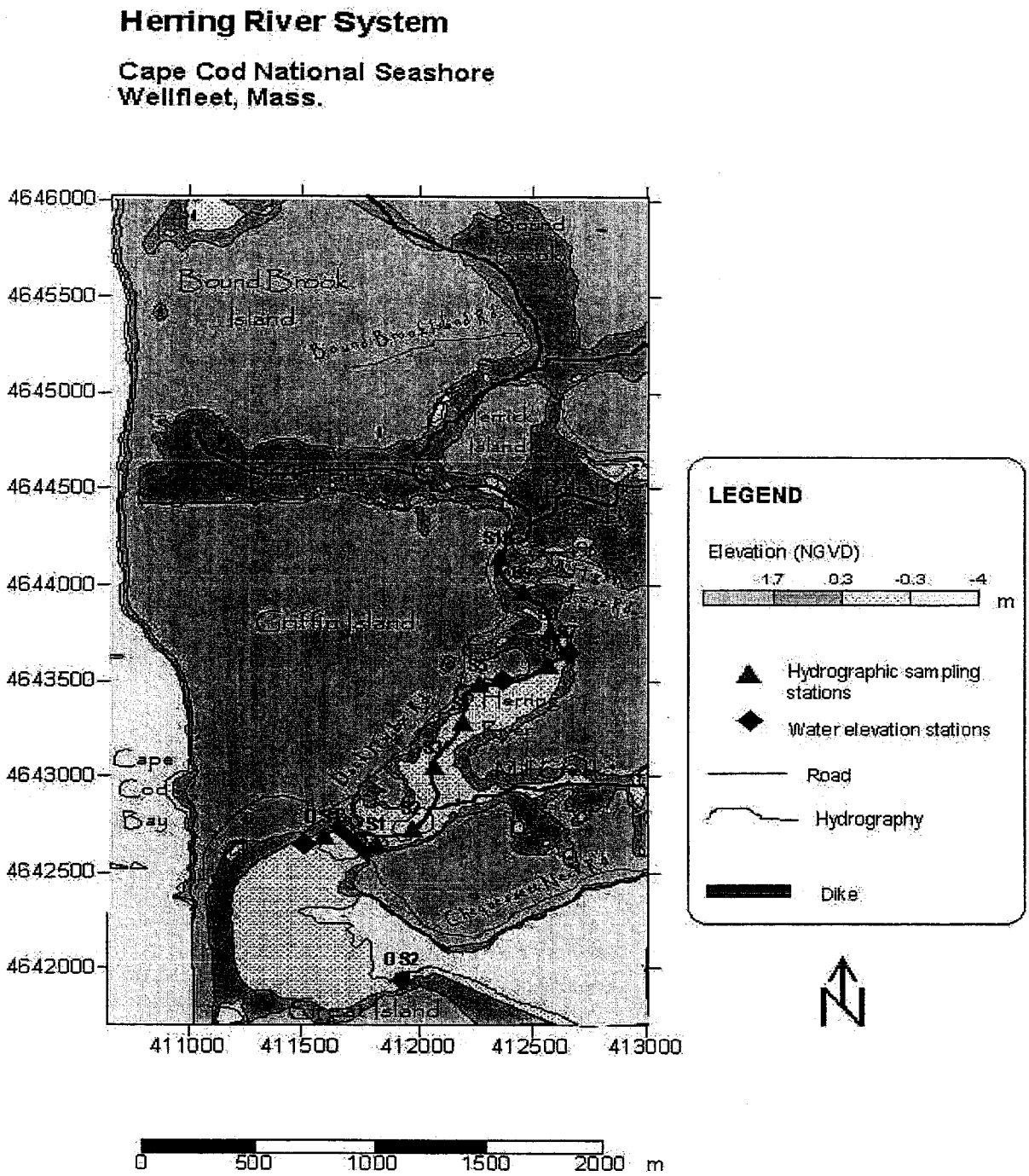

Fig. 1

Figure 1 Herring River study area. Also shown are the locations of the dike at Chequesset Neck Road, High Toss Road, and several of the principal tributaries discharging into the river. The locations of hydrographic sampling stations and the time series measurements are also noted.

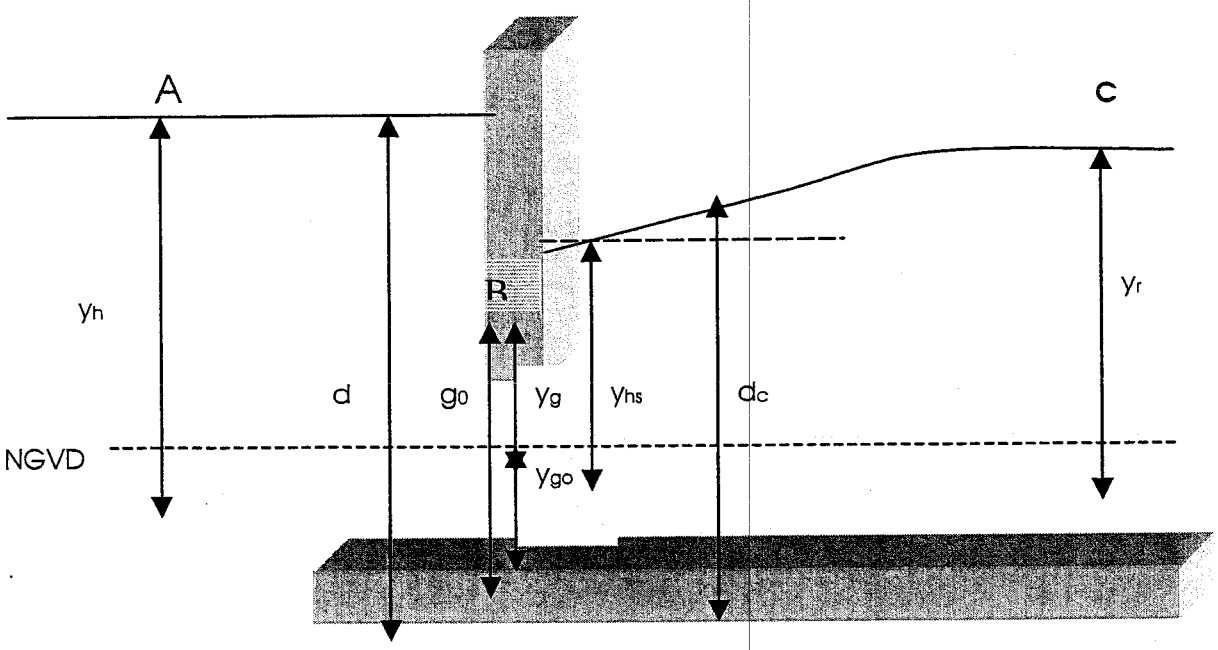

Figure 2 Schematic and definition sketch for flow under a sluice gate.

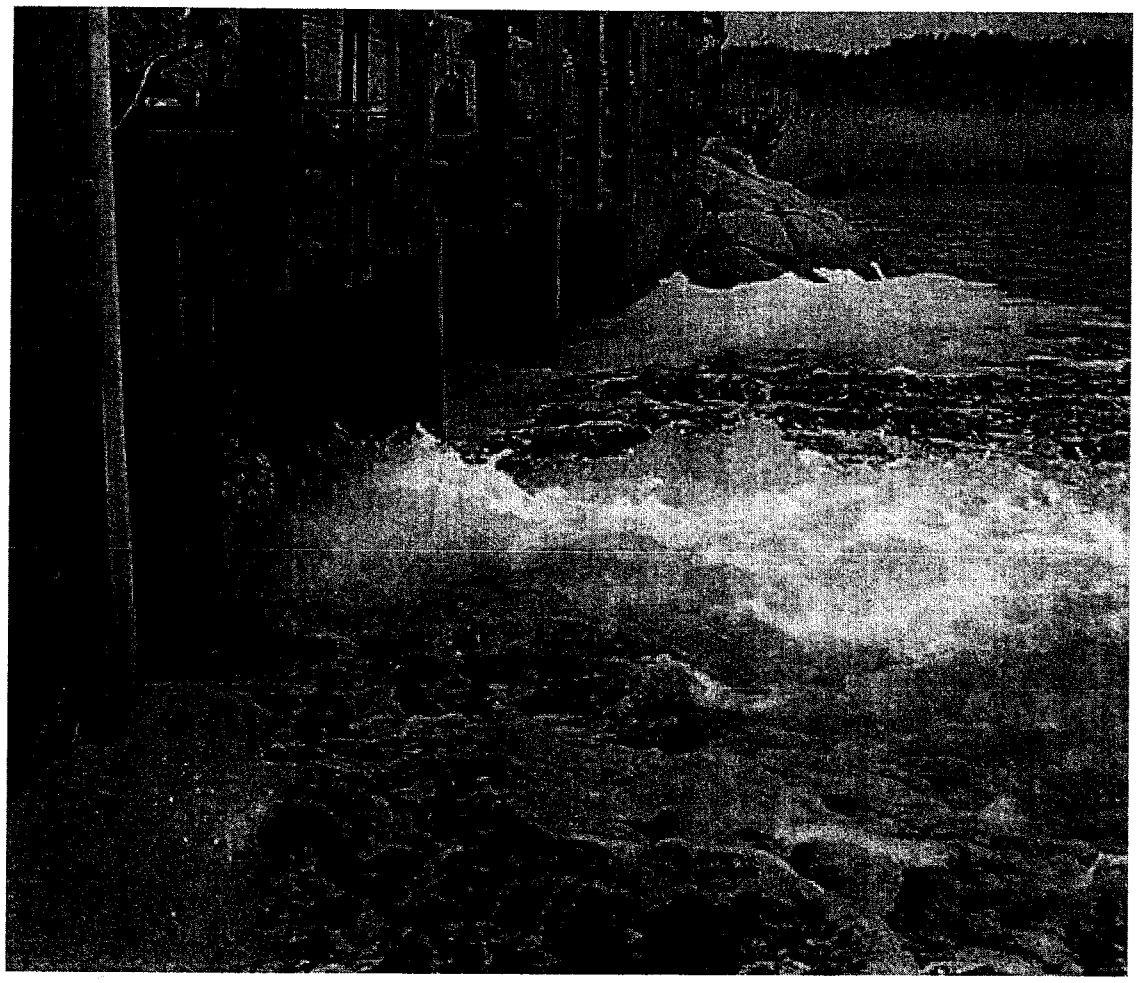

Figure 3a Photograph of the Herring River dike viewed from the landward side. The three openings in the dike are fitted with a sluice gate (left side, closest to the viewer) and two flapper tidal gates (center and right side, furthest from viewer). Currents are flooding at the time of the photograph.

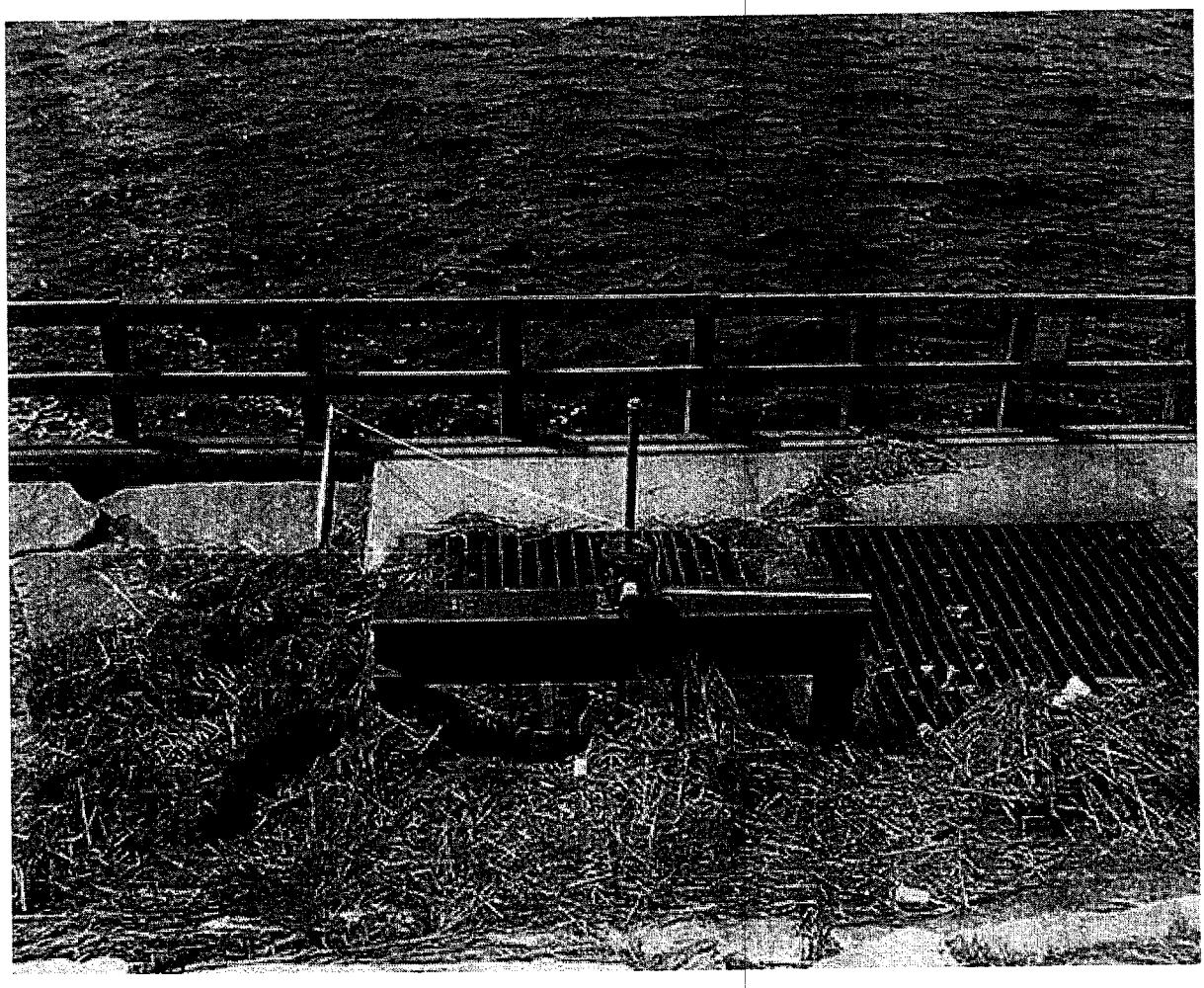

Figure 3b Photograph of the Herring River dike viewed from the Chequessett Road looking seaward. The three openings in the dike are fitted with a sluice gate (left side) and two flapper tidal gates (center gate on right side, second gate not shown). The hand operated mounting bracket, with adjustment screw for the sluice gate, is clearly shown.

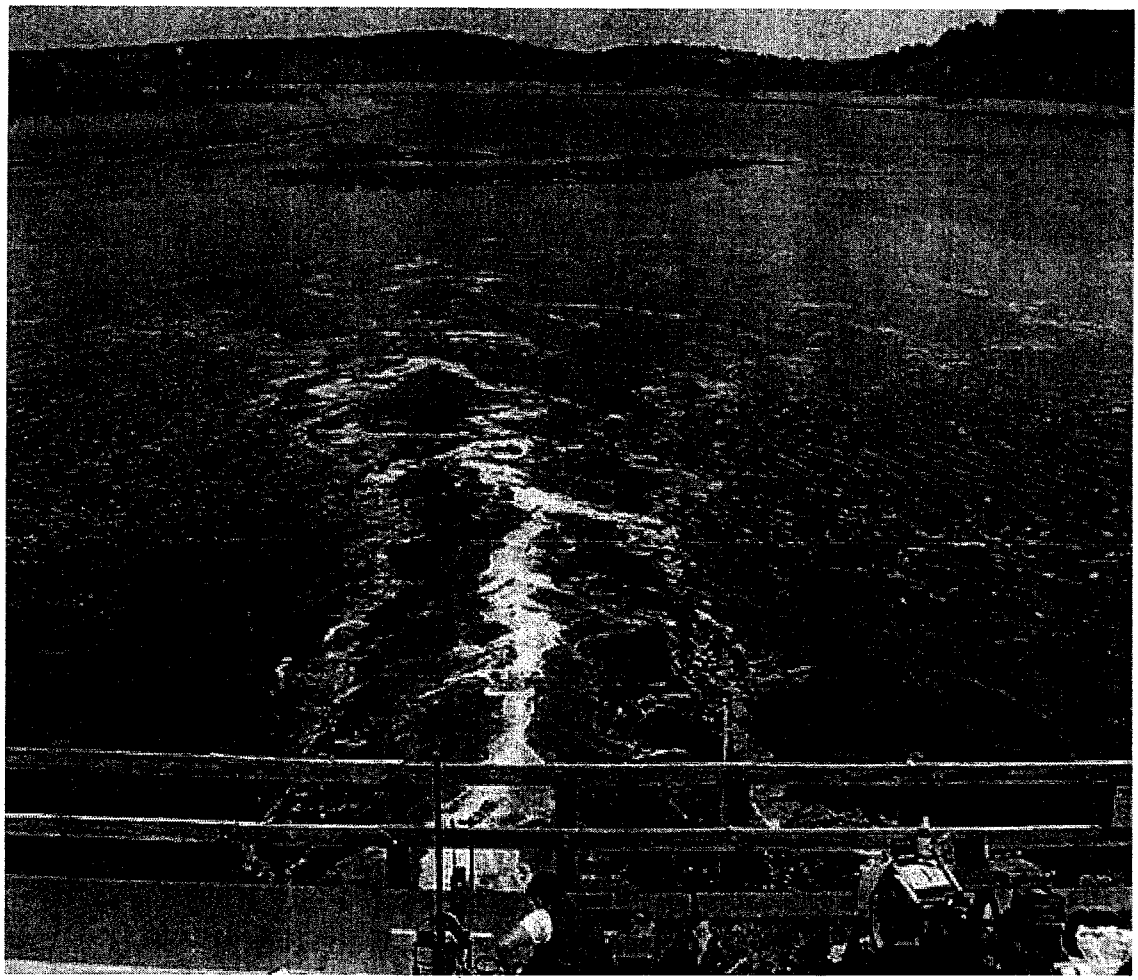

Figure 3c Photograph of the Herring River dike viewed from the landward side. The three openings in the dike are fitted with a sluice gate (right side, with emerging sinuous plume) and two flapper tidal gates (center and left side). Currents are flooding at the time of the photograph. The emergent flood tide delta is clearly evident.

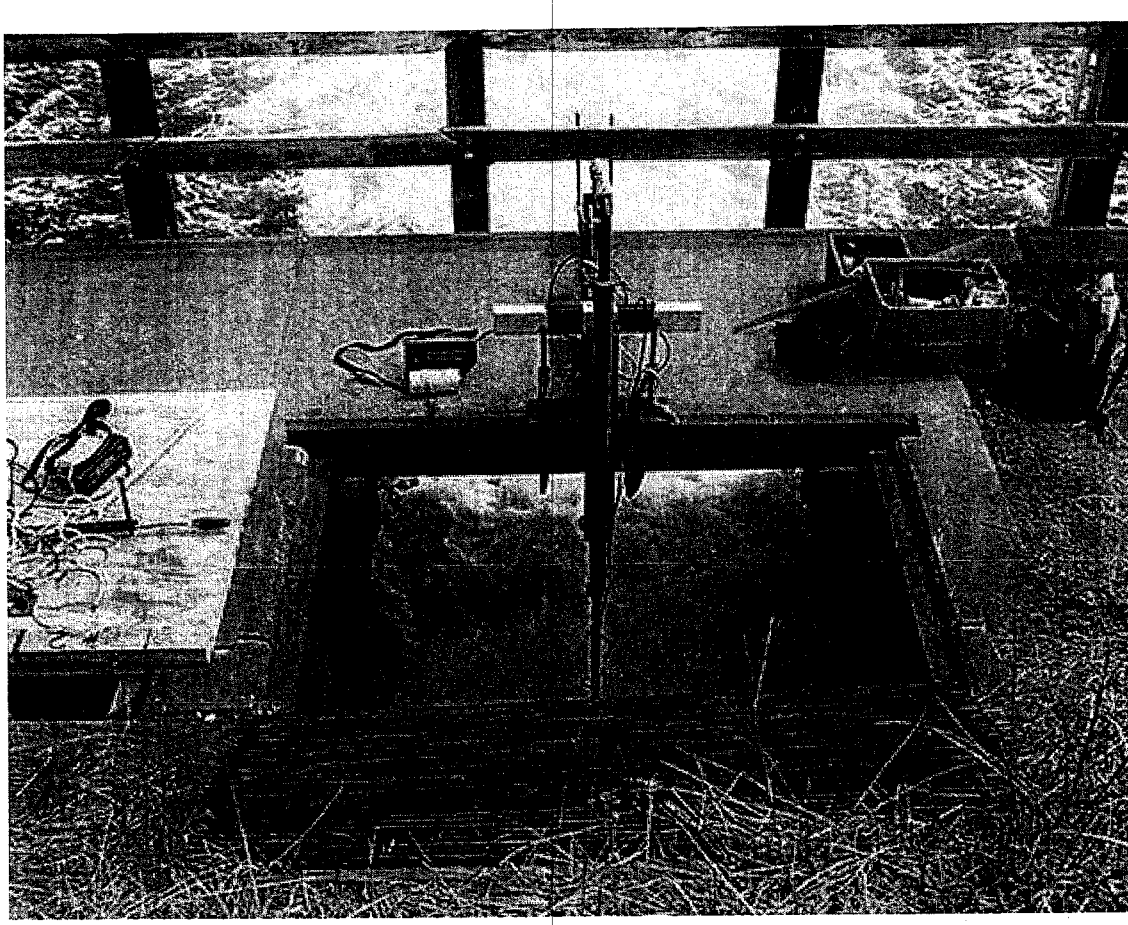

Figure 4 Mounting system used to make measurements of the currents on the landward side of the dike in the culvert outfitted with a sluice gate.

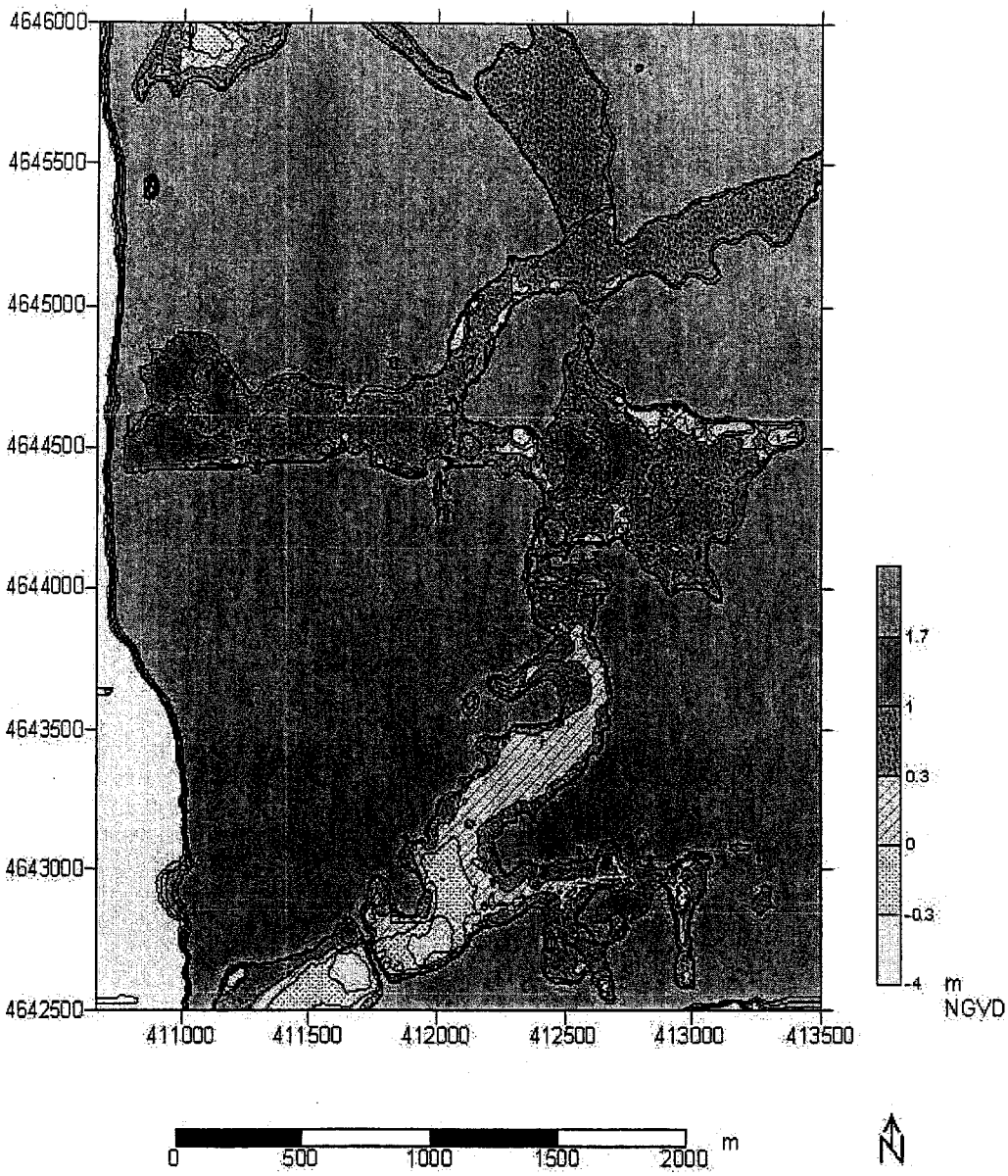

Figure 5a Topographic and bathymetric contours (plan view) for the Herring River system based on US Geological Survey 0, 1, and 3 m topographic contour data and high resolution GPS transects performed by Portnoy and Adams, National Park Service, Wellfleet, MA. All elevations are referenced to NGVD.

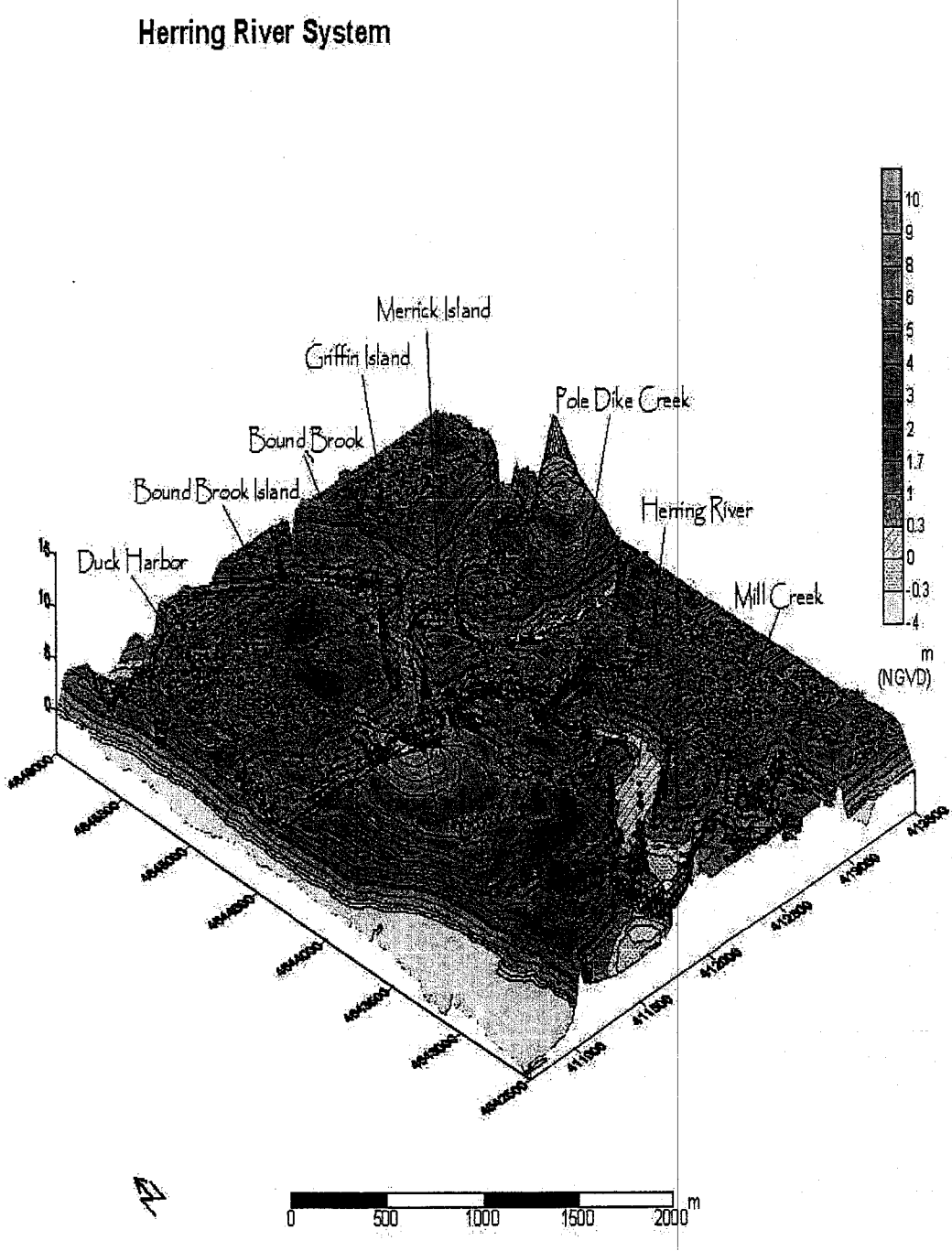

Figure 5b Topographic and bathymetric contours (three dimensional perspective view) for the Herring River system based on US Geological Survey 0, 1, and 3 m topographic contour data and high resolution GPS transects performed by Portnoy and Adams, National Park Service, Wellfleet, MA. All elevations are referenced to NGVD.

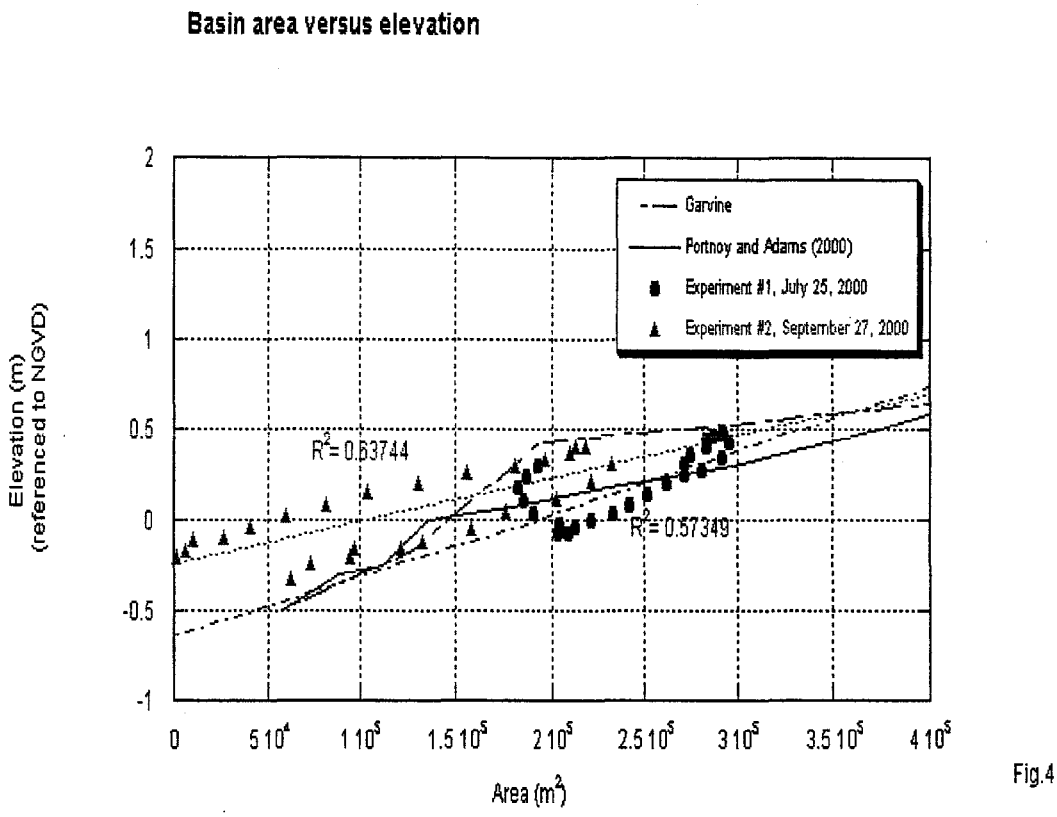

Figure 6a Surface area versus sea surface elevation for the portion of Herring River between the dike and High Toss Road. Estimates of this relationship from data collected by Portnoy and Adams for the present study and by Garvine (Roman, 1978) from an earlier study are shown. Estimates based on the two intensive tidal cycle surveys (Experiment #1, July 25, 2000 and #2, September 27, 2000) are also provided.

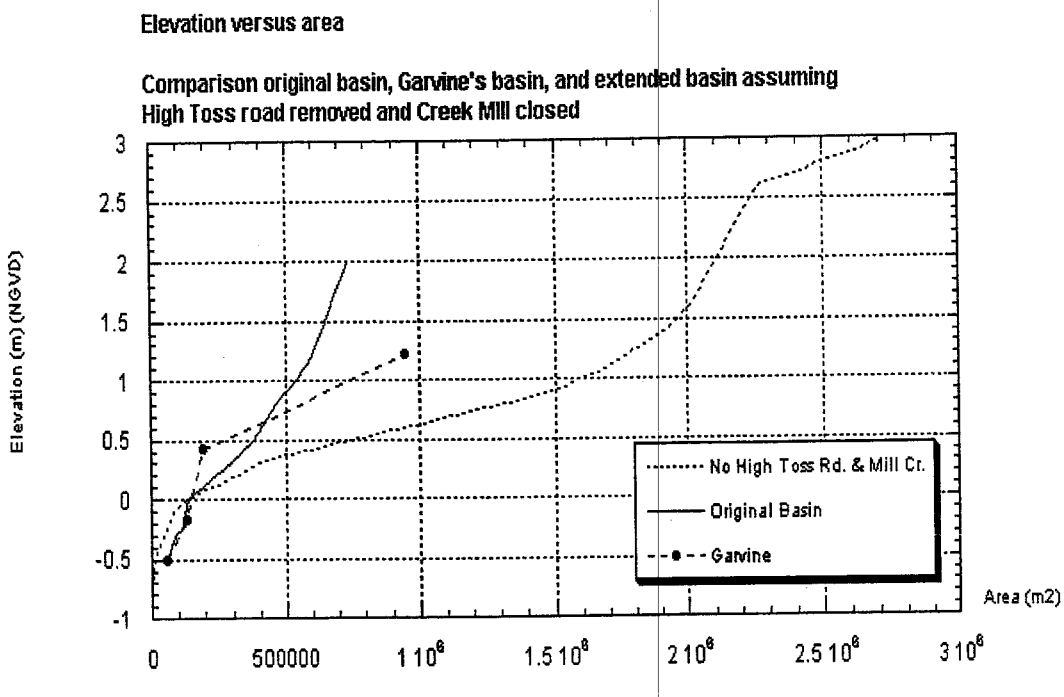

Figure 6b Surface area versus sea surface elevation for the portion of Herring River between the dike and High Toss Road, based on data collected by Portnoy and Adams for the present study and by Garvine (Roman, 1987). Also shown is a similar curve for a restoration option that includes the entire Herring River system, minus Mill Creek.

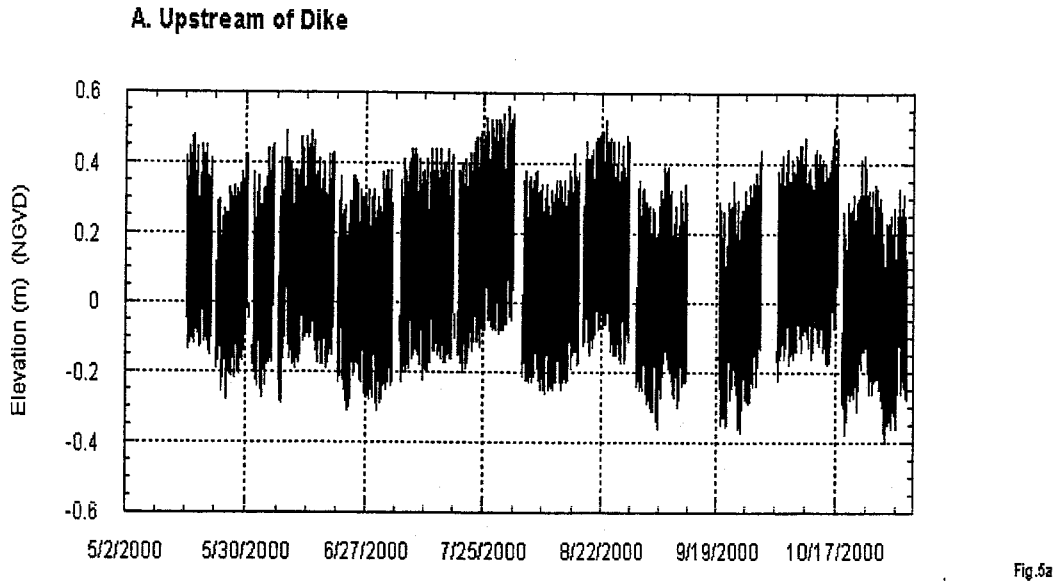

Figure 7a Time series of the sea surface elevation upstream (a) and downstream (b) of the dike are shown for the study period. The gaps in the record indicate time periods when the water level sensors were removed for maintenance or downloading of data.

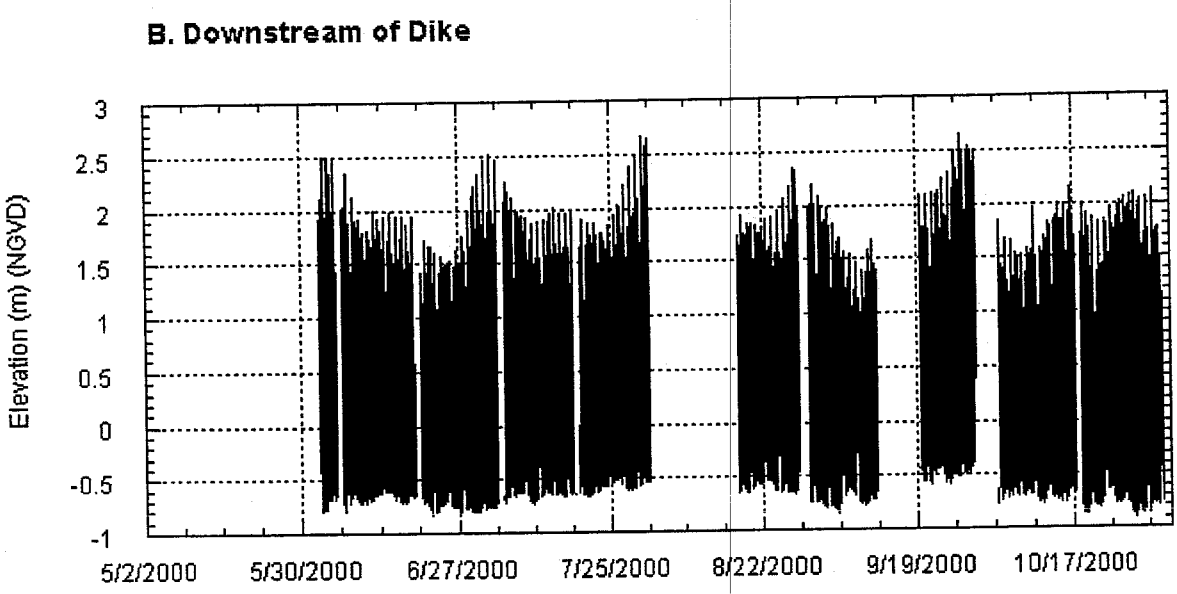

Figure 7b Time series of the sea surface elevation upstream (a) and downstream (b) of the dike are shown for the study period. The gaps in the record indicate time periods when the water level sensors were removed for maintenance or downloading of data.

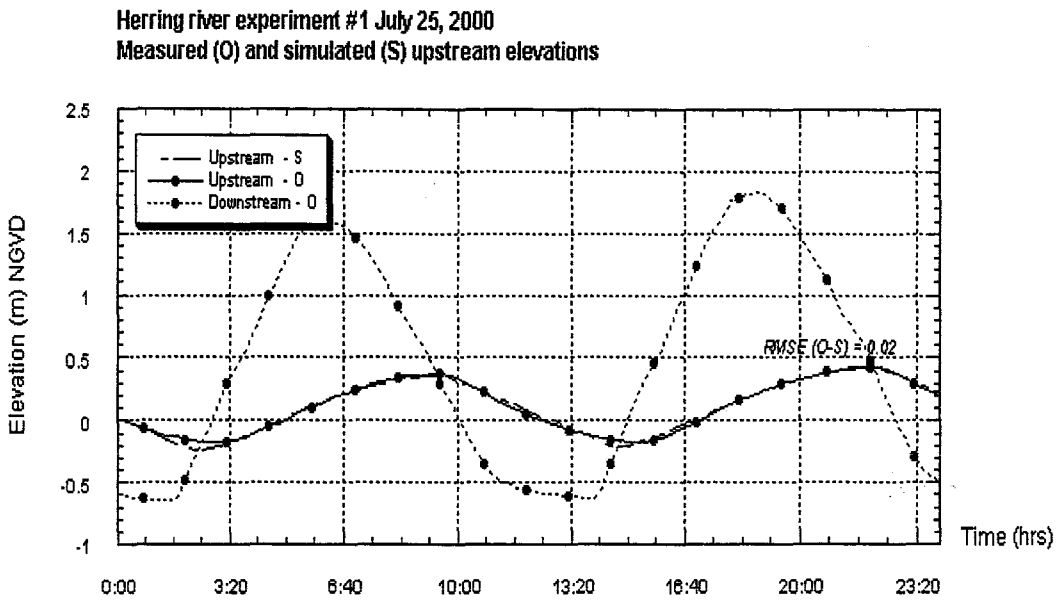

Figure 8 Observations (O) and simulations (S) of the sea surface elevation upstream and downstream of the dike for the July 25, 2000 intensive tidal cycle survey (Experiment #1). The observations were obtained at the sea surface elevation stations noted in Figure 1.

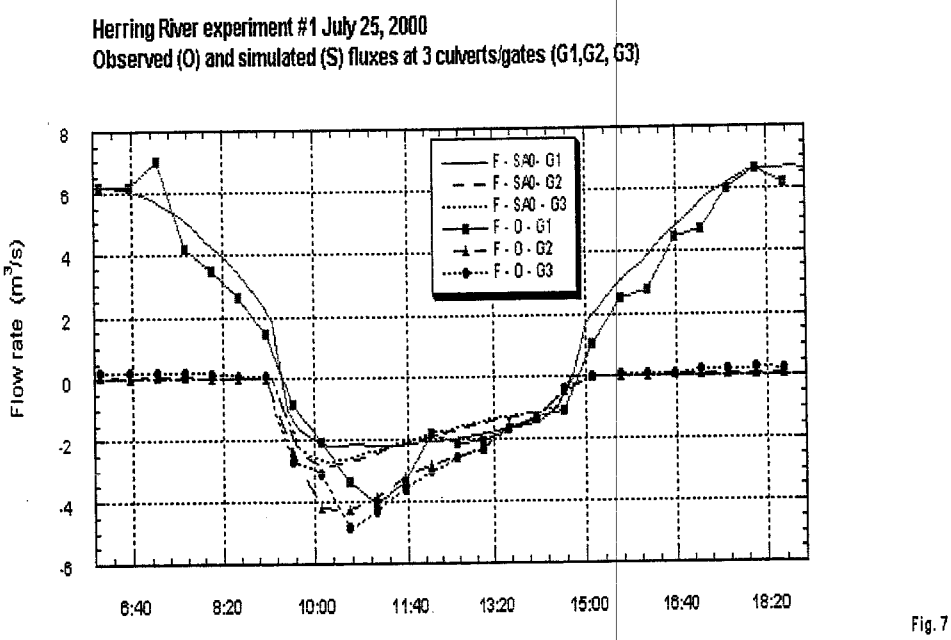

Figure 9 Observations (O) and simulations (S) of the flows through each of the three culverts at the dike for the July 25, 2000 intensive tidal cycle survey (Experiment #1). The culverts or gates are noted by G1 (sluice gate, east), G2(tidal gate, center), and G3 (sluice gate, west).

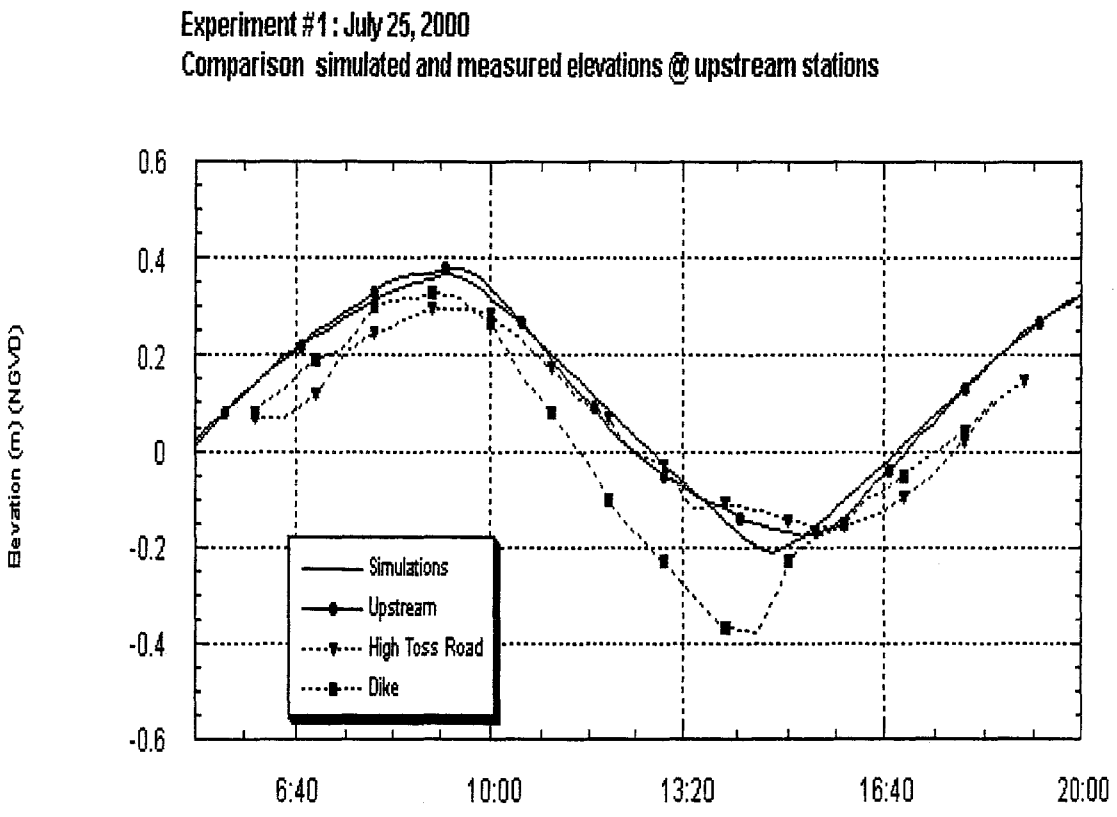

Figure 10 Sea surface elevations versus time for the time period of the July 25, 2000 intensive tidal cycle survey (Experiment #1) as measured at upstream station, High Toss Road, and at the dike. Also shown are simulations at the upstream station for this same period.

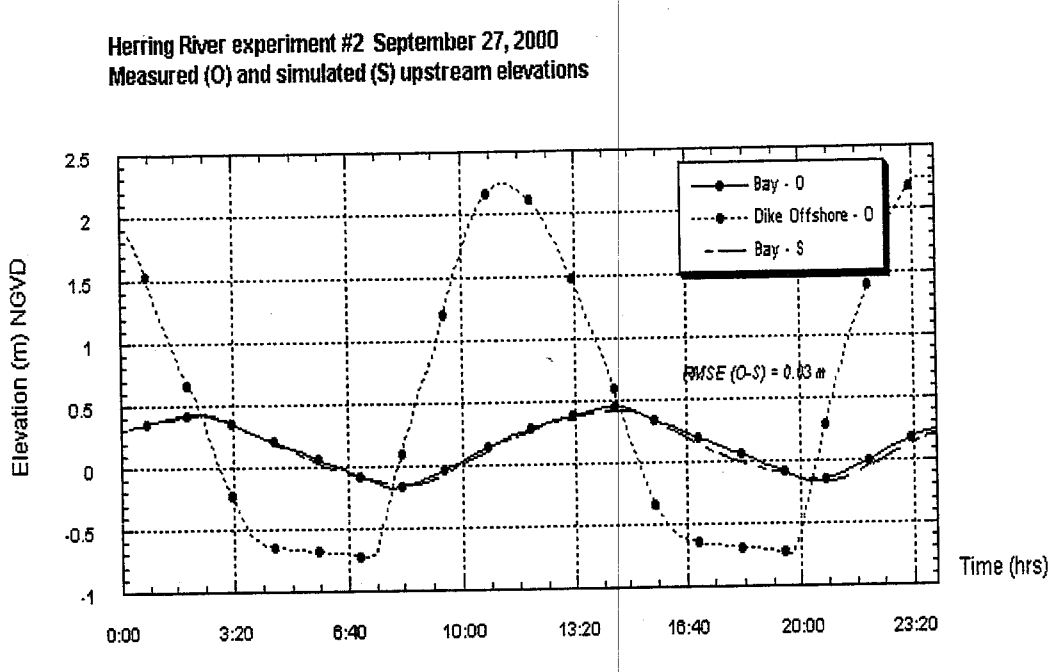

Figure 11 Observations (O) and simulations (S) of the sea surface elevation upstream and downstream of the dike for the September 27, 2000 intensive tidal cycle survey (Experiment #2). The observations were obtained at the sea surface elevation stations noted in Figure 1.

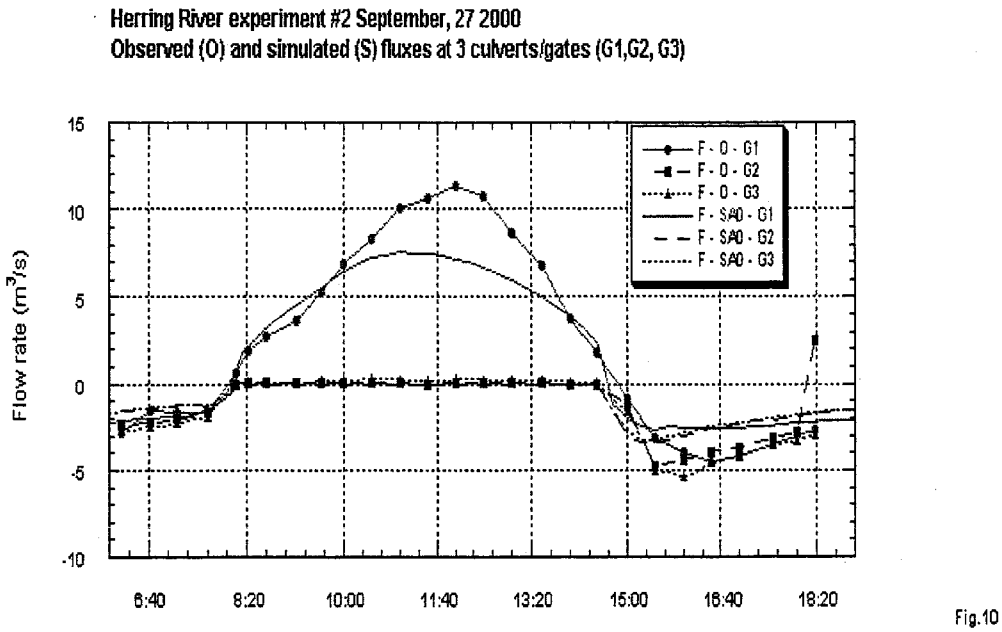

Figure 12 Observations (O) and simulations (S) of the flows through each of the three culverts at the dike for the September 27, 2000 intensive tidal cycle survey (Experiment #2). The culverts or gates are noted by G1 (sluice gate, east), G2 (tidal gate, center), and G3 (sluice gate, west).

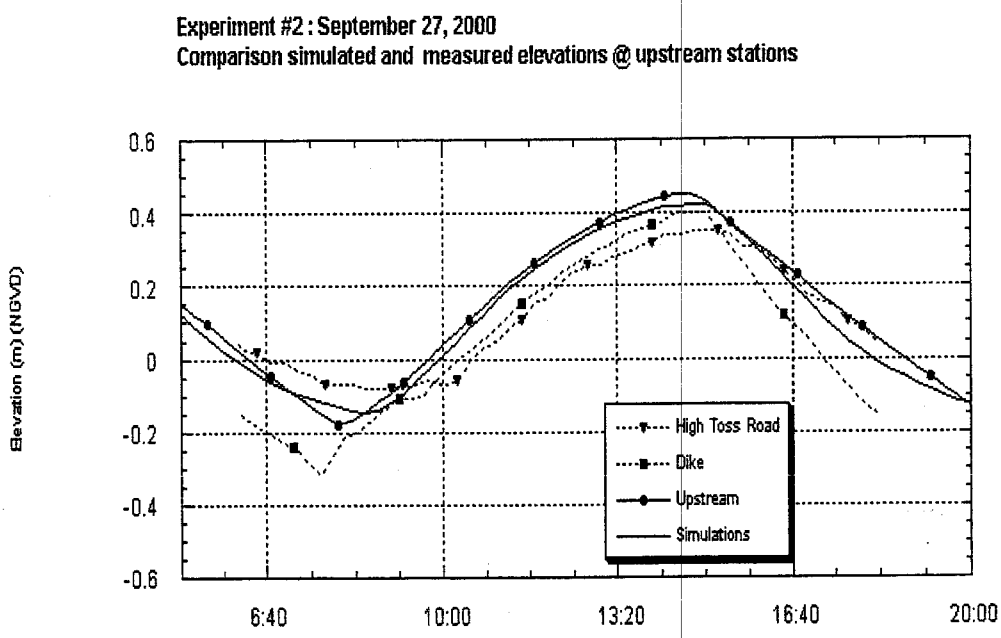

Figure 13 Sea surface elevations versus time for the time period of the September 27, 2000 intensive tidal cycle survey (Experiment #2) as measured at upstream station, High Toss Road, and at the dike. Also shown are simulations at the upstream station for this same period.

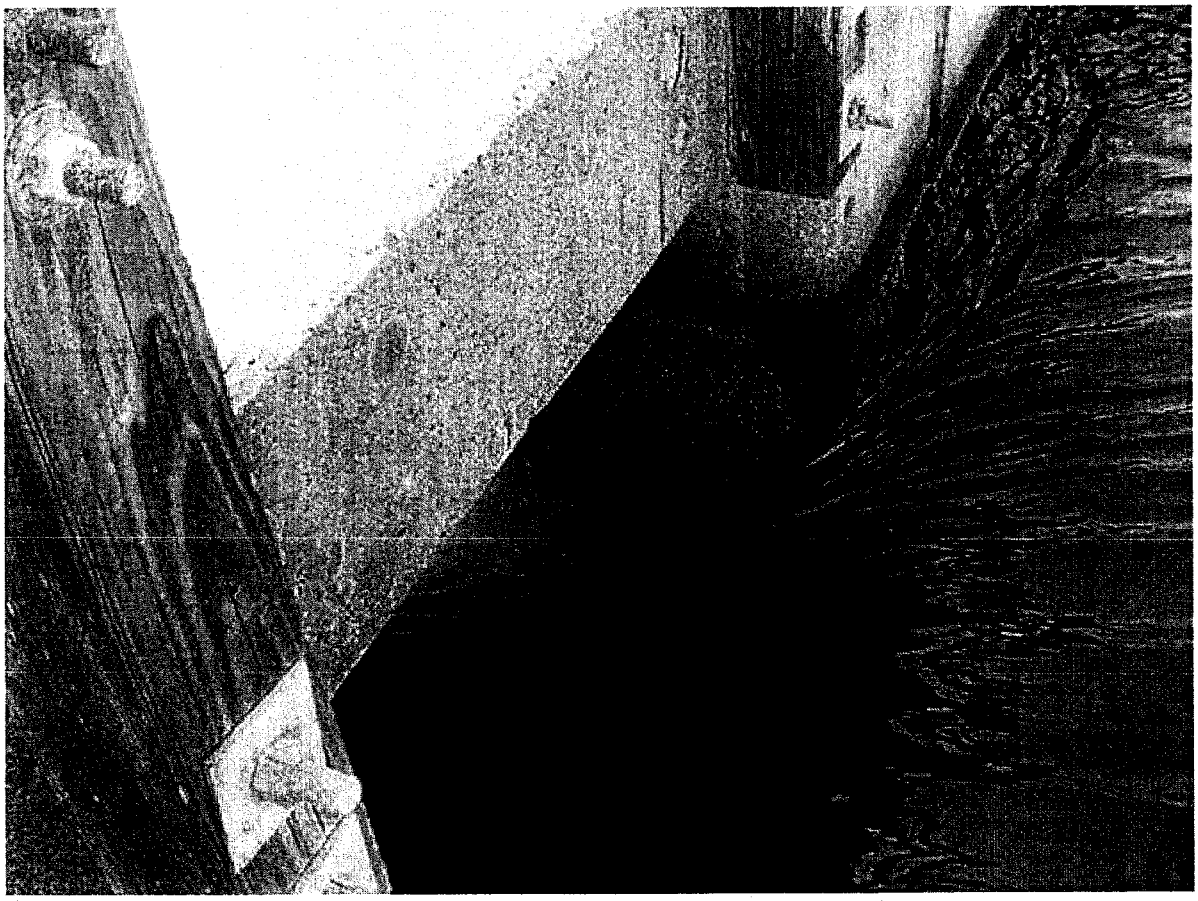

Figure 14a Close-up photograph on the river side of the dike showing the draw down effect associated with ebb flow entering the culvert.

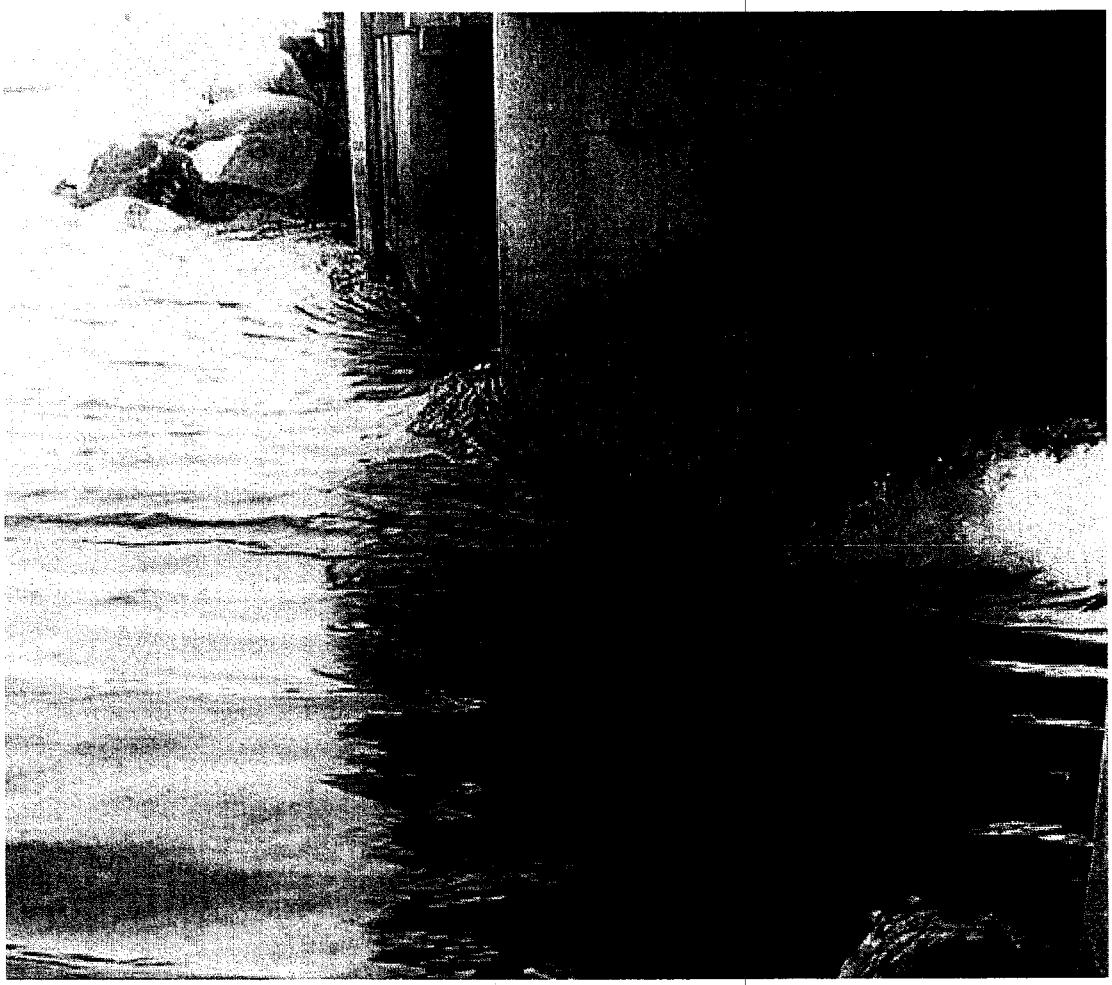

Figure 14b Photograph of the river side of the dike showing ebb flow entering the center and eastern culverts. The difference in water elevation between the river and in the entry region of the culverts is clearly noted. The staff used to measure water level in the vicinity of the culverts during the intensive tidal cycle surveys is clearly seen.

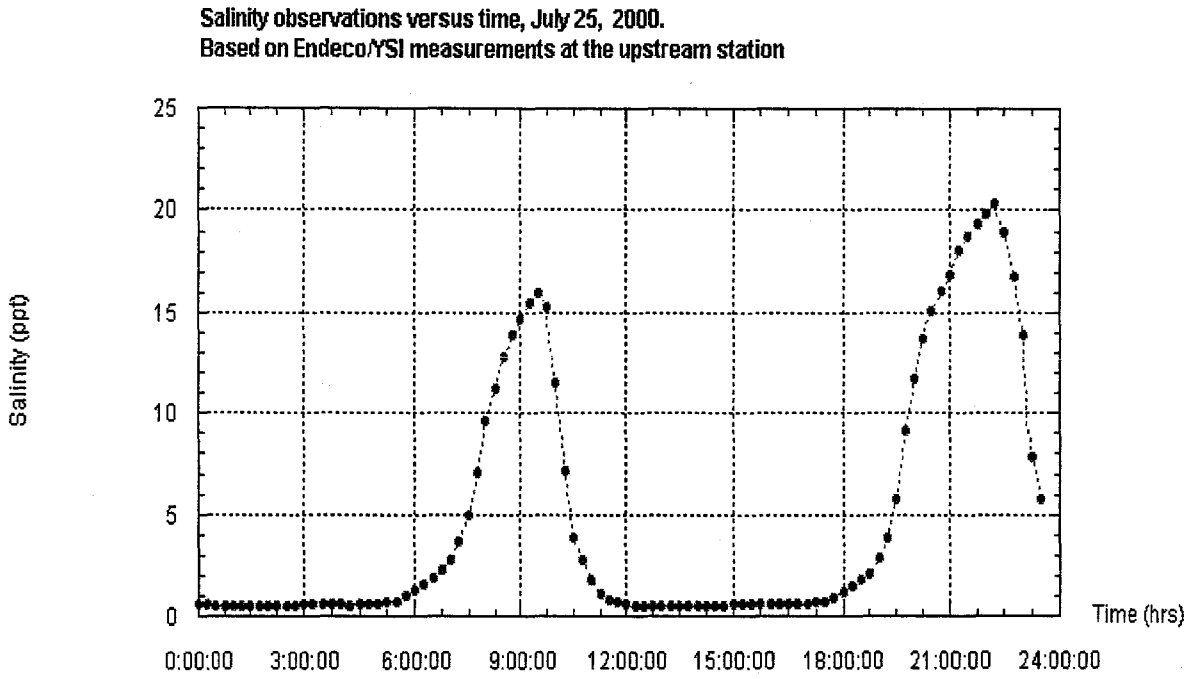

Figure 15 Salinity time series from the YSI/Endeco 6000 water quality sensing system during the July 25, 2000 deployment

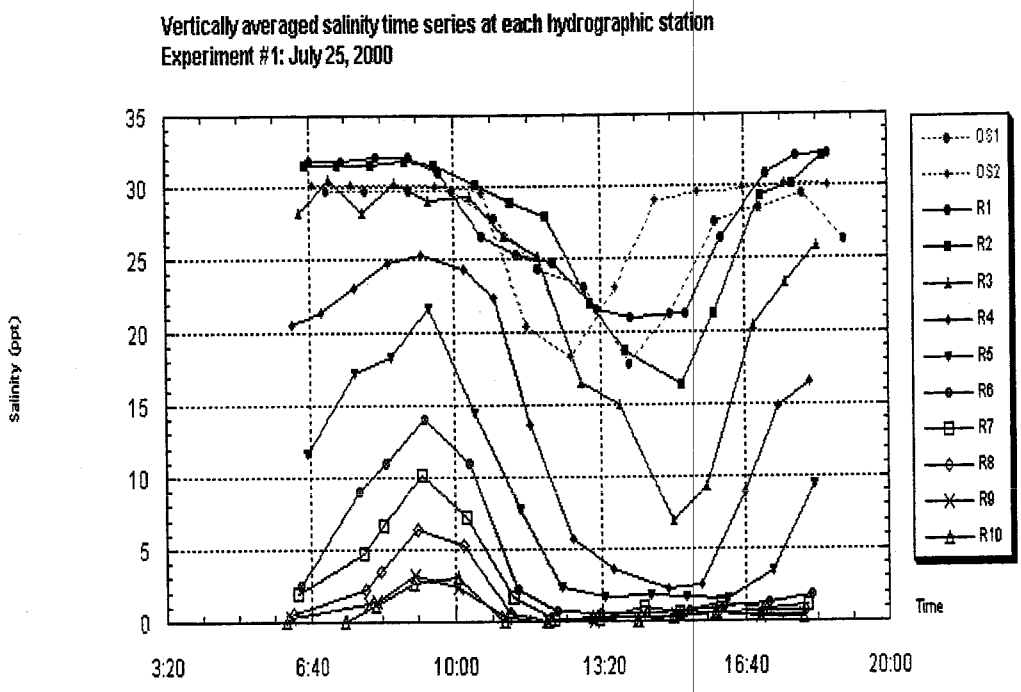

Figure 16 Times series of the salinity at each station during the July 25, 2000 intensive tidal cycle survey. Station locations are shown in Figure 1. Stations with an OS prefix are located seaward of the dike and stations with an R prefix are located landward of the dike.

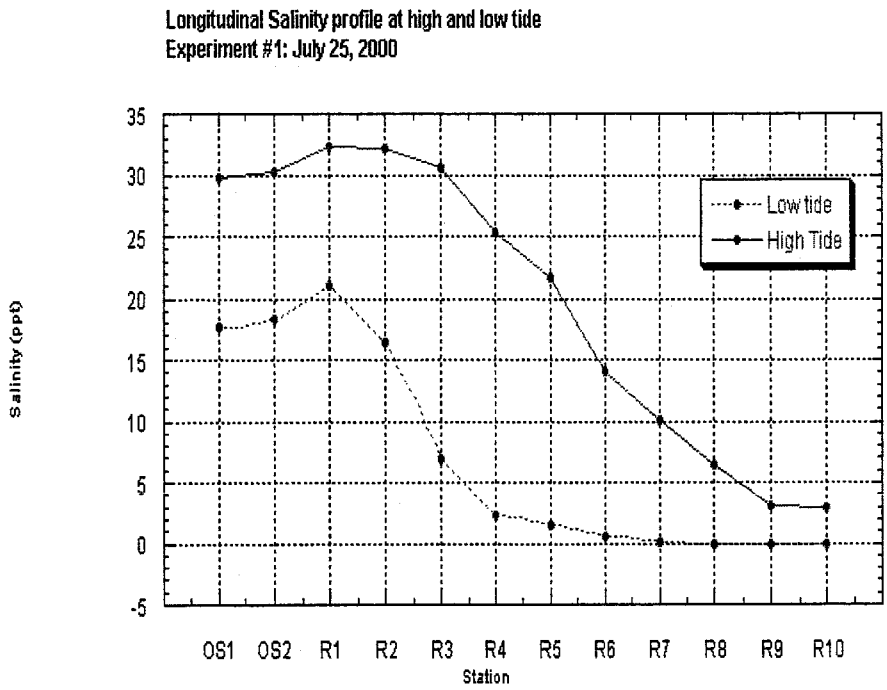

Figure 17 Vertically averaged high and low tide salinity versus distance upstream (in terms of station number; see Figure 1) for the July 25, 2000 intensive tidal cycle survey.

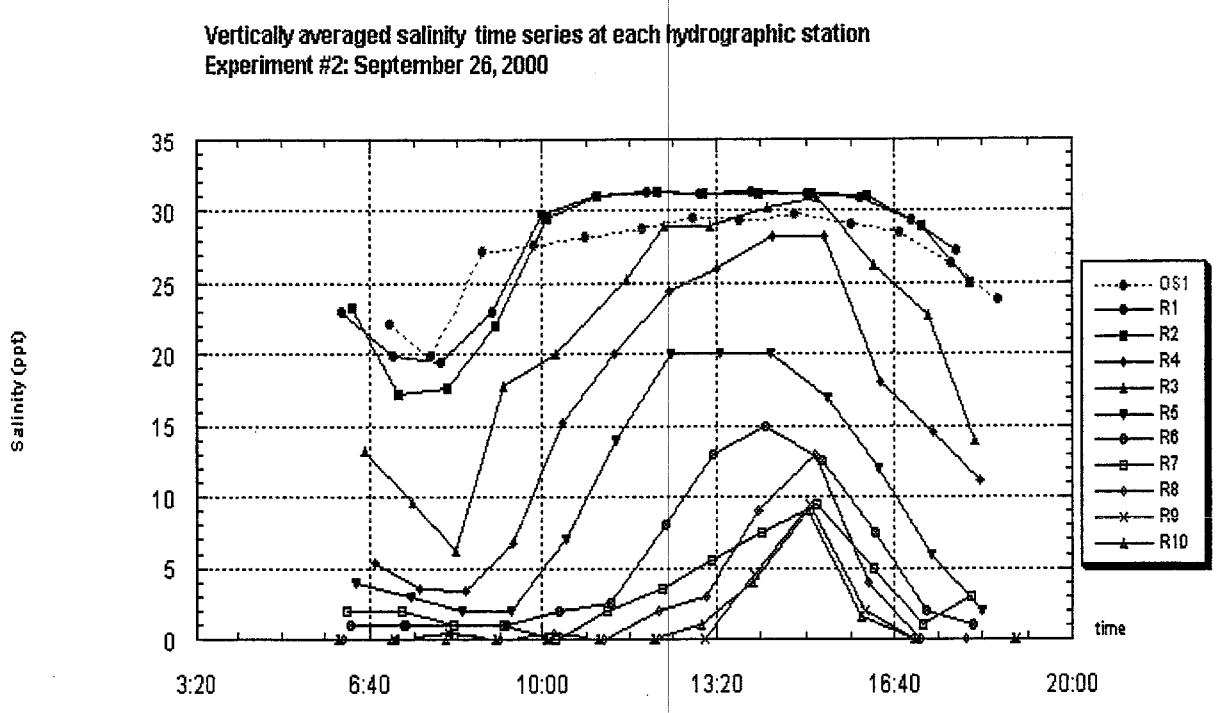

Figure 18 Times series of the salinity at each station during the September 27, 2000 intensive tidal cycle survey. Station locations are shown in Figure 1. Stations with an OS prefix are located seaward of the dike and stations with an R prefix are located landward of the dike.

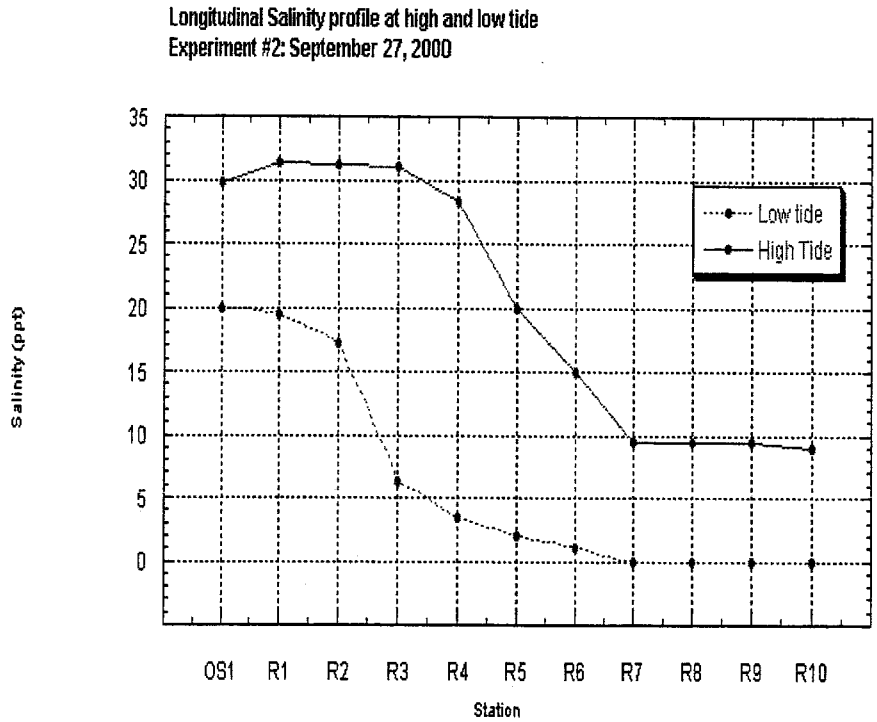

Figure 19 Vertically averaged high and low tide salinity versus distance upstream (in terms of station number; see Figure 1) for the September 27, 2000 intensive tidal cycle survey.

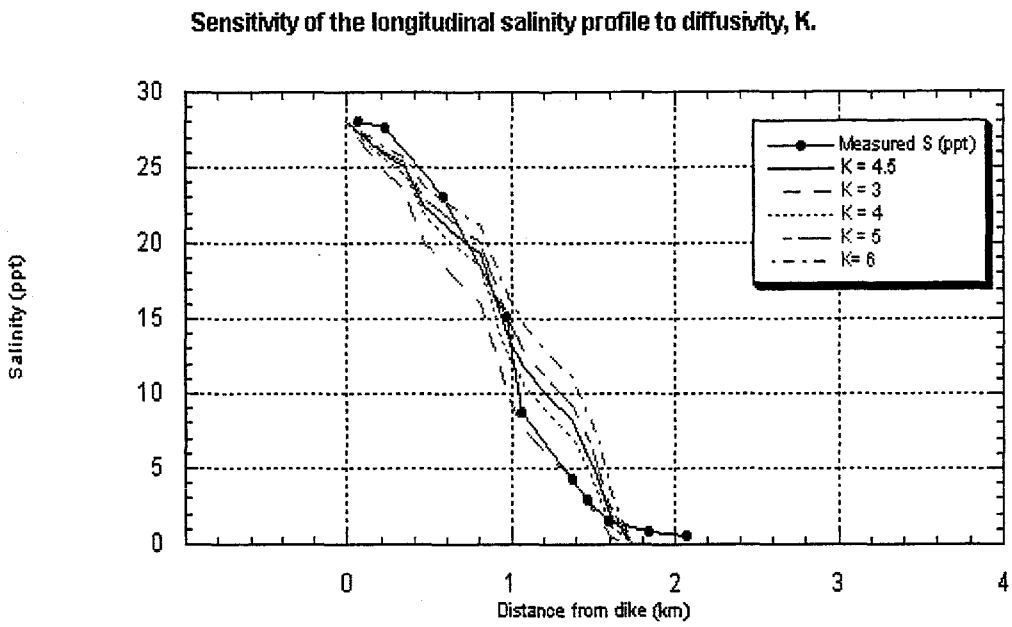

Figure 20 Comparison of the observed and model predicted salinity versus distance upstream from the dike for various values of the longitudinal dispersion coefficient for the July 25, 2000 intensive tidal cycle survey

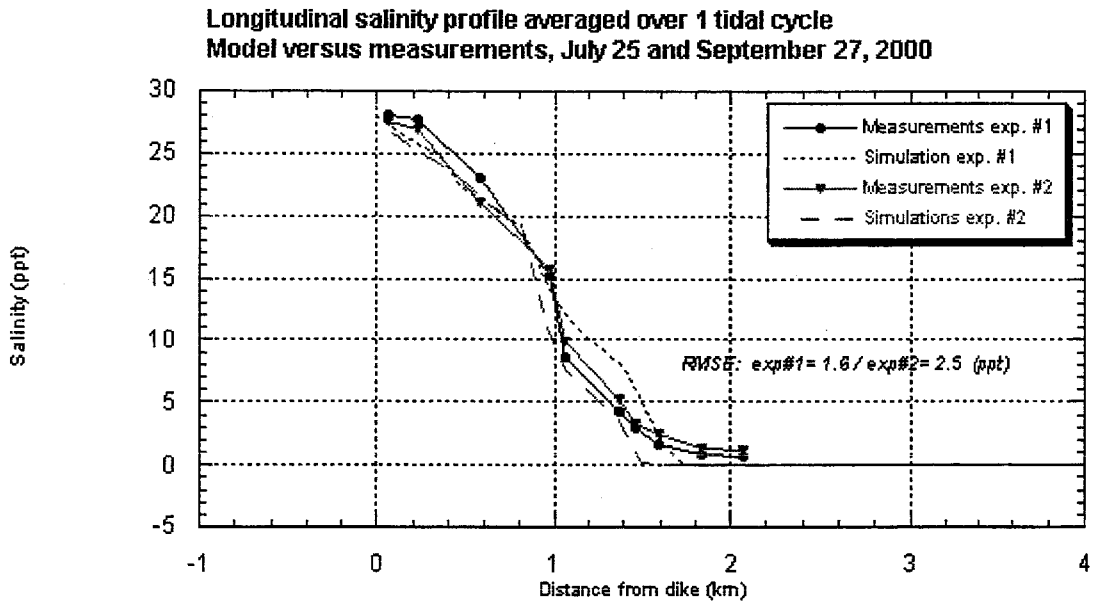

Figure 21 Mean longitudinal salinity profile based on hydrographic data collected during the July 25, 2000 intensive tidal cycle survey (Experiment #1). Also shown is model simulation and associated rms error.

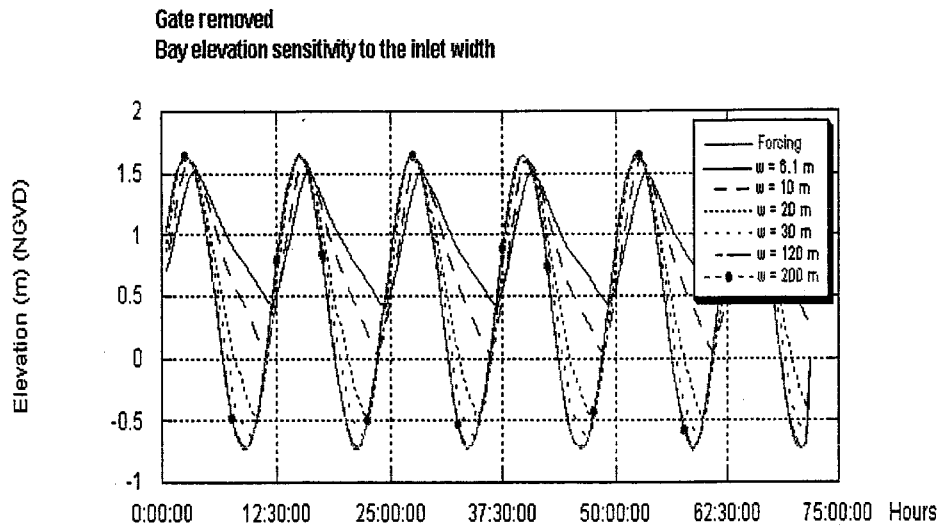

Figure 22 Model predicted surface elevation in the river as a function of time for various opening widths in the dike. Also shown for reference is the forcing used for each simulation.

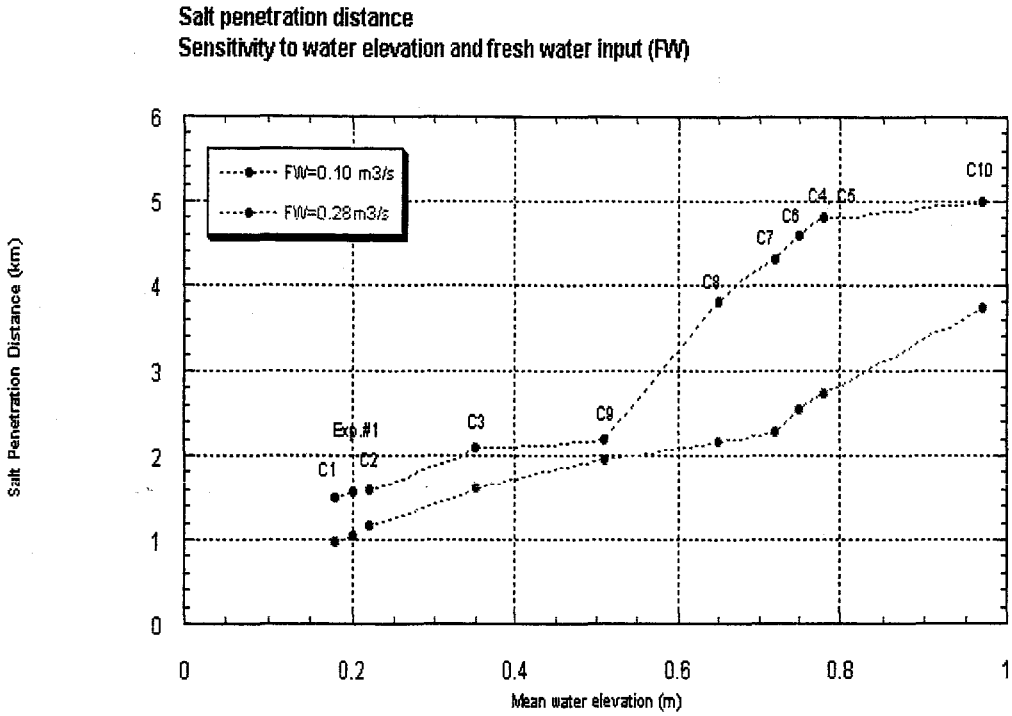

Figure 23 Model predicted salt penetration distance versus mean water elevation for the various restoration options. The option case numbers are provided. Results are presented for high and low water freshwater flow rates

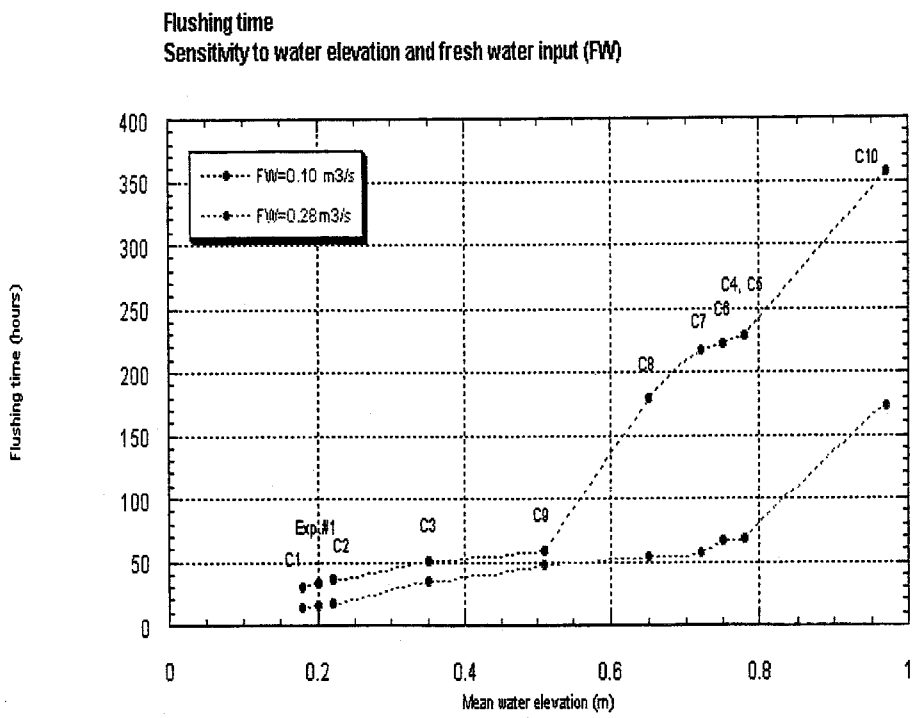

Figure 24 Model predicted flushing time versus mean water elevation for the various restoration options. The option case numbers are provided. Results are presented for high and low water freshwater flow rates

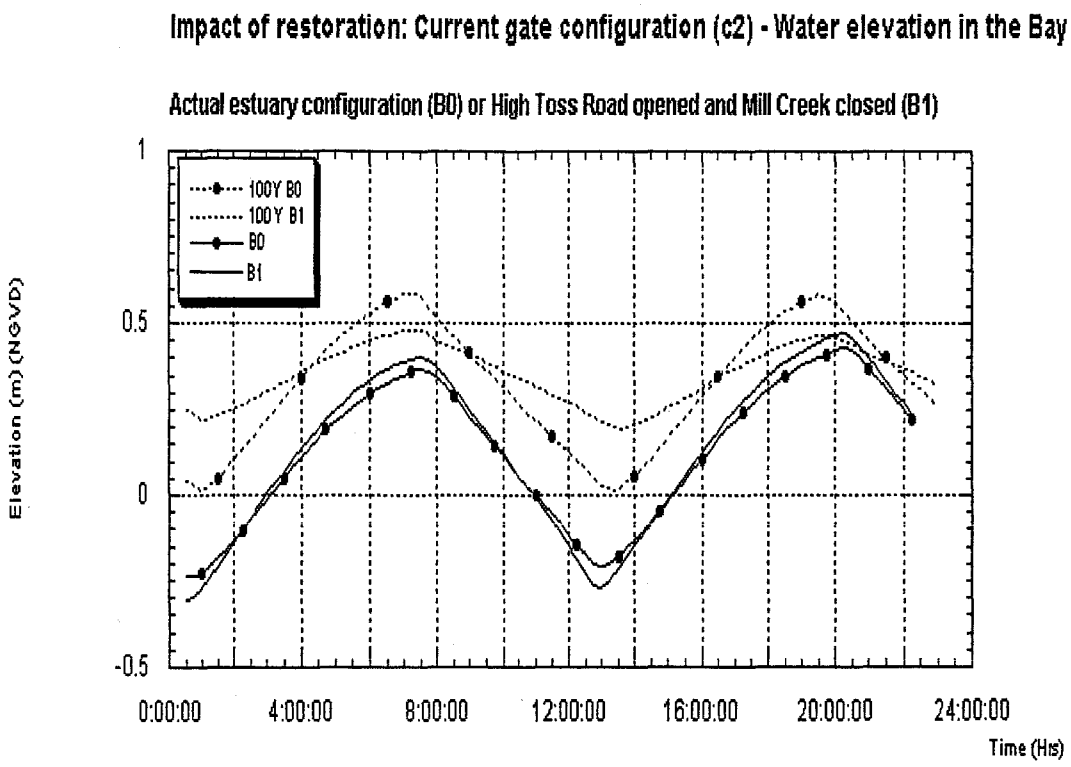

Figure 25a Model predicted time series of sea surface elevation in Herring River for Cases C2 (a), C5 (b), and C10 (c), for mean tidal and 100 yr storm forcing and two basin geometries.

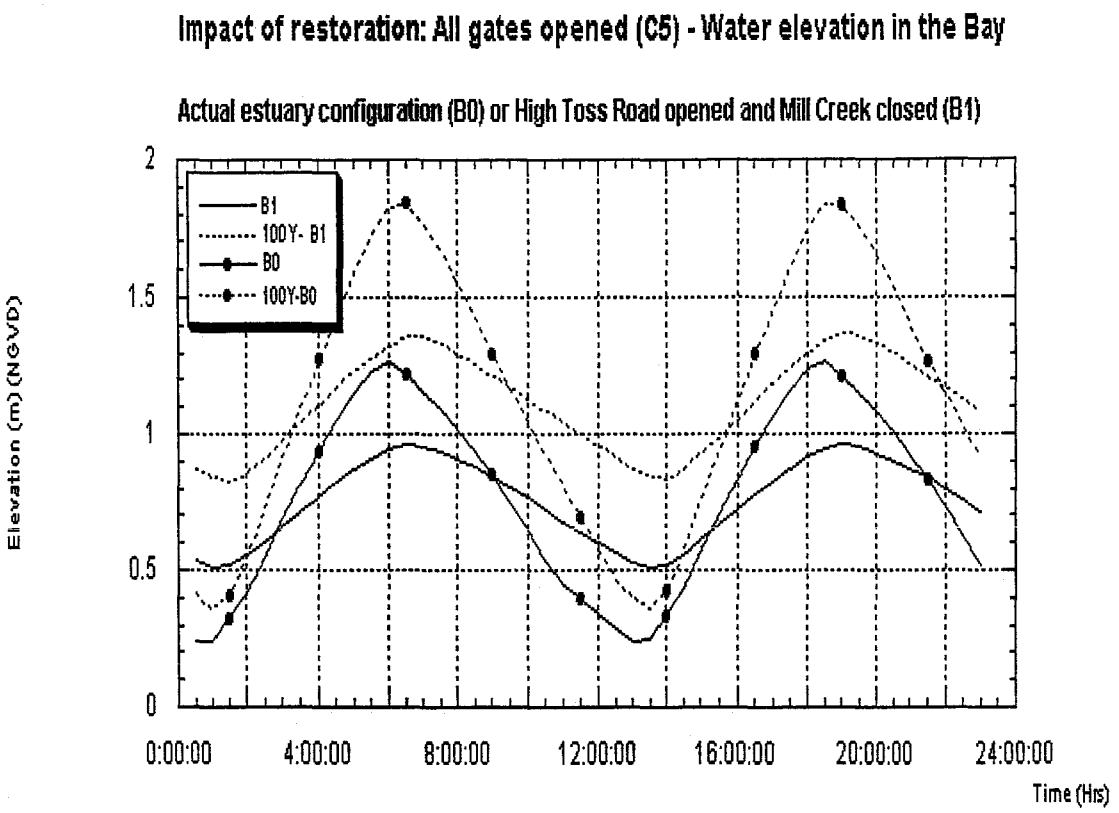

Figure 25b Model predicted time series of sea surface elevation in Herring River for Cases C2 (a), C5 (b), and C10 (c), for mean tidal and 100 yr storm forcing and two basin geometries.

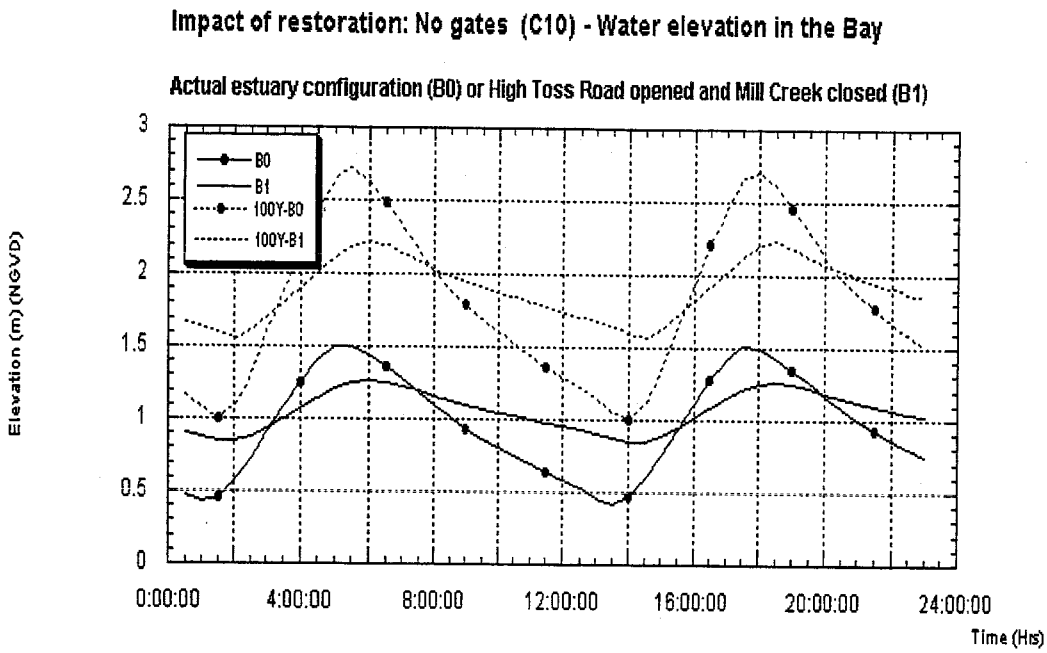

Figure 25c Model predicted time series of sea surface elevation in Herring River for Cases C2 (a), C5 (b), and C10 (c), for mean tidal and 100 yr storm forcing and two basin geometries.